博士論文

Phenomenological Theory of Physiological States, Energetics, and Growth of Cells

（細胞の生理学的状態、エネルギー論、成長の現象論的理論）

姫　岡　優　介

Contents

Chapter 1

Introduction

1.1 Introduction

1.1.1 General Motivation : Why we see the living things as "living things"?

While we still poorly understand the inherent characteristic(s) of living things, almost all people might agree that the living things are strikingly different from non-living matters. Now, on what grounds do we think living things are living? We have some traditional criteria for defining what the living things are; "living things" have a boundary separating their internal entity from external environment, metabolism, and the ability of self-proliferation. The criteria might be helpful to distinguish the living things and non-living things. These criteria just rephrase common features obtained from the observations of what we see as "living things", and the criteria (might) never tell us why we see them as "living". For example, metabolism is just a collection of chemical reactions, and thus, we can easily reconstruct a part of metabolism in beakers. Also, if we place candles densely and ignite one of the candles, the candle fire will propagate and increase the number of fires. This phenomenon looks like the self-replication of fire, and there are chemical reactions in the candle fires corresponding to very simple metabolism. Still, it might be inherently different from the self-replication of living things[1].
We, human beings, have encountered such elusive phenomena and concepts, for example, the arrow of time and information, and have elucidated them by constructing quantitative theories. The arrow of time was, to some extent, understood by establishing the second law of thermodynamics, and also, information was defined, in the style of Shannon, as a quantity which helps to reduce the number of possible choices. The final goal of the author is to construct such quantitative theory (not epistemology) of living things which enables us to understand why we clearly distinguish the living things from non-living things as the second law of thermodynamics provides one explanation why does time seem to go forward.

[1] Of course, candle fires do not have the boundary, however, each candle separates each fire, and thus, at least we can distinguish each fire. While the role of the boundary is not only establishing individuality, to some extent, the propagation of candle fires is very similar to the life phenomenon if we judge this phenomenon pedantically based on the criteria.

To accomplish this purpose, we have to investigate the characteristic features what we think are the essences of living things. Thus, in this thesis we do not take an inductive approach, i.e. highlight what living things are by collecting the common features of them, but take a deductive approach. We focus on some features of living things obtained by observations and try to investigate the general consequence emerging from the features. Specifically, we focus on two themes; consequence of the autonomy to energetic property of cellular systems, and the growth laws in starved conditions.

The energetics of autonomous cellular growth

Cells generally take up substrates from the external environment and convert them into the ingredients for their growth and energy source for the self-maintenance. Needless to say, we know that cells cannot sustain their lives in the chemical equilibrium at which all chemical reactions are balanced, and thus, no energy is transducted thereby. In this sense, the constant consumption of chemicals through cellular metabolism makes cells possible to live. Then, it is natural to wonder the characteristics of this conversion process; how cells allocate the substrates to its growth and self-sustainment.
In thermodynamics conversion process is formulated by the Carnot engine. S. Carnot pointed out by studying the ideal model of engines that the process of converting the heat to mechanical work has an upper limit on efficiency represented by the temperature difference in the heat baths, and the engine reaches the upper bound by the quasi-static operation. Here, one may regard the cellular systems as the energy-conversion systems which convert the chemical potential of substrates into their growth and self-sustainment. On the other hand, the striking difference between Carnot-type engines and cells lies in an autonomous feature. Carnot-type engines never produce their components such as piston and cylinder, whereas, cells produce their components as a result of energy conversion. We expect that this autonomous feature leads to the distinct characteristic nature of energy conversion such as the efficiency of the process.

Phenomenological growth laws under slow growth conditions

I. Prigogine conceptualized living things by proposing "dissipative structure" [1]. He regarded living things as a consequence of the self-organization in non-equilibrium states. His idea paved the way to relate an emergence of living things to order-disorder transitions in non-equilibrium states and the bifurcation phenomena discussed in dynamical systems theory. The idea encouraged to bridge a gap between the researches for living things and non-living matters, but still, the idea is suspicious because many organisms can sustain their lives for a long time period even in the substrate-poor environments, while the ordinary dissipative structures cannot exist in a closed system or a low-flux conditions[2, 3, 4].
To focus on the nature of living things under low flux conditions, we study the stationary phase of bacteria. Bacteria typically show four distinct growth phases in batch culture conditions, namely, lag, exponential, stationary, and death phase.

In the exponential phase and death phase, the population of bacteria simply increases or decreases in time, respectively. On the other hand, in the stationary phase that appears in the lack of resources, the growth rate and death rate of the bacteria are strongly suppressed as if the bacteria are sleeping[2]. Thus, the stationary phase might be strikingly different from the exponential phase in which constant consumption of substrates supports the growth of bacteria allowing for the far-from-equilibrium condition that is assumed in dissipative structure.

1.1.2 Why Phenomenological Theory?

In this thesis, we study the characteristic nature of cells by using phenomenological models of cells, without details of precise metabolic processes for cellular growth such as Flux Balance Analysis[5] because we aim to construct the universal theory for cellular growth and energetics. For our purpose, such detailed models are not suitable because one of the main aims of the detailed models is to give quantitative predictions for cellular growth, and thus, the specific details for each species are significant, and universality in living systems takes a second place for such researches[2].
Since the cellular systems consist of complex systems of gene regulation and metabolism, the impact of phenomenological approach is naïvely suspicious. There are several successful phenomenological laws on the cellular growth, however, for example, Monod equation, Pirt's relation, and the relationship between the amount of ribosomal RNA and the growth rate[3, 6, 7]. Because of the simplicity of these laws, they do not always hold. Still, it is confirmed that they provide a reasonable model to understand the cellular physiology for certain conditions. What makes such simple, phenomenological laws possible? As an example, let us remember the movement of a ball under gravity. The equation of the motion of it with initial velocity $\mathbf{v}_0$ is given as $\dot{\mathbf{v}}(t) = -g\mathbf{e}_y, \mathbf{v}(0) = \mathbf{v}_0$, where g and $\mathbf{e}_y$ represent the gravitational acceleration and unit vector of the vertical axis, respectively. To predict the motion of the ball in extremely accurately, we have to include the effect of the shape of the ball, rotation, and friction with air, and so on. However, we know that in most cases, we can omit these "miscellaneous factors". In such condition, it is sufficient to assume the ball as a point mass, and gravity as only force imposed onto the ball. When can we model biological systems like this ball? Here, we briefly review some conditions which might make phenomenological approach reasonable.

[2]For example, we seek the universal theory which picks up the common features from E.coli to humans, however, even two different strains of E.coli have slightly different metabolic pathways and kinetic parameters, and this difference could result in different growth rate or other objective functions. Thus, the researchers cannot ignore such difference for the purpose of quantitative prediction.

0th-order kinetics

In this section, we review two mechanisms which lead to 0th-order reactions. When a certain reaction obtains the 0th-order dependency on certain substrates, the rate of chemical reaction is independent of their concentrations, and thus, it contributes to reducing the complexity of cellular metabolism.

Michaelis-Menten kinetics

Almost all chemical reactions occurring in cells are catalyzed by enzymatic proteins (we call them as "enzymes" hereafter). Enzyme usually forms a complex with its corresponding ligands first, and thereafter, converts it into the product and deforms the complex. Kinetics of such enzymatic reaction is known to follow Michaelis-Menten equation given as

$$\text{production rate} = v_{\max}\frac{[E][S]}{K+[S]},$$

where $[E]$ and $[S]$ represents the concentration of enzyme and substrate, respectively. $v_{\max}$ is the maximum production speed of product, and K is the dissociation constant.
A significant characteristic of the kinetics is that if the concentration of substrate is sufficiently larger than the dissociation constant ($K \ll [S]$), the kinetics turns to be the 0th order chemical reaction of the substrate. It makes the kinetics of chemical reaction simple.

Rate-Limiting substrates

There is another mechanism which leads to the 0th order chemical reaction against certain substrates. Let us introduce simple chemical reaction pathways composed of the elemental reactions described below (schematic representation of reactions is shown in Fig.1.1(a))

$$\begin{aligned} \emptyset &\rightarrow x, \\ \emptyset &\rightarrow y, \\ x+y &\rightarrow z, \\ x &\rightarrow \emptyset, \\ y &\rightarrow \emptyset, \\ z &\rightarrow \emptyset, \end{aligned}$$

where, molecular species x and y are supplied from the external environment (or other pathways), and also, chemicals x and y are spontaneously degraded with the rate ϕ. Produced z molecule is consumed with the rate v. Here, we study the dynamics of the consumption of z molecule. To clarify that 0th order sensitivity stems from a mechanisms different from Michaelis-Menten kinetics, we model all

chemical reactions by mass-action kinetics[3]. Then, the differential equations for the concentration of x, y, and z are given by

$$\begin{aligned}
\dot{[x]} &= J_x - [x][y] - \phi[x], \\
\dot{[y]} &= J_y - [x][y] - \phi[y], \\
\dot{[z]} &= [x][y] - v[z],
\end{aligned}$$

where J_x and J_y represent the supply rate of chemical x and y, respectively. ϕ and v are rate constants for spontaneous degradation of x and y, and consumption of z.

Fig.1.1.(b) and (c) show the consumption flux of z denoted by J as a function of J_x and J_y. Even though there is no trivial saturation effect caused by the Michaelis-Menten kinetics, J turns to be the 0th order reaction of J_x. This saturation effect simply stems from the lack of molecule y. As shown in Fig.1.1.(d), the steady concentration of y decreases in the order of magnitude at the point at which J saturates for each J_y value. At the steady state, production rate and consumption rate have to be balanced for each molecule. If we omit the spontaneous degradation of x and y for the simplicity[4], to $J = J_x$ and $J = J_y$ must hold in the steady state. This condition simply leads $J = \min\{J_x, J_y\}$, and for $J_x > J_y$, chemical y is the substrate that rate limits. Such condition for the balance of influx/efflux also leads to the insensitivity of certain reactions on the non-rate-limiting chemical species.

Growth rate as Global Constraint

There are $\sim 4,300$ proteins even in *E.Coli* cell[8]. Here, the cell state with all chemical concentrations including the concentrations of other metabolites is represented by the phase space of more than $4,300$-dimension. Then, it would be almost impossible for a simple model with just a few variables to successfully capture the nature of cells. However, a recent study revealed that the concentration of chemical species cannot change in this high-dimensioned space without restriction when the cell achieve stable growth[9]. Their dynamics are constrained by the volume growth of the cell.

To see this constraint, let us introduce the dynamics of chemical species inside cells in a general form. When we assume the chemical species are well-mixed, and thus, the spatial structure inside the cell can be omitted, the change in chemical concentrations is written as

$$\dot{x_i} = f_i(\mathbf{x}, \mathbf{y}) - \mu(\mathbf{x}, \mathbf{y}) x_i, \ (0 \leq i \leq N-1) \tag{1.1}$$

where $\mathbf{y}$ is the external parameters (for example the external concentration of substrates),x_i and f_i represent the concentration of ith chemical species, and its

[3]Mass-action kinetics is valid for non-enzymatic reactions, and also, enzymatic reactions under low-substrate concentration regime in which the concentration of substrates is sufficiently smaller than the dissociation constant.

[4]Since we set ϕ as sufficiently smaller than other parameters in the calculation of Fig.1.1, this assumption is valid.

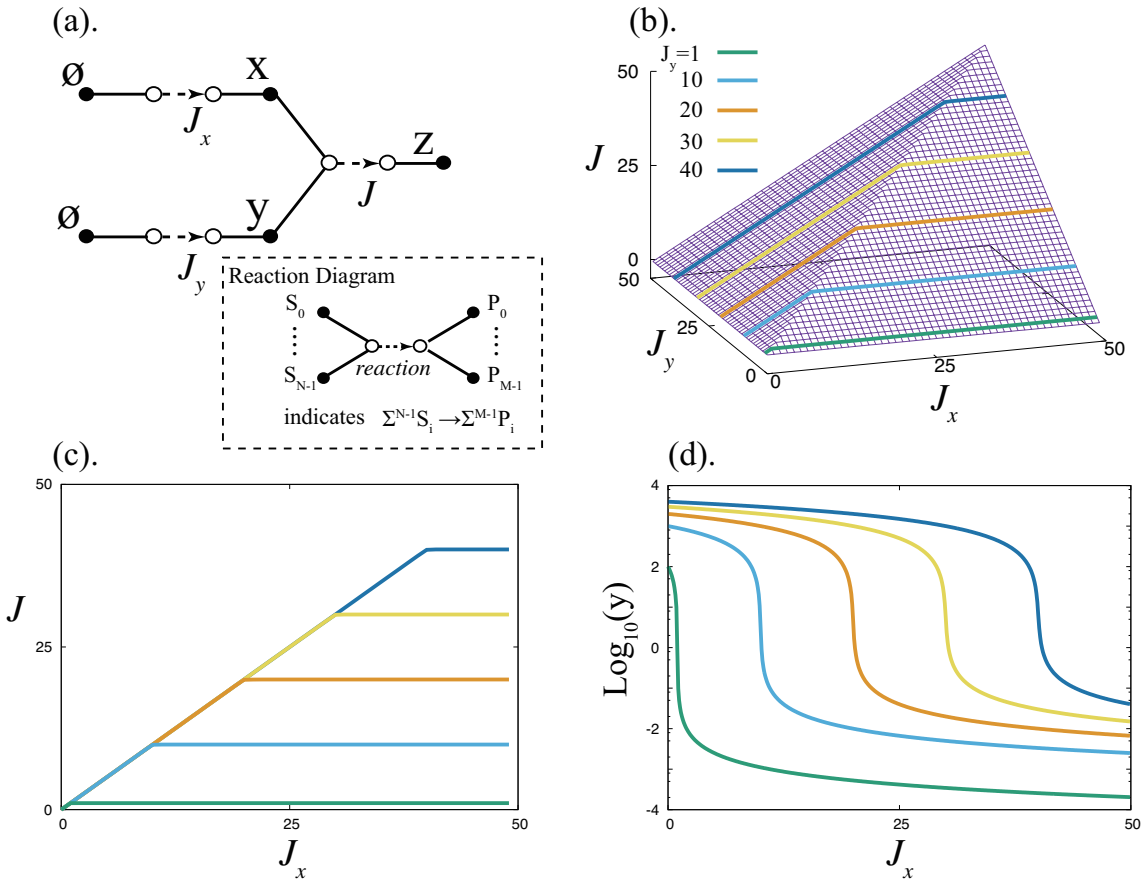

Figure 1.1: (a). Reaction diagram of our example. For the sake of visibility, the spontaneous degradation and consumption reactions are not depicted in the diagram. (b). Three-dimensional plot of the steady value of $J(J_x, J_y)$. Also, $J(J_x, J_y)$ values for several J_y values are overlaid as a function of J_x. (c). $J(J_x, J_y)$ values for several J_y values are plotted as functions of J_x. (d). Steady concentrations of $[y]$ are plotted as functions of J_x. Line with the same color has the same value of J_y among (b)-(d). Parameter values are set to be $\phi = 10^{-2}$ and $v = 1.0$.

change by all the collection of the chemical reactions including interactions between with environment, respectively. μ is the specific growth rate of the cell ($\mu = \frac{d}{dt} \ln V$ with V as the volume of the cell). The growth rate of the cell is determined by the rates of some chemical reactions and the concentrations of certain chemical species. Here, we perform variable transformation $X_i = \ln x_i$ with an assumption $x_i \neq 0$. Then we get

$$\dot{X}_i = F_i(\mathbf{X}, \mathbf{y}) - \mu(\mathbf{X}, \mathbf{y}), \ (0 \leq i \leq N-1),$$

where F_i is f_i/x_i. At the steady state, $\dot{X}_i = 0$ holds, which implies that the production rate of ith chemical species normalized by its steady concentration is equal to the specific growth rate μ for all i. If the steady concentration of ith chemical is twice the concentration of jth chemical, the production rate of ith chemical has to be twice of the production rate of j. It is the simplest constraint for a cell that doubles all chemical components without changing the compositional ratio of chemical species. Now, $F_0 = F_1 = \cdots = F_{N-1} = \mu$ holds, which imposes $N-1$ conditions to the steady state of N-dimensional dynamical system (Eq.(1.1)). This leads to a constraint on the change in chemical compositions.

1.1.3 Overview of this thesis

We first study the energetics of cellular growth in Chapter.2 and Chapter.3, and thereafter, we study the phenomenological laws of bacterial growth under substrate-poor conditions (or low-growth conditions) in Chapter.4 and Chapter.5.

Chapter.2 Energetic efficiency of cellular growth

Cells generally convert external nutrient resources to support metabolism and growth. Understanding the thermodynamic efficiency of this conversion is essential to determine the general characteristics of cellular growth. Using a simple protocell model with catalytic reaction dynamics to synthesize the necessary enzyme and membrane components from nutrients, the entropy production per unit-cell-volume growth is calculated analytically and numerically based on the rate equation for chemical kinetics and linear nonequilibrium thermodynamics. The minimal entropy production per unit-cell growth is found to be achieved at a nonzero nutrient uptake rate rather than at a quasistatic limit as in the standard Carnot engine. This difference appears because the equilibration mediated by the enzyme exists only within cells that grow through enzyme and membrane synthesis. Optimal nutrient uptake is also confirmed by protocell models with many chemical components synthesized through a catalytic reaction network. The possible relevance of the identified optimal uptake to optimal yield for cellular growth is also discussed.

Chapter.3 Efficient metabolic reaction facilitated by the temporal separation of anabolism and catabolism

Cells generally convert nutrient resources to products via energy transduction. Accordingly, the thermodynamic efficiency of this conversion process is one of

the most essential characteristics of living organisms. However, although these processes occur under conditions of dynamic metabolism, most studies of cellular thermodynamic efficiency have been restricted to examining steady states; thus, the relevance of dynamics to this efficiency has not yet been elucidated. Here, we develop a simple model of metabolic reactions with anabolism-catabolism coupling catalyzed by enzymes. Through application of external oscillation in the enzyme abundances, the thermodynamic efficiency of metabolism was found to be improved. This result is in strong contrast with that observed in the oscillatory input, in which the efficiency always decreased with oscillation. This improvement was effectively achieved by separating the anabolic and catabolic reactions, which tend to disequilibrate each other, and taking advantage of the temporal oscillations so that each of the antagonistic reactions could progress near equilibrium. In this case, anti-phase oscillation between the reaction flux and chemical affinity through oscillation of enzyme abundances is essential. This improvement was also confirmed in a model capable of generating autonomous oscillations in enzyme abundances. Finally, the possible relevance of the improvement in thermodynamic efficiency is discussed with respect to the potential for manipulation of metabolic oscillations in microorganisms.

Chapter.4 Phenomenological laws of lag phase and stationary phase

The quantitative characterization of bacterial growth has attracted substantial attention since Monod's pioneering study. Theoretical and experimental works have uncovered several laws for describing the exponential growth phase, in which the number of cells grows exponentially. However, microorganism growth also exhibits lag, stationary, and death phases under starvation conditions, in which cell growth is highly suppressed, for which quantitative laws or theories are markedly underdeveloped. In fact, the models commonly adopted for the exponential phase that consist of autocatalytic chemical components, including ribosomes, can only show exponential growth or decay in a population; thus, phases that halt growth are not realized. Here, we propose a simple, coarse-grained cell model that includes an extra class of macromolecular components in addition to the autocatalytic active components that facilitate cellular growth. These extra components form a complex with the active components to inhibit the catalytic process. Depending on the nutrient condition, the model exhibits typical transitions among the lag, exponential, stationary, and death phases. Furthermore, the lag time needed for growth recovery after starvation follows the square root of the starvation time and is inversely related to the maximal growth rate. This is in agreement with experimental observations, in which the length of time of cell starvation is memorized in the slow accumulation of molecules. Moreover, the lag time distributed among cells is skewed with a long time tail. If the starvation time is longer, an exponential tail appears, which is also consistent with experimental data. Our theory further predicts a strong dependence of lag time on the speed of substrate depletion, which can be tested experimentally. The present model and theoretical analysis provide universal growth laws beyond the exponential phase, offering insight into how cells halt growth without entering the death phase.

Chapter.5 Cell death induced by nutrient

In Chapter.4 , we constructed a model exhibiting three distinct phases, namely, active, inactive, and death phases, and found a law on the dependence of average lag time on the starvation time and maximum growth rate, and distribution form of lag time over cells, in agreement with experiments. Lag time of the model cell depends on the process of the starvation, but it does not show the dependence on the process of the substrate recovery. However, such dependence is experimentally known as sugar induced cell death (SICD). If the starved cell is incubated to the water or unusable carbon source medium, cells remain being starved. When a cell is incubated to the glucose medium without any other nutrient (i.e, without nitrogen source, inorganic substrates, and so on), however, the cell rapidly dies. In contrast, if the cell is incubated to the glucose medium with other non-carbon nutrient sources, it easily resurrects. Hence the cell death is triggered by glucose, the nutrient source

To study such problem, we introduced additional components into the previous model; energy currency molecules such as ATP and ADP. The model cell takes up two types of nutrients from the external environment. The first kind of substrate is used to produce macromolecules, and the second one is used for the conversion reaction from ADP to ATP. The model cell needs active form of energy currency molecules (ATP) to produce macromolecules and increase the fraction of the growth-facilitating component among the total macromolecules.

By computing the steady states and dynamics of this model cell, we found that the model cell had death attractor for all substrate conditions. The cells could be attracted to the death attractor depending on which substrate concentration was recovered first. SICD is explained accordingly from this model.

Chapter 2

Entropy production of a steady-growth cell with catalytic reactions

2.1 Introcution

A cell is a system that transforms nutrients into substrates for growth and division. By assuming that the nutrient flow from the outside of a cell is an energy and material source, the cell can be regarded as a system to transform energy and matter into cellular reproduction. It is important to thermodynamically study the efficiency of this transformation[10, 11, 12, 13, 14]. Regarding material transformation, the yield is defined as the molar concentration of nutrients (carbon sources) needed to synthesize a molar unit of biomass (cell content) and has been measured in several microbes [6, 15, 16, 17, 18]. As the conversion of nutrients to cell content is not perfect and material loss to the outside of a cell occurs as waste, the yield is generally lower than unity. The yield also changes with nutrient conditions, and measurements in several microbes show that the yield is maximized at a certain finite nutrient flow rate. The basic logic underlying the optimization of yield at a finite nutrient flow rate rather than at a quasi-static limit is not fully understood. A cell can also be regarded as a type of thermodynamic engine to transform nutrient energy into cell contents. It is necessary to study the thermodynamic efficiency or entropy production during the process of cell reproduction.The thermodynamic efficiency of metabolism has been measured in several microbes under several nutrientconditions[17, 19, 20, 21, 22, 23], and Westerhoff and others computed it by applying the phenomenological flow-force relationship of the linear thermodynamics to catabolism and anabolism [13, 13, 24] to show that the efficiency is optimal at a finite nutrient flow. Although such a phenomenological approach is important for technological application, a physiochemical approach is also necessary to highlight difference between cellular machinery and the Carnot engine by characterizing the basic thermodynamic properties in a simple protocell model. Indeed, when viewed as a thermodynamic engine, a cell has remarkable differences from the standard Carnot-cycle engine.

The cell sits in a single reservoir, without a need to switch contacts between different baths. The cell grows autonomously to reproduce. To consider the nature of such a system, it is necessary to establish the following three points distinguishing the cell from the standard Carnot engine [25].

First, cells contain catalysts (enzymes). The enzyme exists only within a compartmentalized cell encapsulated by a membrane and thus enables reactions to convert resources to intracellular components to occur within a reasonable time scale within a cell but not outside the cell. Without the catalyst, extensive time is required for the reaction. Thus, the reaction is regarded to occur only in the presence of the catalyst. This leads to an intriguing non-equilibrium situation: Let us consider the reaction $R+C \rightleftharpoons P+C$ with R as the resource, P as the product, and C as the catalyst. Then, under the existence of C, the system approaches an equilibrium concentration ratio with $[R]/[P] = \exp(-\beta(\mu_R - \mu_P))$ and μ_R and μ_P as the standard chemical potential of the resource and product, respectively, and with β as the inverse temperature. In contrast, outside the cell, R and P are disconnected by reactions within the normal time scale [1]; therefore, their concentration ratio can take on any value. In this sense, a cell can be regarded as a machinery which has ability to equilibrate extracellular environment.

Second, while considering the dynamical process, it is important to note that the catalysts are synthesized within the cell as a result of catalytic reactions. The time scale to approach equilibrium can depend on the abundance of the catalyst, which depends on the reaction dynamics themselves. Based on the first and second points mentioned above, the approach to equilibrium in the intracellular environment depends on catalyst abundance, which also depends on the flow rate of nutrients from outside the cell. Hence, the thermodynamic efficiency could show non-trivial dependence upon the nutrient flow.

Third, cell volume growth results from membrane synthesis from nutrient components, facilitated by the catalyst, whereas the concentrations of catalyst and nutrient are diluted by cell growth, which results in a non-standard factor for thermodynamic characteristics.

These three issues, which are fundamental to cell reproduction, are mutually connected and thus inherent to a self-reproducing, or autopoietic, system. In contrast to dynamical systems studies for self-reproduction in catalytic reaction networks [27, 28, 29, 30], however, the thermodynamic characteristics for such systems have not been fully explored.

On the other hand, there are extensive studies on thermodynamic efficiency for a system that operates at a nonequilibrium condition with a finite velocity, as well as the optimality on the power efficiency [31, 32, 33, 34], with some applications to molecular motors [35, 36]. However, the above three issues that are essential to reproducing cells are not discussed in the traditional thermodynamic context so far. In particular, with the encapsulated catalysts that exist only within a cell, reactions that do not exist at the outside of a cell can progress within a cell within

[1] Of course, if we wait for a huge amount of time, the reaction between R and P could occur ultimately, even without catalysts. However, the enzymes often facilitate the time scale of the order of 10^7 to 10^{19} [26], so that within the normal time scale we are concerned, the reaction can be regarded not to occur at the outside.

a normal time scale we are concerned. In the standard time scale, the equilibration is possible only within a cell, whose speed is facilitated by the enzymes which are produced as a result of the intra-cellular reactions. How this autonomous regulation of time scale together with the cell volume growth influences on the thermodynamic efficiency is the main concern of this chapter, which has not been investigated earlier.
In the present study, we determine these characteristics using simple reaction dynamics consisting of the nutrient, catalyst, and membrane. In Sec.2, we consider a simple protocell model consisting of a membrane precursor and catalyst under a given nutrient flow. The entropy production by chemical production per unit cell volume growth is shown to be minimized at a certain finite nutrient flow. The mechanism underlying this optimization is discussed in relation to the abovementioned three characteristics of a cell. The entropy production by material flow is discussed in Sec.2 and basically does not change the conclusion described above. A protocell model consisting of a variety of catalysts that form a network, together with nutrients and membrane precursors, has been investigated to confirm that the conclusion described above is not altered. The biological relevance of our results is discussed in Sec.3.

2.2 Entropy production of an autopoietic cell

2.2.1 Two-component model

First, we study the entropy production rate σ resulting from the intracellular reaction for the minimal protocell model consisting only of the synthesis of the enzyme and membrane precursor from the nutrient, which then leads to cellular growth [7, 16, 37, 38](see FIG.2.1 for schematic representation). The model consists of nutrient, membrane precursor, and enzyme, where the enzyme and membrane precursor are synthesized from the nutrient under catalysis by the enzyme. Moreover, by assuming that the diffusion constant of the nutrient is sufficiently large, the internal nutrient concentration is regarded to be equal to the external nutrient concentration. Based on the rate equation for chemical kinetics, our model is given by the following two-component ordinary differential equation

$$\begin{aligned} \frac{dx}{dt} &= \kappa_x x(kr - x) - x\lambda, \\ \frac{dy}{dt} &= \kappa_y x(lr - y) - \phi y - y\lambda. \end{aligned} \tag{2.1}$$

where the variables x and y denote the concentrations of the enzyme and membrane precursor, respectively, whereas $\lambda \equiv \frac{1}{V}\frac{dV}{dt}$ denotes the cell volume growth rate to be determined. Here, the first terms with κ in both the equations represent the change in the concentrations by the reaction $N \rightleftharpoons E$, and $N \rightleftharpoons M_p$, respectively, and the term ϕy is due to the consumption of the membrane precursor molecules to produce the membrane ($M_p \rightarrow$ Membrane), while the last terms represent the dilution of the concentrations of all chemical species due to the volume expansion with the rate λ. Here, the notation of parameters is as follows:

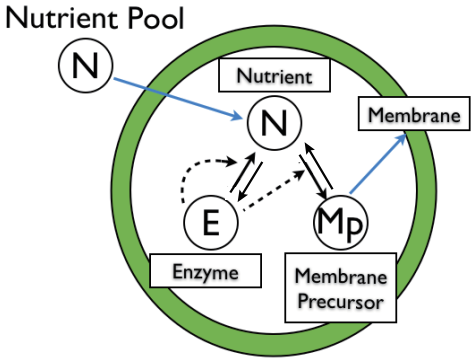

Figure 2.1: Schematic representation of our three-component protocell model. N, Mp, and E denote nutrient, membrane precursor, and enzyme, respectively. The nutrient is taken up from the extracellular nutrient pool by diffusion, indicated by a blue arrow. All chemical reactions, indicated by black solid arrows, are reversible and catalyzed by the enzyme, as indicated by dashed arrows. Membrane precursors are transformed to the membrane as indicated by the green ring with some leaks. The membrane growth results in an increase in cell volume.

- r : nutrient (i.e. resource) concentration
- $k = e^{-\beta(\mu_x - \mu_r)}$, $l = e^{-\beta(\mu_y - \mu_r)}$: the rate constant of each chemical reaction, with μ_r, μ_x and μ_y as the standard chemical potential of nutrient, x, and y, respectively.
- κ_i : catalytic capacity of the enzyme for i component $(i = x, y)$[2].
- ϕ : consumption rate of the membrane precursor to produce the membrane, such that the volume growth rate λ is given by $\lambda = \gamma\phi y$, where γ is the conversion rate from membrane molecules to cell volume.

In the stationary state, λ takes a positive constant value of $y > 0$ for $r > 0$ [3]. Thus, the protocell volume increases exponentially in time. Here, we define the entropy production rate per unit volume at this steady growth state as σ. In computing σ, spatial inhomogeneity is not considered through the assumption of local homogeneous equilibrium. Thus, the entropy produced during the doubling

[2]In other words, the forward and backward reaction rates are given by $\kappa_x k$ and κ_x, $\kappa_y \ell$, κ_y, respectively. We used the present parameterization, to separate the timescales of chemical reactions as represented as κ_i, $(i = x, y)$, from the ratios of forward to backward reactions that are given by the exponential of the free energy difference.

[3]In our model, another stationary solution $(x, y) = (0, 0)$ exists. However this solution is an unstable fixed point of the differential equation for $X > 0$.

in the cell volume is given by

$$\begin{aligned} S &= \int_0^T \int_{V(t)} \sigma \ dV dt, \\ &= \int_0^T V_0 e^{\lambda t} \sigma dt, \\ &= \frac{\sigma}{\lambda} V_0. \end{aligned} \tag{2.2}$$

where V_0 is the initial cell volume and T is doubling time of the cell [4].
We denote $\eta \equiv \sigma/\lambda$ as the entropy production per unit cell-volume growth. Generally, if η is smaller, the thermodynamic efficiency for a cell growth is higher. For larger η, more energetic loss occurs in the reaction process. Hereafter, we study the dependence of η on the nutrient condition and the growth rate λ.
In this subsection, we consider only the entropy production by the chemical reaction; the entropy production by the flow of chemicals from the outside of the cell will be considered in the next section. The calculation of entropy production rate among different components is performed by virtually introducing chemical baths for different components that are mutually in disequilibrium and then applying linear non-equilibrium thermodynamics for calculation. This may result in stringent requisites; however, this step is adopted to address the thermodynamic efficiency of a cell with growth, as general steady-state thermodynamics are not established currently.
Then, the entropy production rate by the reactions is given by $\sigma = \sum_i J_i \frac{A_i}{T}$, where J_i is the chemical flow and A_i is the affinity for each reaction. Here we set $T = 1$ without losing generality.
For calculation, we assume that κ_x and κ_y are identical for simplicity, denoted as κ. Then, by rescaling the variables as

$$\begin{aligned} \tilde{x} &= x\gamma, \quad \tilde{y} = y\gamma, \\ \tilde{r} &= lr\gamma, \quad \tau = t\phi. \end{aligned} \tag{2.3}$$

Eq.(2.1) is written as

$$\begin{aligned} \frac{d\tilde{x}}{d\tau} &= \tilde{\kappa}\tilde{x}(\tilde{k}\tilde{r} - \tilde{x}) - \tilde{x}\tilde{y}, \\ \frac{d\tilde{y}}{d\tau} &= \tilde{\kappa}\tilde{x}(\tilde{r} - \tilde{y}) - \tilde{y} - \tilde{y}^2, \end{aligned} \tag{2.4}$$

where $\tilde{\kappa} = \frac{\kappa}{\phi\gamma}$ and $\tilde{k} = k/l$. The stationary solution of the equation for $\tilde{\kappa} = 1$ is given by

$$\tilde{x} = \frac{\tilde{k}\tilde{r}(1 + \tilde{k}\tilde{r})}{1 + \tilde{r} + \tilde{k}\tilde{r}}, \qquad \tilde{y} = \frac{\tilde{k}\tilde{r}^2}{1 + \tilde{r} + \tilde{k}\tilde{r}}.$$

[4]This is nothing but the relationship between the total entropy production through cell reproduction and the entropy production per time and volume. Specific contribution of material flow, cell volume growth, and reactions to the entropy roduction rate σ will be analyzed below.

Following this assumption, the entropy production rate by chemical reaction σ at the stationary state is calculated as $\sigma = \sigma_x + \sigma_y$ with $\sigma_i = J_i \frac{A_i}{T}$ for the enzymatic reaction $i = x$ and for the membrane reaction $i = y$. Here, the flows are given by $\tilde{J}_x = \tilde{\kappa}\tilde{x}(\tilde{k}\tilde{r} - \tilde{x})$ and $\tilde{J}_y = \tilde{\kappa}\tilde{x}(\tilde{r} - \tilde{y})$, whereas the affinities are given by $A_x = T\ln(\tilde{k}\tilde{r}/\tilde{x})$ and $A_y = T\ln(\tilde{r}/\tilde{y})$. We omit the tilde for affinities because the affinities are not affected by scale transformation. Therefore, we obtain

$$\tilde{\sigma} \;=\; \tilde{\kappa}\tilde{x}(\tilde{k}\tilde{r} - \tilde{x})\ln(\tilde{k}\tilde{r}/\tilde{x}) + \tilde{\kappa}\tilde{x}(\tilde{r} - \tilde{y})\ln(\tilde{r}/\tilde{y}).$$

The dependence of $\tilde{\eta} \equiv \tilde{\sigma}/\tilde{y} = \gamma\eta$ upon $\tilde{k}$ and $\tilde{r}$, thus obtained, is plotted in FIG.2.2 for $\tilde{\kappa} = 1$. As shown, the entropy production per unit growth shows a non-monotonic dependence on the nutrient concentration and is minimized at a non-zero nutrient concentration. Because nutrient uptake rate is a monotonic function of nutrient concentration, this result means that the entropy production per unit growth η is minimal at a finite nutrient uptake rate. This result is in strong contrast with the thermal engine, where the entropy production is minimal at a quasi-static limit. FIG.2.3(a),(b) shows the entropy production per unit

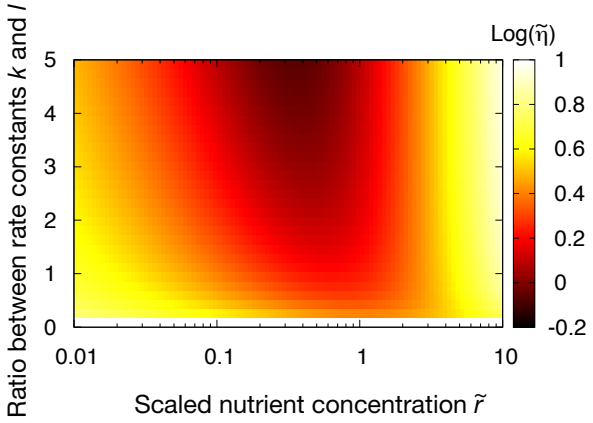

Figure 2.2: The logarithm of $\tilde{\eta}$ plotted as a function of scaled nutrient concentration $\tilde{r}$ and $\tilde{k} = k/l$, the ratio between two rate constants, with the color code given in the side bar. It is calculated from the solutions of Eq.(2.4). The parameter $\tilde{\kappa}$ is chosen to be 1.0. For given $\tilde{k}$, there is an optimal nutrient concentration that gives the minimum $\tilde{\eta}$.

growth $\sigma_x/\lambda, \sigma_y/\lambda$ for each reaction which produces component x and y, respectively. This shows that the non-monotonic dependence on the nutrient in FIG.2.2 is attributable to σ_y/λ. As mentioned above, an important characteristic of cells is that intracellular reactions are facilitated by enzymes that are autonomously synthesized. Thus, the equilibrium distribution of chemicals in the presence of enzymes is different from the external chemical distribution. The decrease in η under low nutrient concentrations is explained accordingly: The extracellular concentrations of the nutrient and of the membrane precursor are far from equilibrium in the presence of catalysts. Therefore, their intracellular concentrations under conditions of low nutrient uptake remain far from equilibrium and still similar to the

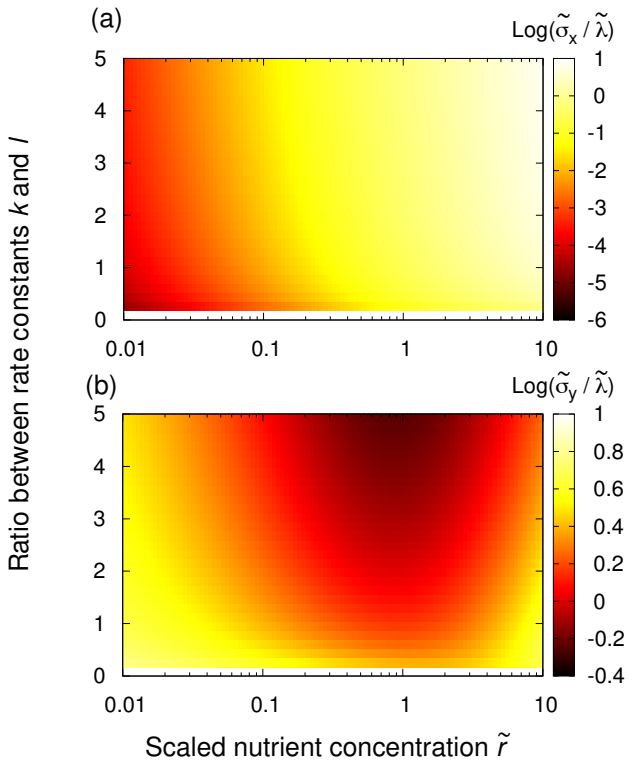

Figure 2.3: The logarithm of the rescaled entropy production rate per unit rescaled growth rate $\tilde{\sigma_x}/\tilde{\lambda}$ and $\tilde{\sigma_y}/\tilde{\lambda}$ for the enzyme and membrane precursor synthesis reactions, respectively, plotted as a function of the rescaled nutrient concentration $\tilde{r}$ and the ratio between rate constants $\tilde{k}$, computed by Eq.(2.4). (a). $\tilde{\sigma_x}/\tilde{\lambda}$ for the enzyme producing reaction and (b) $\tilde{\sigma_y}/\tilde{\lambda}$ for the membrane precursor producing reaction.

external concentrations because of insufficiency of the enzyme. However, when the amount of nutrient uptake increases, the amount of enzyme increases and the system approaches intracellular equilibrium; therefore, the entropy production per unit growth decreases.
In contrast, with further increases in nutrient uptake, the entropy production rate increases as a result of the increase in cellular growth; entropy production rate $\sigma = \sum_i J_i \frac{A_i}{T}$ by the reaction increases linearly with the reaction speed J_i. In the steady state, the reaction speed J_i is roughly estimated by λp_i, with p_i as the concentration of the product of the ith reaction, because the dilution due to cell volume expansion and production of chemical reaction should be balanced. For example, the dynamics of the enzyme concentration are given by $\frac{dx}{dt} = x(kr-x)-\lambda x$. At steady state, the enzyme production rate $x(kr - x)$ is balanced with λx according to Eq.(2.1). Thus, σ_x increases with λx. In summary, for a cell with a high growth rate, increased enzyme abundance is needed, which, however, leads to higher entropy production rate [5].
In contrast, if the enzyme concentration is fixed externally, the entropy production per unit growth η is minimized at the zero limit of nutrient concentration. In this case, the reaction dynamics Eq.(2.1) are reduced to

$$\frac{dy}{dt} = c(lr - y) - \phi y - \phi y^2. \tag{2.5}$$

where c is a constant representing the concentration of the enzyme. In this case, the stationary solution is given by $y = \frac{1}{2}[\ -(1 + c/\phi) + \sqrt{(1 + (c\phi)^2) + 4clr/\phi}\ ]$, and accordingly $\eta^{-1} = (1+y)\ln(lr/y)$. There is no optimal nutrient concentration in this expression because $\frac{\partial \eta^{-1}}{\partial r}$ is always positive for any $r, l > 0$. This is consistent with the explanation mentioned above for Eq.(2.4). If the enzyme abundance is fixed to be independent of the nutrient uptake, the speed of approaching equilibrium is not altered by the nutrient condition; therefore, the entropy production just increases monotonically because of the cell volume growth.

2.2.2 Additional entropy production by material flow

Thus far, we considered only entropy production by chemical reactions. In addition, the material flow also contributes to entropy production, which is taken into account here.
To discuss the flow of nutrients, the dynamics of the nutrient concentration cannot be neglected. By including the temporal evolution of the nutrient concentration,

[5] For membrane production in Eq.(2.1), $(\phi+\lambda)y$ balances with the synthesis of the membrane precursor, but the tendency does not change. The increase of entropy production rate with λ mentioned above does not mean that the factor λ would totally be canceled with the factor σ in Eq.(2.2). The intra-cellular state concentrations of chemicals depend on λ, so that σ/λ has further dependence on λ.

the dynamics of the cellular state are given by

$$\begin{aligned}
\frac{dr}{dt} &= -\kappa_x x(kr - x) - \kappa_y x(lr - y) \\
&- r\lambda + D(r_{\rm ext} - r), \\
\frac{dx}{dt} &= \kappa_x x(kr - x) - x\lambda, \\
\frac{dy}{dt} &= \kappa_y x(lr - y) - \phi y - y\lambda.
\end{aligned} \tag{2.6}$$

where x, y and r are the enzyme, membrane precursor, and nutrient concentration, respectively, and $\lambda = \frac{1}{V}\frac{dV}{dt} = \gamma\phi y$. The rate constants k and l are determined by the standard chemical potential of each chemical. Additionally, the nutrient is taken up with rate D from the extracellular environment with a concentration $r_{\rm ext}$.

Entropy production by chemical flow is derived from nutrient uptake and membrane consumption, which (again by assuming linear nonequilibrium thermodynamics) are given by $\vec{J_r} \cdot \nabla(-\mu_r/T)$ and $\vec{J_y} \cdot \nabla(-\mu_y/T)$, respectively, where $\vec{J_i}$ is the material flow of component i and μ is the chemical potential. Integration of the terms with the spatial gradient over a space results in $D(r_{ext} - r)\frac{r_{ext}-r}{r}/T$ and $\phi y/T$ [6].We neglect the entropy production of the solvent with the assumption that intra- and extracellular solvent concentrations are identical [7]. The contribution of dilution of the nutrient resulting from cellular growth is approximated as $\sigma_{d,r} \approx r\lambda$ by using the formula of entropy change resulting from the isothermal expansion of an ideal solution [8]; for other species, we use the same formula.

We choose that $\kappa_x, \kappa_y, D, \gamma$ and ϕ are equal to unity and that $l = k$, for the sake of simplicity. Indeed, the characteristic behavior of η is independent of this choice. Then, the fixed-point solutions of Eq.(2.6) are obtained against two parameters k and $r_{\rm ext}$. From the solution, the entropy production per unit growth is computed, as shown in FIG.2.4(a). We note that here again the minimal η is achieved for a finite nutrient uptake, i.e., under nonequilibrium chemical flow. In FIG.2.4(b),

[6]The entropy production rate of material flow under a one-dimensional gradient of chemical concentration $u_i(x)$ (of the spcies i at the position x) is estimated as follows; $\int_a^b J_i(x)\frac{d}{dx}(-\mu_i(x)/T)dx \approx \int_a^b D_i(u_i(b) - u_i(a))\Big(\frac{u_i(b)-u_i(a)}{(b-a)u_i(a)}\Big)\frac{dx}{T} = \frac{D_i}{T}\frac{(u_i(b)-u_i(a))^2}{u_i(a)}$, by assuming that $b - a$ is small. To neglect possible correction by the spatial inhomogeneity on the entropy production by reaction, it might be necessary to assume that the spatial gradient is restricted at round the membrane, and not extends through the cells, while this correction would be smaller.

[7]The extracellular membrane concentration is assumed to be zero in our model; Eq.(2.1), we adopted entropy production rate of membrane consumption as a diffusion process.

[8]Entropy production during isothermal expansion of an ideal solution from the initial volume V_i to a terminal volume V_t is $\Delta S = \ln(V_t/V_i)$ per unit mole. Because λ is the volume expansion rate in this context and $V_t = V_i + \lambda\Delta t$, the change in entropy density is written as $\Delta s_v = \ln(1 + \lambda\Delta t)$ per unit mole. The approximated formula is obtained by expanding $\ln(1 + \lambda\Delta t)$ into the Taylor series and taking the limit of Δt to zero. Of course, $\frac{\Delta s_v}{\Delta t}$, entropy change per unit time of the system, is generally different from the entropy production rates because there is increase in the entropy due to the heat flow from the environment, so that the entropy production by the expansion can be smaller. At any rate, the above Δs_v is smaller than the other entropy production terms, and the estimate here is not essential to our result.

we plotted η_{flow}, the entropy production excluding that derived from the chemical reaction. It increases monotonically with the external nutrient concentration. Entropy production is primarily derived from chemical reactions; therefore, the conclusion of subsection A is unchanged.
Note that the so-called thermodynamic efficiency is defined as $\eta_{th} = -\frac{J_a \Delta G_a}{J_c \Delta G_c}$ where J_c and J_a are the rates of catabolism and anabolism, and ΔG_c and ΔG_a are the affinities of catabolism and anabolism [13, 19]. Here, the optimality with regard to entropy production η also leads to the optimal thermodynamic efficiency, which, in the present case, is computed by $\eta_{th} = \frac{J_y \mu_y}{J_r \mu_r}$ where $J_r = D(r_{ext} - r)$ and $J_y = \phi y$ are the absolute values of the uptake (and consumption) flow of chemical species r (and y), and μ_i is the chemical potential of the ith chemical species. It is computed by using the chemical potential of nutrient $\mu_r = {\mu^0}_r + T \ln(r/r_0)$ with ${\mu^0}_r$ as the standard chemical potential for the nutrient and r_0 as its standard concentration (The chemical potential for x and y are computed in the same way). This thermodynamic efficiency also takes a local maximum value at a non-zero nutrient uptake rate (see FIG.2.5).

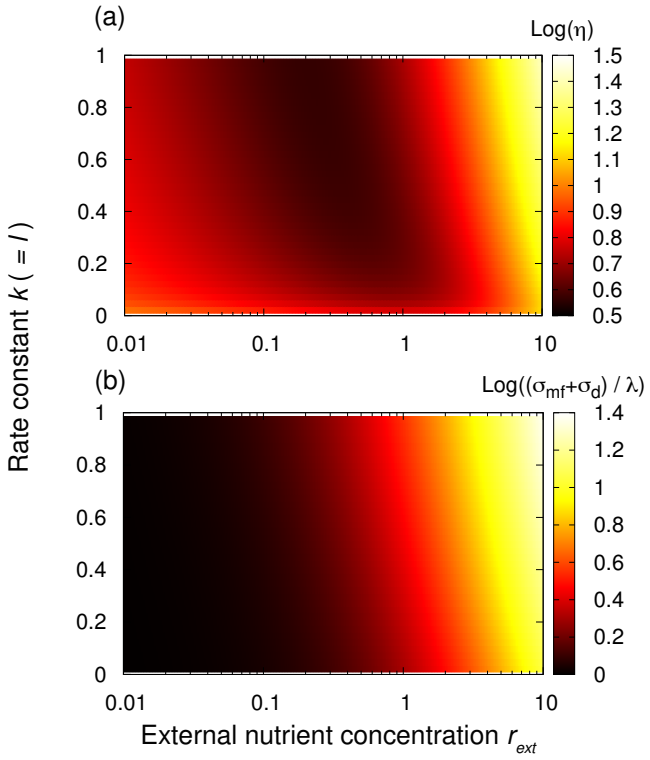

Figure 2.4: The entropy production plotted as a function of the external nutrient concentration r_{ext} and the rate constant $k(= l)$, calculated from the fixed-point solution of Eq.(2.6); (a) the logarithm of total entropy production per unit cell growth, η; and (b) the logarithm of the entropy production per unit growth by material flow (σ_{mf}/λ) and dilution (σ_d/λ) only. The parameters are chosen to be $\kappa_x = 1.0,\ \kappa_y = 1.0,\ D = 1.0,\ \phi = 1.0,\ \gamma = 1.0$, and $l = k$.

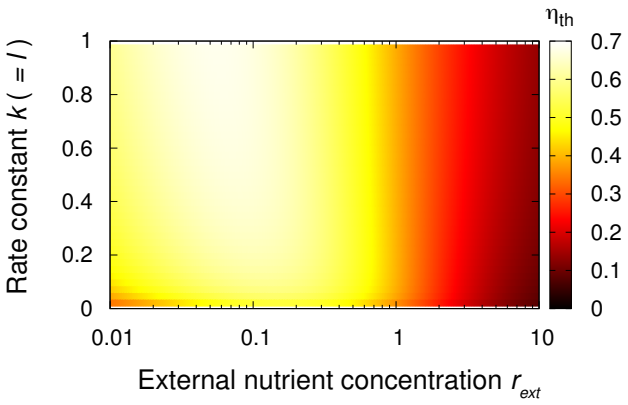

Figure 2.5: The thermodynamic efficiency for the model Eq.(2.6) plotted as a function of the external nutrient concentration r_{ext} and the rate constant $k(= l)$. The parameters were set as $\mu_r = 0.0$, $D = 1.0$, $\phi = 1.0$, $\gamma = 1.0$ and $\kappa_x = \kappa_y = 1.0$. The standard concentrations were chosen to be 10^{-8}.

2.3 Extension to a multi-component model

It is worthwhile to check the generality of our result for a system with a large number of chemical species as in the present cell. For this purpose, we introduce a model given by

$$\begin{aligned}
\frac{dx_1}{dt} &= \sum_{j=1}^{N}\sum_{k=2}^{N-1}(C(1,j;k)k_{1j}x_j - C(j,1;k)k_{j1}x_1)x_k \\
&+ (X_1 - x_1) - x_1\lambda, \\
\frac{dx_i}{dt} &= \sum_{j=1}^{N}\sum_{k=2}^{N-1}(C(i,j;k)k_{ij}x_j - C(j,i;k)k_{ji}x_i)x_k \\
&- x_i\lambda, \quad (1 < i < N-1), \\
\frac{dx_N}{dt} &= \sum_{j=1}^{N}\sum_{k=2}^{N-1}(C(N,j;k)k_{Nj}x_j - C(j,N;k)k_{jN}x_N)x_k \\
&- \phi x_N - x_N\lambda, \\
\lambda &= x_N.
\end{aligned} \tag{2.7}$$

where the variables x_1, x_N, and x_i $(1 < i < N)$ denote the concentrations of the nutrient, membrane precursor, and enzymes, respectively, and X_1 is the external concentration of the nutrient. Each element of the reaction tensor $C(i,j;k)$ is unity if the reaction of j to i catalyzed by k exists; otherwise, it is set to zero. Here, the nutrient and the membrane precursor cannot catalyze any reaction, whereas the other components $i = 2, ..N-1$ form a catalytic reaction network [28, 39, 40, 41]. All chemical reactions are reversible in our model; therefore $C(i,j;k)$ is equal to unity if and only if $C(j,i;k)$ equals unity. For the sake of simplicity, we assume

that catalytic capacity, nutrient uptake rate, membrane precursor consumption rate, and the conversion rate from membrane molecule to cell volume are unity. The standard chemical potential μ_i for each chemical species is assigned by uniform random numbers within $[0, 1]$, whereas k_{ij} is given by $\min\{1, \exp(-\beta(\mu_i - \mu_j))\}$ accordingly [40].
Numerical simulations reveal that there again exists an optimal point of η for each randomly generated reaction network of $N = 100$. The dependence of η on the nutrient concentration is plotted in FIG.2.6(a), overlaid for different networks. Although the nutrient concentration to give the optimal value is network-dependent, it always exists at a finite nutrient concentration; therefore, the entropy production is minimized at a non-zero nutrient concentration. To determine a possible relationship with the optimality of η and equilibrium in the presence of a catalyst We also computed the Kullback-Leibler (KL) divergence of the steady state distribution from the equilibrium Boltzmann distribution [25] as a function of the external nutrient concentration, expressed as

$$D_{KL}(\mathbf{p}||\mathbf{q}) = \sum_{i=1}^{N} p_i \ln \frac{p_i}{q_i}. \tag{2.8}$$

where p_i and q_i are $p_i = e^{-\mu_i}/(\sum_j e^{-\mu_j})$ and $q_i = {x^{st}}_i/(\sum_j {x^{st}}_j)$, respectively (${x^{st}}_i$ is the concentration of the i th chemical species in the steady state.) The KL divergence for each network shows non-monotonic behavior, as shown in FIG.2.6(b). Although the optimal nutrient concentration does not agree with the optimum for η, each KL divergence decreases in the region where η is reduced. In this sense, it is suggested that the reduction of η in our model Eq.(2.7) is related to the equilibration process of abundant enzymes synthesized as a result of a relatively high rate of nutrient uptake as discussed for Eq.(2.1) and Eq.(2.6).

2.4 Summary and Discussion

To discuss the thermodynamic nature of a reproducing cell, we have studied simple protocell models in which nutrients are diffused from the extracellular environment and necessary enzymes for the intracellular reactions are synthesized to facilitate chemical reactions, including the synthesis of membrane components, which leads to the growth of cell volume. In the models, cell growth is achieved through nutrient consumption by the reactions described above. We computed η, which is the entropy production per unit cell volume growth and found that the value was minimized at a certain nutrient uptake rate. This optimization stems from the constraint that cells have to synthesize enzymes to facilitate chemical reactions, i.e., the autopoietic nature of cells. In general, the concentrations of nutrients and membrane components in extracellular environments are different from those in equilibrium achieved in the presence of enzymes, and the intracellular state moves towards equilibrium by synthesizing enzymes to increase the speed of chemical reactions. The equilibration reduces the entropy per unit chemical reaction. However, faster cell volume growth leads to a higher dilution of chemicals; therefore,

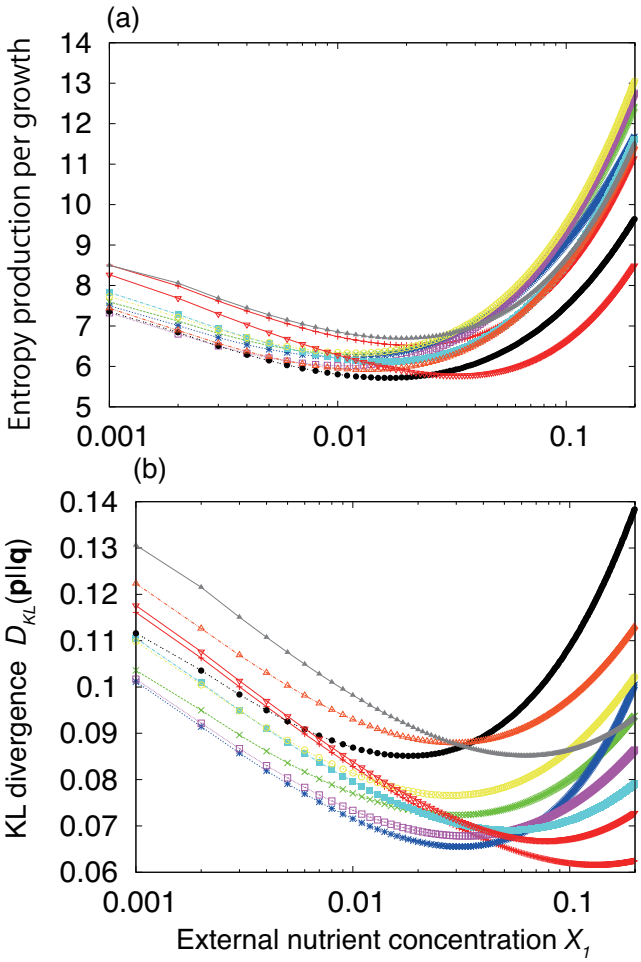

Figure 2.6: The entropy production and deviation from equilibrium calculated from the steady-state solution of the multi-component model Eq.(2.7), plotted as a function of the external nutrient concentration. The results of 10 randomly generated networks are overlaid. (a)η ; entropy production rate per growth rate, and (b)Kullback-Leibler divergence of the steady-state distribution from the Boltzmann distribution defined in Eq.(2.8). The number of chemical species is set as 100, whereas the parameter ϕ is chosen to be unity, and the ratio of the average number of reactions to the number of chemical species is set to 3.

faster chemical reactions are required to maintain the steady-state concentration of chemicals. Because entropy production rate by the reaction increases (roughly linearly) with the frequency of net chemical reactions, η then increases for a higher growth range. Thus, the existence of an optimal nutrient content is explained by the requirement for reproduction mentioned in the introduction, i.e., equilibration of non-equilibrium environmental conditions facilitated by the enzyme, autocatalytic processes to synthesize the enzyme, and cell-volume increase resulting from membrane synthesis.

In the present model, all chemical components thus synthesized are not decomposed; they are only diluted. However, each component generally has a specific decomposition time or deactivation time as a catalyst. We can include these decomposition rates, which can also be regarded as diffusion to the extracellular environment with a null concentration. Then, the equilibration effect is clearer, although the results regarding optimal nutrient uptake are unchanged.

Note that in the present cell model, there is only a single stationary state, given the external condition. In a complex reaction system as in the present cell, there can be multiple stationary states, with different growth rates and the selection process among them is also important [42, 43]. Comparison of thermodynamic efficiency among different states will be also important [9].

In the present study, we focused on the case with a single entropy production that corresponds to dissipated energy per unit growth. In microbial biology, however, material loss is discussed as biological yield, as mentioned in the introduction, and it is thus reported that the optimal yield is achieved at a certain finite nutrient flow. Material loss is not directly included in the present model; therefore, we cannot discuss the yield derived directly from entropy production. However, it may be possible to assume that energy dissipation is correlated with material dissipation. For example, the stoichiometry of metabolism is suggested to depend on dissipated energy [46]. Here, metabolism consists of two distinct parts: catabolism and anabolism. For catabolism, the energy is transported through energy currency molecules such as ATP, NADPH, and GTP, which are synthesized from the nutrient molecule. In this process, molecular decomposition also occurs, leading to the loss of nutrient molecules. In addition, the abundance of energy-currency molecules and the utilized energy are correlated. Hence, for both catabolism and anabolism, the energy dissipation and material loss are expected to be correlated. Indeed, a linear relationship between the yield and the inverse of thermodynamic loss (i.e., quantity similar to $1/\eta$ here) is suggested from microbial experiments [46, 47].

Considering the correlation between energy and matter, the minimal entropy production at a finite nutrient flow that we have shown here may provide an explanation for the finding of optimal yield at a finite nutrient flow. Future studies should examine the relationship between minimal entropy production and optimal yield in the future by choosing an appropriate model that includes ATP synthesis and waste products in a cell. Currently, although our models are too simple to capture

[9] There is no reason that a state with smaller entropy production is selected, and in contrast, there are proposals that a maximal one are selected [44, 45].

such complex biochemistry in a cell, they should initiate discussion regarding the thermodynamics of cellular growth.

Chapter 3

Enzyme oscillation can enhance the thermodynamic efficiency of cellular metabolism: consequence of anti-phase coupling between reaction flux and affinity

3.1 Introduction

Cells uptake external nutrients from energy sources and transform them into all of the components required for growth, maintenance, and survival, such as the cell membrane and catalysts. The efficiency of these reaction processes, collectively referred to as "metabolism", is an important factor for the fitness of a cell. Given that intracellular reactions are catalysed by enzymes, the efficiency of such reactions also depends on the enzyme concentrations and their dynamics. Therefore, as cells regulate enzyme concentrations through protein expression dynamics, the potential relationship between metabolic efficiency and enzyme dynamics is an important issue warranting investigation [48, 49].

Although enzymes cannot alter the equilibrium condition itself [50], they do change the speed of chemical reactions drastically. Indeed, enzymes generally facilitate chemical reactions in the order of 10^7 to 10^{19} [26], and many reactions within a cell could be almost completely halted by reducing the amount of the corresponding enzyme. In general, the relaxation process to equilibrium is controlled by the enzyme abundances, and thus so is the time scale for the metabolic reactions.

Furthermore, the abundance of each enzyme can change autonomously over time within a cell. Hence, together with the external flow that maintains the system out of equilibrium, the internal time scales are changed autonomously. In this sense, a cell is regarded as a machine with autonomous changes in time scale that functions in transforming nutrients into useful products via energy transduction [49, 51, 52, 53, 54, 55]. Although there are extensive studies on thermodynamic

nature for a non-autonomous system that operates at a non-equilibrium condition with a finite velocity [31, 32, 33, 56], to date, the characteristic nature of such autonomous machinery has not been studied in the context of non-equilibrium chemical thermodynamics. Hence, investigations of the thermodynamic nature of dynamic metabolic processes are not only important to resolve basic questions in cellular biophysics but can also provide insight for non-equilibrium physics.

Metabolic processes can be generally classified into anabolism and catabolism. The former is a synthesis process of biomolecules from nutrients, which typically involves consumption of energy by transforming ATP to ADP, whereas the latter involves decomposition of nutrients into smaller molecules, and consequently releases energy with a change from ADP to ATP. Through this metabolism, chemical resources are transformed into products along with the energy transduction between ATP and ADP. The thermodynamic efficiency of such energy transduction processes has been extensively studied [13, 17, 19, 21, 24, 57, 58, 59, 60]. However, so far, these studies have primarily focused on the behaviours in the steady state, without consideration of the time-dependent dynamics in the reaction flux and concentrations of enzymes and substrates.

In contrast, there are a variety of time-dependent (non-steady) processes in cellular metabolism, such as those observed in the cell cycle [61, 62], cyclic AMP signaling [63], circadian rhythms [64, 65] glycolytic oscillation [66, 67, 68, 69, 70, 71, 72, 73], and yeast metabolic cycle (YMC) [74, 75, 76, 77, 78]. The enzyme concentrations change in time during these dynamic processes, which then alters the time scale of the reaction processes, as mentioned above. Thus, it is important to study the characteristics of such "dynamic" processes of cellular metabolism, and uncover the potential influence of the cyclic process on the thermodynamic efficiency of the metabolic processes.

Toward this end, we here introduce a simple model of coupled anabolic and catabolic reactions, each of which is catalysed by a corresponding enzyme and uses typical energy currency molecules (ATP and ADP). In particular, we demonstrate that temporal changes in enzyme concentrations are required to achieve higher thermodynamic efficiency under the condition in which available enzymes are limited.

In Section 2, the Nutrient, Waste, Substrate, Product (NWSP) model is described and implemented by applying periodic oscillations of the abundances of enzymes for anabolism and catabolism. This model showed improved thermodynamic efficiency compared to the steady-state condition. This result was then extended to the case with autonomous oscillations resulting from internal catalytic reaction dynamics, which confirmed the relevance of oscillation in enzyme abundances for thermodynamic efficiency. The observed increase in the efficiency due to the oscillation in enzyme abundances is in strong contrast with the general condition of a decrease in thermodynamic efficiency due to oscillatory inputs. In Section 3, we discuss the biological relevance of these results for the dynamic control of enzyme abundances.

3.2 NWSP Model

Here, we introduce a simple model for a metabolic process consisting of anabolism and catabolism, by extending the model introduced by Westerhoff et al.[13, 17]. In the Westerhoff model, anabolism (process for the synthesis of biomolecules) and catabolism (process for the digestion of nutrients) are analysed using linear non-equilibrium thermodynamics, in which the deviation from chemical equilibrium is assumed to be small, and the steady chemical reaction flow and thermodynamic force (affinity) are proportional [79]. To incorporate oscillatory dynamics, we extended this model so that the chemical concentrations change according to the rate equation of the chemical reactions. Specifically, our model consists of four chemical species, i.e., Nutrient, Waste, Substrate, and Product, in addition to the energy currency molecules ATP and ADP, and involves two catalytic enzymes for anabolism and catabolism, E_a and E_c, respectively. The catabolic reaction decomposes nutrients to waste with the aid of the catalyst E_c, simultaneously transforming ADP into ATP, whereas the anabolism reaction synthesizes a product from a substrate with the aid of E_a, by consuming energy with the change from ATP to ADP. As a consequence of the coupled reactions of catabolism and anabolism, the product is synthesised from a substrate by consuming a nutrient. If the enzyme concentrations are constant, there is a steady flow generated from nutrient and substrate to waste and product, depending on the concentrations of the chemical spoecies, as in the Westerhoff model. Here, we introduce a periodic change in the concentration of each enzyme, and study the effect of this temporal change in enzyme concentrations on the thermodynamic efficiency of this metabolism. Thus, to reflect all of these reaction dynamics, our model is given by

$$
\begin{aligned}
\frac{d[\mathrm{Nutrient}]}{dt} &= -J_c + \Big([\mathrm{Nutrient}]_{\mathrm{ext}} - [\mathrm{Nutrient}]\Big) \\
\frac{d[\mathrm{Waste}]}{dt} &= J_c + \Big([\mathrm{Waste}]_{\mathrm{ext}} - [\mathrm{Waste}]\Big) \\
\frac{d[\mathrm{Prod}]}{dt} &= -J_a + \Big([\mathrm{Prod}]_{\mathrm{ext}} - [\mathrm{Prod}]\Big) \\
\frac{d[\mathrm{Subs}]}{dt} &= J_a + \Big([\mathrm{Subs}]_{\mathrm{ext}} - [\mathrm{Subs}]\Big) \\
\frac{d[\mathrm{ATP}]}{dt} &= Ja + Jc \\
\frac{d[\mathrm{ADP}]}{dt} &= -Ja - Jc \\
J_c &= [E_c](t)\Big([\mathrm{Nutrient}]\cdot[\mathrm{ADP}] - [\mathrm{Waste}]\cdot[\mathrm{ATP}]\Big) \\
J_a &= [E_a](t)\Big([\mathrm{Product}]\cdot[\mathrm{ADP}] - [\mathrm{Substrate}]\cdot[\mathrm{ATP}]\Big),
\end{aligned}
\tag{3.1}
$$

where $[\cdot]$ represents the intracellular concentration of chemical species, and $[\cdot]_{\mathrm{ext}}$ represents the external concentration. If E_c and E_a were constant, and the external concentrations of chemicals were close to be equilibrium values, the model system (3.1) would be reduced to that introduced by Westerhoff. Note that the total

concentration of ATP and ADP is conserved according to (3.1). However, the enzyme concentration changes with time as

$$\begin{aligned} [E_i] &= \kappa(1 + \sigma_i \lambda f(t)) \\ \sigma_i &= \begin{cases} +1 & (i = c) \\ -1 & (i = a), \end{cases} \end{aligned}$$

where $f(t)$ is a given periodic function with period T that satisfies,

- $\max[f(t)] = 1, \min[f(t)] = -1$
- $\int_0^T f(t)dt = 0.$

With the first condition, λ gives the amplitude of the oscillations in the enzyme concentration (relative to the steady-state value). The second condition is imposed so that the average concentration is not altered by the periodic change, which facilitates comparison between the steady and oscillatory cases. The average concentration of enzymes is given by the parameter κ, which controls the time scale of the chemical reactions. The sign parameter σ_i is introduced to represent the difference in the phase of enzyme oscillations between catabolism and anabolism. Here, we mainly consider the case in which catabolism and anabolism proceed in an anti-phase manner, and the case with an in-phase will be briefly discussed later.

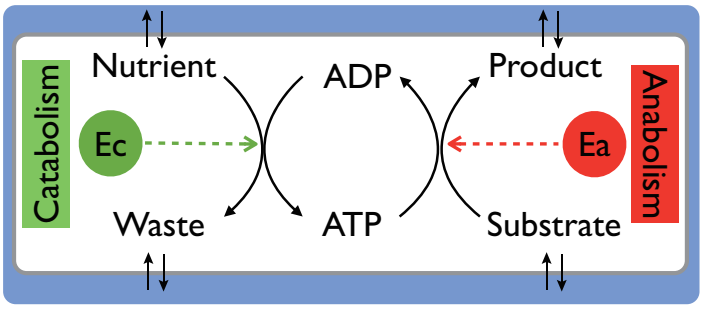

Figure 3.1: Schematic representation of the NWSP model. Nutrient, Waste, Product, and Substrate molecules diffuse in and out of the cell through the external environment. Enzyme concentrations $[E_c]$ and $[E_a]$ are periodically changed externally in order to study the influence of oscillations on the thermodynamic efficiency.

3.2.1 Remarks on oscillatory input

Before presenting the results for the enzyme oscillation, we provide brief remarks on the general consequence of oscillations in substrate concentration.

In general, cellular metabolism can be described as a transduction system of chemical energy. Therefore, it can be expected that oscillatory reaction dynamics

would increase the dissipation in energy transduction compared with the steady-state case. For example, let us consider the simplest reversible chemical reaction $X \rightleftharpoons Y$, with X as the substrate and Y as the product. Then, it can be clearly proven with linear non-equilibrium dynamics that dissipation in the chemical reaction represents a minimum for the steady state (for details, see the Supplement). In general, such oscillations do not change the time scale for the equilibration, and never improve the thermodynamic efficiency.

In contrast, the enzymes themselves can change the time scale for the reaction, which facilitates the equilibration process. Hence, with appropriate oscillatory dynamics in enzyme concentrations, higher thermodynamic efficiency may be achieved, which we will explore in this section.

3.2.2 Characteristic dynamics

Figure 3.2 shows an example of the time series of the concentrations of nutrients, substrates, waste, product, ATP, and ADP, where the periodic function $f(t)$ is chosen as successive switches by a step function with period 1. Specifically, for $t \in [0.0, 0.5)$, $[E_c] = \kappa$ and $[E_a] = 0.0$, and for $t \in [0.5, 1.0)$, $[E_c] = 0.0$ and $[E_a] = \kappa$, where $[E_c]$ and $[E_a]$ change periodically. In the example given in Figure 2, the enzyme is switched four times at $t = 0.0, 0.5, 1.0$, and 1.5. Changes in the concentrations of ATP and ADP reflect this enzyme switching, whereas the concentrations of the nutrient and waste are not changed substantially at $t \approx 0.5$ (and $t \approx 1.5$). This is why the chemical reaction Nutrient + ADP $\rightleftharpoons$ Waste + ATP is almost relaxed to equilibrium at that time point, and the affinity of the reaction, i.e. the flux, is approximately zero. On the other hand, the product and substrate do not change at $t \approx 0.0$ (and $t \approx 1.0$) for the same reason.

Here, we introduce the average thermodynamic efficiency of metabolism to

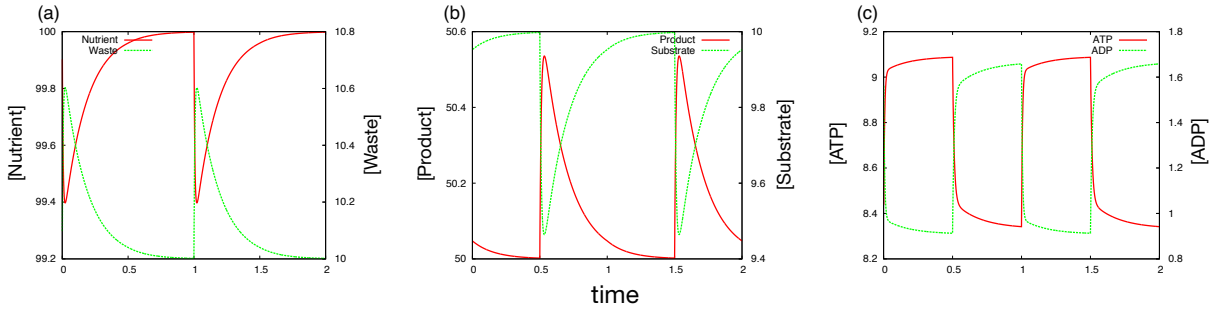

Figure 3.2: An example of the time series of chemical concentrations in the NWSP model (3.1) plotted over two periods. The periodic function $f(t)$ is chosen to be a step function with period 1. We set $[\mathrm{Nutrient}]_{\mathrm{ext}} = 100.0, [\mathrm{Waste}]_{\mathrm{ext}} = 10.0, [\mathrm{Product}]_{\mathrm{ext}} = 50.0, [\mathrm{Substrate}]_{\mathrm{ext}} = 10.0, [\mathrm{ATP}, \mathrm{ADP}]_{\mathrm{total}} = 10.0$, and $\kappa = 0.1$.

study the relevance of oscillatory metabolism for energy transduction. This model of thermodynamic efficiency was originally introduced by Westerhoff et al. [13, 17]

as a ratio of the output of Gibbs free energy to the input of Gibbs free energy, given by $\eta = -J_a A_a / J_c A_c$, where J_i and A_i are the chemical reaction flux and affinity (difference in the Gibbs free energy between the substrate and product of the reaction), respectively [80]. However, this model of the thermodynamic efficiency of metabolism was originally considered in the steady state without a temporal change in chemical concentrations. Therefore, to deal with the case of a time-dependent chemical reaction system, we here extend the definition of the thermodynamic efficiency as follows:

$$\begin{aligned} \eta(\lambda, \kappa) &= -\frac{\int_0^T J_a(t) \cdot A_a(t) dt}{\int_0^T J_c(t) \cdot A_c(t) dt} \\ A_c &= G_{\text{nutrient}} - G_{\text{waste}} \\ A_a &= G_{\text{product}} - G_{\text{subst}}, \end{aligned} \tag{3.2}$$

where G_i is the chemical potential (sum of the standard chemical potential and activity due to a difference in concentration from the standard) of chemical species i, κ is the rate constant of the chemical reaction, and λ is the amplitude of enzyme oscillations relative to the steady state. By setting $\lambda = 0$ (without oscillation), this definition (3.2) is of the same form used for the steady-state metabolism model [13]; thus, it is a natural extension to incorporate the oscillatory case.

Rigorously speaking, this definition of thermodynamic efficiency is justified only near equilibrium. Nevertheless, it is expected that η provides at least an approximately good measure for the efficiency of chemical energy transduction in consideration of oscillatory reaction dynamics.

3.2.3 Influence of oscillation on the thermodynamic efficiency

In this subsection, we demonstrate the dependence of η on the amplitude λ of the oscillation of enzyme concentrations and their average κ values. The efficiency is plotted as a function of the amplitude λ and rate constant κ in Figure 3.3. Here, the steady state is given by $\lambda = 0$, while $\lambda = 1$ corresponds to the switch between two separated states, in which one of the enzymes (E_a or E_c) vanishes so that the corresponding reaction is halted. From the numerical results in Figure 3.3, we find that the incorporation of oscillatory metabolism improves the average efficiency when κ is small. However, note that the average flux, $< J > (\lambda, \kappa) = -T^{-1} \int_0^T J_a(t) dt$, is not improved (see Figure.3.12).

In Figure 3.4, the efficiency is compared between the steady ($\lambda = 0$) and full oscillatory ($\lambda = 1$) cases. This comparison further confirmed that the efficiency $\eta(\lambda, \kappa)$ is improved with oscillations in the small κ region. Note that $\eta(\lambda, \kappa)$ is not a monotonic function of λ for a certain range of κ values. The crossover point of the amplitude at which the efficiency for the oscillation case exceeds that for the steady case depends on κ, whereas the oscillation case is always advantageous as long as κ is small. This advantage of dynamic (chemical) energy transduction for thermodynamic efficiency is in strong contrast with the energy conversion observed

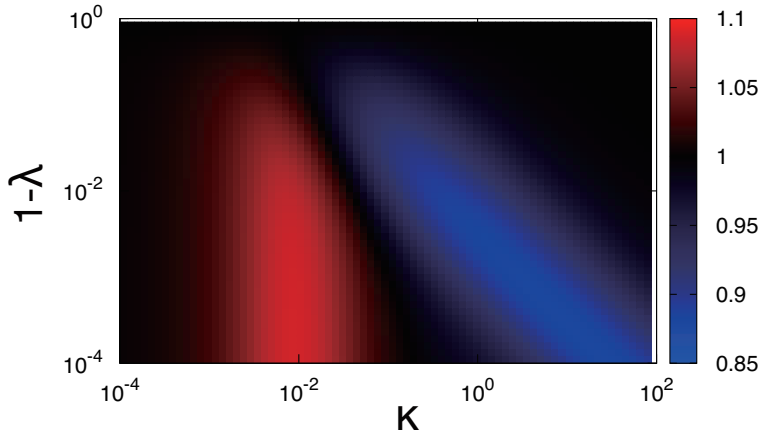

Figure 3.3: Heat map of the average thermodynamic efficiency with oscillations in enzyme concentrations relative to that in the steady state. The horizontal and vertical axes are κ and $1.0 - \lambda$, respectively. The colour bar represents $\eta(\lambda, \kappa)/\eta(\lambda = 0, \kappa)$. The thermodynamic efficiency η is improved for the small κ region. The step periodic function, with period $T = 200.0$, was adopted to model the change in enzyme concentration. Parameters were set as follows: $[\text{Nutrient}]_{\text{ext}} = 10.0$, $[\text{Waste}]_{\text{ext}} = 0.1$, $[\text{Prod}]_{\text{ext}} = 1.0$, $[\text{Subs}]_{\text{ext}} = 0.05$,and $[\text{ATP}] + [\text{ADP}] = 100.0$.

in the dynamic input change, in which the efficiency is always decreased by the oscillation, as discussed above.

In the following, we will focus on how this observed improvement in efficiency is actually achieved. Firstly, loss in efficiency is caused by the dissipation of Gibbs free energy in each chemical reaction. Then, the amount of dissipation is reduced when each reaction progresses close to its equilibrium. If κ, the time scale for the catalytic reaction, is sufficiently larger than that of material flux (which is set to unity), the system is near equilibrium and the loss is small; indeed, this loss is smallest at the steady state. However, when κ is small, the "chemical coupling" between the two reactions (anabolism and catabolism) hinders the approach to equilibrium. In the present case, the two reactions are coupled with the energy currency ATP and ADP. Equilibration of catabolism results in an excess of ATP compared to ADP, which results in a far-from-equilibrium condition for the anabolism reaction (Of course, whether equilibration of one elemental reaction dis-equilibrates the other will depend on how the two reactions are coupled energetically; in particular, this will depend on the values of standard chemical potentials. However, as long as $\int J_c dt > 0, \int J_a dt < 0$ and $G_{\text{Substrate}} < G_{\text{Product}}$, synthesis of the product (P) relies on the free energy of ATP synthesised from the nutrient, and this coupling form is generally true for coupling between catabolic and anabolic reactions. Thus, increasing the reaction time scale of catabolism produces more ATP, which then dis-equilibrates the anabolic reaction.).

Thus, the elemental reaction processes dis-equilibrate each other in the present coupled reaction system. In the steady state, these two reactions progress in a

moderately dis-equilibrated condition when κ is small. In contrast, the oscillatory reaction can separate the process into two time regimes. The first regime is the situation for E_c, in which the catabolism reaction progresses near equilibrium and the anabolism reaction occurs far from equilibrium and is almost halted as $E_a \sim 0$. On the other hand, in the time regime with $E_a > 0$ and $E_c \sim 0$, anabolism progresses near equilibrium, and catabolism is almost halted. Thus, most of the reaction events for the two temporal regimes occur near their equilibria, and thus the dissipation is suppressed in these two regimes. On the other hand, during the switch time between $E_c \gg E_a$ and $E_a \gg E_c$, the dissipation would be increased. Thus, the total efficiency depends on the difference between the gain in the suppression from one of the reactions and the loss caused by the oscillation. This characteristic is not observed when the enzymes oscillate in an in-phase manner. In the in-phase oscillation, the enzymes facilitate the catabolic and anabolic reactions equally, and each reaction hinders the approach to the other reaction's equilibrium, as observed in the steady state.

To quantify the gain and loss of this oscillatory chemical reaction system, we calculated the energy gain $G_{\rm gain}$ and loss $G_{\rm loss}$ using the following equation:

$$\begin{aligned} G_{\rm gain} &= \sum_{i=c,a} \int_0^T \theta(A_i^{\rm st} - A_i^{\rm os}(t)) J_i^{\rm os}(t)(A_i^{\rm st} - A_i^{\rm os}(t))dt \\ G_{\rm loss} &= \sum_{i=c,a} \int_0^T \theta(A_i^{\rm os}(t) - A_i^{\rm st}) J_i^{\rm os}(t)(A_i^{\rm os}(t) - A_i^{\rm st})dt \\ \theta(x) &= \begin{cases} 1 & (x > 0) \\ 0 & (x < 0), \end{cases} \end{aligned} \tag{3.3}$$

where A_i^j is the affinity (Gibbs free energy difference) of the reaction, and J_i^j is the corresponding flux, where $i = c$ for catabolism and $i = a$ for anabolism; and $j = {\rm st}$ for $\lambda = 0$ (the steady case) and $j = {\rm os}$ for $\lambda = 1$ (full oscillatory case). Thus, $G_{\rm gain}$ ($G_{\rm loss}$) represents the amount of reduced (excess) Gibbs free energy compared with that of the steady-state value. The value of κ at which the gain exceeds the loss is approximately equal to the value where $\eta(\lambda = 1, \kappa)$ is larger than $\eta(\lambda = 0, \kappa)$, as shown in Figure 3.4. In summary, by progressing the chemical reaction closer to the equilibrium and suppressing the reaction further from equilibrium, the efficiency is increased compared to that of the steady case.

This improvement in efficiency can also be interpreted from a different perspective. Figure 3.6 shows the time series of the flux and affinity of the catabolic reaction. When the flux is not close to zero, the affinity is close to zero, and thus the reaction progress near equilibrium. By contrast, when the affinity is not close to zero, the flux is close to zero, except at the time point of enzyme switching, and this far-from-equilibrium reaction occurs only at a very low rate. Thus, thermodynamic loss is suppressed throughout the process. In Figure 3.6, we illustrate this negative correlation between flux and affinity for catabolism, which was also confirmed for anabolism.

It is important to note that this characteristic cannot be realized under the

condition of linear thermodynamics without a change in the enzyme concentrations, in which thermodynamic flux increases with the affinity. Thus, the flux can be controlled only by changing the affinity of the chemical reaction, and the two are always positively correlated. In contrast, in the present case, by changing the concentration of the catalytic enzyme, the time scale of the chemical reaction is changed. Accordingly, the flux can be increased even for a low-affinity state, and can be suppressed for a high-affinity state.

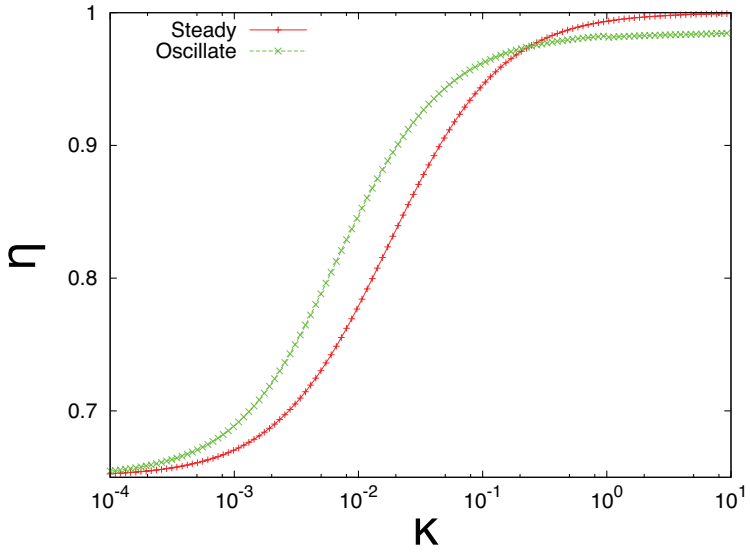

Figure 3.4: The average thermodynamic efficiency $\eta(\lambda, \kappa)$ for the steady ($\lambda = 0$) and oscillatory ($\lambda = 1$) cases plotted against the rate constant of the chemical reaction κ. The average thermodynamic efficiency for the oscillatory case is higher for the small κ region. The choice of function and parameters is identical with that described in Figure3.3.

3.3 Extension to an autonomous chemical reaction model

So far we have demonstrated that the thermodynamic efficiency of metabolism (coupling between anabolism and catabolism) can be improved by incorporation of an oscillatory chemical reaction. However, the model introduced in the last section cannot generate the chemical oscillation autonomously; thus, this model does not account for the possible energetic cost from generating the chemical oscillation. Since the chemical oscillation is generated as a dissipative structure at the far-from-equilibrium condition, generating the oscillation itself requires a certain amount of excess dissipation [81]. Therefore, it is important to investigate whether or not a chemical reaction system capable of generating autonomous

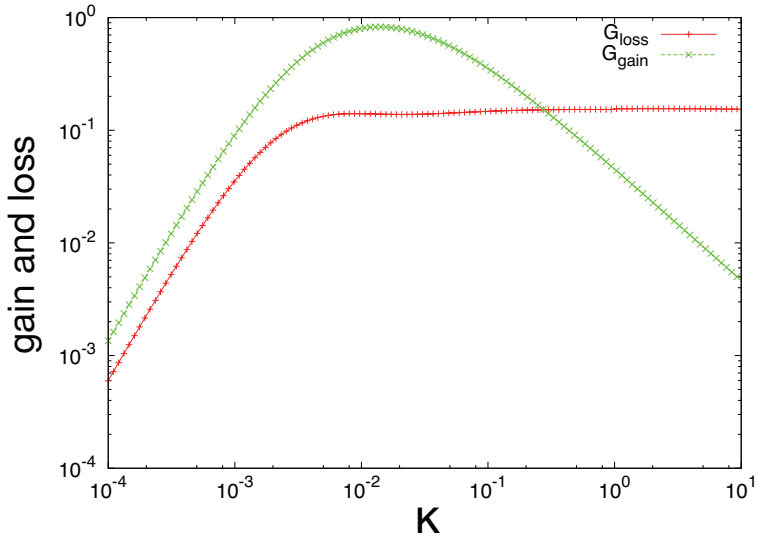

Figure 3.5: The thermodynamic loss and gain with oscillatory metabolism calculated using (3.3). At the value of κ for which the loss and gain are balanced, $\eta(\lambda = 0, \kappa) \approx \eta(\lambda = 1, \kappa)$ holds as in Figure 3.4. The choice of the periodic function and parameter values is identical with that of Figure 3.3.

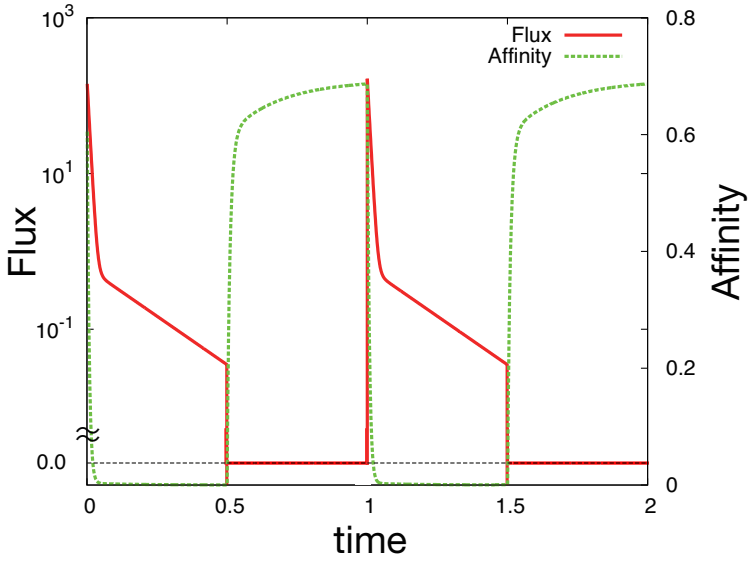

Figure 3.6: Time series of the flux (red) and affinity (green) under enzyme switching plotted over two time periods. A step periodic function with period $T = 1$ was adopted for $f(t)$.The flux and affinity ocillate with an anti-phase.

oscillation can improve thermodynamic efficiency. To address this question, we developed a three-catalyst model in which chemical oscillation appears under a given flow from resource chemicals to product.

Our model consists of nine chemical species, $x, y_i, z_i, (i = 1, 2, 3)$, substrate, and product. Chemical reactions were constructed by coupling between catabolic (energy-generating) and anabolic (energy-consuming) reactions, as shown in the schematic in Figure 3.7. There are two types of catalytic reactions, $x+substrate \rightleftharpoons y_i+product$ and $y_i+substrate \rightleftharpoons z_i+product$, and each reaction is catalysed by y_i. The system takes up x and the substrate from the external environment, and x is converted into z via the above two reactions, resulting in the simultaneous synthesis of two products. The produced z molecules and products are transported into the environment. In the model, the reaction to covert x into z via y is assumed to be a catabolic reaction, and the chemical reaction between the substrate and the product is regarded as anabolism. Therefore, the reaction $substrate \rightarrow product$ is driven by the coupled chemical reactions $x \rightarrow y_i$ and $y_i \rightarrow z_i$.

In developing this model, we referred to the example of a repressilator [82], in which the expression of three proteins is mutually inhibited to generate the oscillation. However, given the present focus of a reaction system involving a catalytic reaction, there is no direct inhibition. Instead, each of the three components y_i mutually catalyse the decomposition of y_{i+1} into z_{i+1} ($y_{i+1}+substrate \rightleftharpoons z_{i+1}+product$). Hence, the y_is suppress the abundances of each other, which introduces effective mutual inhibition, as in a repressilator.

Here, for the sake of simplicity, we assume that the consumed substrate or synthesised product is quickly supplied by or transported to the external environment, respectively; thus, their internal concentrations are kept constant. Therefore, there are only 7 variables for $[x]$, $[y_i]$, and $[z_i]$. In addition, by scaling the rate constants according to the concentration of the substrate, the coupling with the anabolic reaction is given by a single parameter ρ. Finally, by assuming the symmetrical case in which the parameters for each species i are homogeneous over the index i, our chemical reaction system is given by

$$\begin{aligned}
\frac{d[x]}{dt} &= -\sum_{i=1}^{3} J_{1,i} + D([X] - [x]) \\
\frac{d[y_i]}{dt} &= J_{1,i} - J_{2,i} \\
\frac{d[z_i]}{dt} &= J_{2,i} + \phi([Z] - [z_i]) \\
J_{1,i} &= \kappa_1 [y_i]([x] - l_1 \rho [y_i]) \\
J_{2,i} &= \kappa_2 [y_{\sigma(i)}]([y_i] - l_2 \rho [z_i]),
\end{aligned} \tag{3.4}$$

where $[\cdot]$ represents the concentration of the corresponding chemical species, κ_1 and κ_2 are the rate constants of each chemical reaction $x + substrate \rightleftharpoons y_i + product$ and $y_i + substrate + z_i + product$, respectively, D and ϕ are the rate of material exchange of x and z with the external environment, respectively, and l_1, l_2, and ρ are the Boltzmann factors of each chemical reaction (i.e. $l_1 = \exp(-\beta(\mu_x - \mu_y))$, $l_2 = \exp(-\beta(\mu_y - \mu_z))$, and $\rho = [\text{product}][\text{substrate}]^{-1} \exp(-\beta(\mu_{\text{substrate}} - \mu_{\text{product}}))$,

where μ_i is the standard chemical potential of chemical species i). $[X]$ and $[Z]$ represent the environmental concentrations of chemical species x and z, respectively, where σ denotes the cyclic permutation on i ($\sigma(1) = 3, \sigma(2) = 1, \sigma(3) = 2$).

We numerically computed the dynamics and attractor of the model by varying the parameter values, and found that the system exhibits Hopf bifurcation from a fixed point to limit-cycle oscillation with the increase in the parameter κ_2. An example of the time series of the concentrations is shown in Figure 3.8.

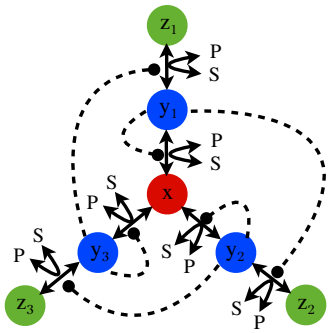

Figure 3.7: Schematic representation of a simple chemical reaction model exhibiting autonomous oscillation. The chemical reaction $x \rightleftharpoons y_i$ is catalysed by y_i, and $y_i \rightleftharpoons z_i$ is catalysed by y_{i-1} species. In each reaction, the product (P) is synthesised from substrates (S) that are externally supplied. An anabolic reaction *substrate* $\rightleftharpoons$ *product* is coupled to each reaction.

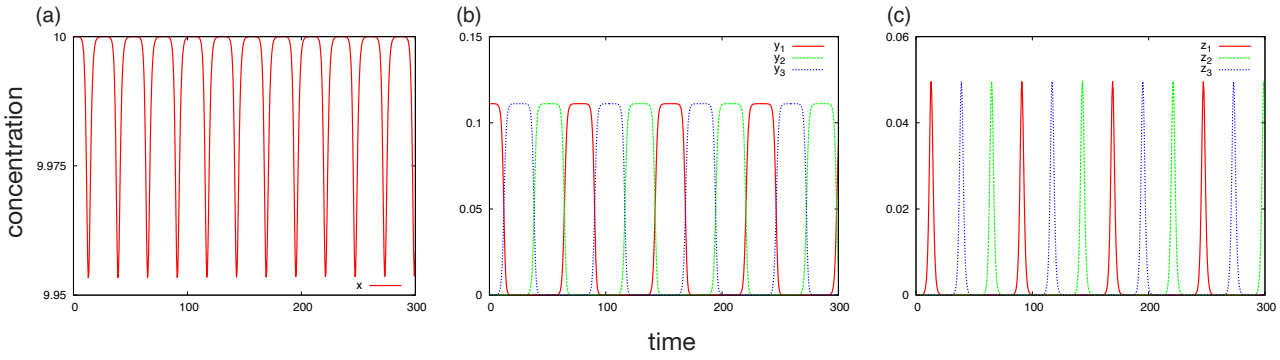

Figure 3.8: Time series of concentrations of species (a) x, (b) y_is, and (c) z_is. Parameters were chosen as follows: $\mu_x = 1.0, \mu_y = 2.0, \mu_z = 0.0, \mu_{\text{product}} - \mu_{\text{substrate}} = 0.5, \kappa_1 = 0.1, \kappa_2 = 20.0, \beta = 3.0, D = \phi = 1.0$, $[X] = 10.0$, and $[Z] = 0.0$.

3.3.1 Relationship between oscillation and dissipation

We now introduce the average thermodynamic efficiency of the energy transduction, as described in Section 2. In our model (3.4), the reactions to convert

x into z via y are regarded as catabolic, and the reactions between the substrate and product are considered to be anabolism. Thus, the average thermodynamic efficiency can be defined as,

$$\eta = -\frac{\sum_{i,j} \int_0^T J_{i,j}(t) A^a_{i,j} dt}{\sum_{i,j} \int_0^T J_{i,j}(t) A^c_{i,j}(t) dt},$$

where $A^c_{i,j}$ ($A^a_{i,j}$) indicates the affinity of the catabolic (anabolic) part of the chemical reaction (i, j), and the time for the average T is chosen to be sufficiently long. Specifically, the parameters are given by $A^c_{1,j} = \ln(x/(l_1 \cdot y_j))/\beta, A^c_{2,j} = \ln(y_j/(l_2 \cdot z_j))/\beta$, and $A^a_{i,j} = -\ln(\rho)/\beta$. The definition of the average thermodynamic efficiency implies the ratio of output to input energy, and η satisfies the inequality $0 \leq \eta \leq 1$ with appropriate conditions: $J_{i,j}(t)$ values are always positive, and $\rho \geq 1$.

Figure 3.9 shows the average flux $< J >$ and η. Both the average flux and the thermodynamic efficiency were improved (or maintained at a high level) by incorporation of the oscillation. The time courses of the flux and affinity for each reaction are shown in Figure 3.10. The flux and affinity of each chemical reaction oscillates out of phase, roughly in anti-phase. Since the thermodynamic dissipation is given by the product between the flux and affinity, it can be reduced by this anti-phase oscillation between the two, as described in Section 2.

To summarise, we introduced a simple chemical reaction system exhibiting autonomous sustainable oscillations, and confirmed that the oscillations increased the average thermodynamic efficiency, which was attributed to the anti-phase oscillation between the flux and affinity.

3.4 Summary and Discussion

We here report the first evaluation of the relevance of oscillatory chemical reactions to thermodynamic efficiency by introducing the NWSP model. In the model, chemical energy is stored by transforming ADP into ATP via a catabolic reaction that converts an imported nutrient into waste, while an anabolic reaction consumes the stored energy to synthesise a product from a substrate, by transforming ATP to ADP. Such a coupling structure between anabolism and catabolism forms the basis of cellular metabolism. Thus, the NWSP model is regarded as a simplified, coarse-grained model for cellular metabolism. Each reaction is catalysed by a corresponding enzyme. Moreover, by introducing oscillations in the abundances of each enzyme, the thermodynamic efficiency of energy conversion was computed and compared between the steady and oscillatory cases.

Under the condition of enzyme limitation, in which the (average) enzyme abundances are insufficient and the chemical reactions can only progress slowly, we found that the oscillation in enzyme abundances improved the thermodynamic efficiency. This improvement stems from the antagonistic nature between anabolism and catabolism. In general, a catabolic reaction generates the energy currency

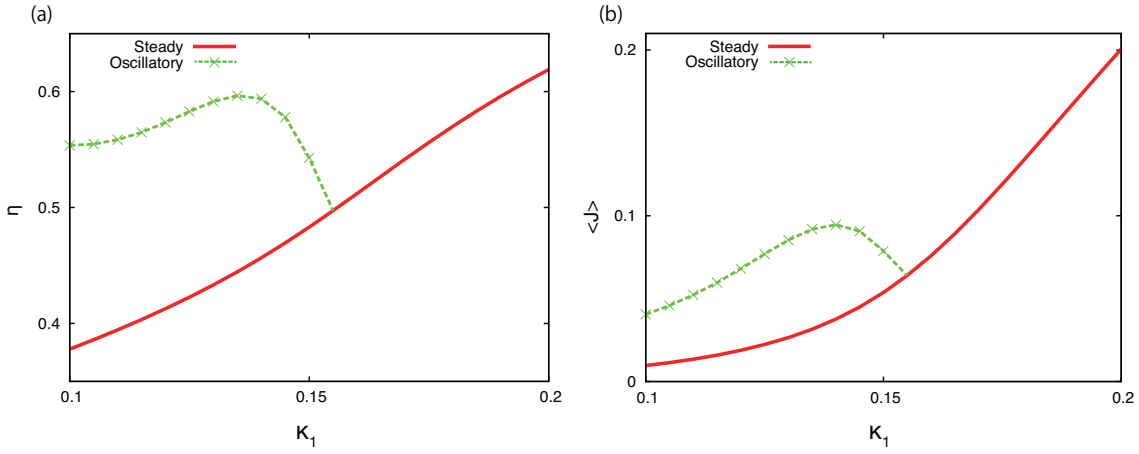

Figure 3.9: (a) The thermodynamic efficiency and (b) average flux of the model, plotted as a function of κ_1, for the oscillation (green) and steady (red) cases. The thermodynamic efficiency is maintained at a higher value by the oscillation for small κ_1 values. In addition, the oscillation also improved the flux. Hopf bifurcation occurs at $\kappa_1 \approx 0.155$, and the oscillatory solution (limit cycle) disappears for $\kappa_1 > 0.155$. The parameters were chosen to be $\mu_x = 1.0, \mu_y = 2.0, \mu_z = 0.0, \mu_{\text{product}} - \mu_{\text{substrate}} = 1.5, \kappa_2 = 250.0, \beta = 1.0, D = \phi = 1.0$, $[X] = 10.0$, and $[Z] = 0.0$.

by breaking a large macromolecule into smaller pieces, whereas anabolism consumes energy to drive the synthesis of a macromolecule. Therefore, these two reaction types tend to dis-equilibrate each other, and thus they will progress far from equilibrium if they progress concurrently under a limited rate, which will consequently increase thermodynamic loss (entropy production). In contrast, if sequential switching between anabolism and catabolism is achieved by oscillations in enzyme abundances, the two reactions become decoupled, and the loss is suppressed. Indeed, we confirmed the improvement in thermodynamic efficiency by imposing anti-phased oscillations in the abundances of enzymes for anabolism and catabolism.

However, the generation of such oscillation can bring about thermodynamic loss by itself. To account for this effect, we also considered a reaction model that can generate autonomous chemical oscillations, by amending the energy-transduction with three enzymes that mutually catalyse their degradation reactions, so that autonomous, repressilator-type, oscillation is possible. The model converts chemical species x into z via the enzymes, along with synthesis of a product from the substrate. By comparing the thermodynamic efficiency between cases, we confirmed again that the thermodynamic efficiency is improved by the emergence of chemical oscillation.

The common mechanism for the improvement in efficiency observed in our two models is the anti-phase oscillation between the chemical reaction flux and affinity. The anti-phase oscillation implies low flux for a high-affinity state and high flux for a low-affinity state. This situation leads to the increase in the thermodynamic

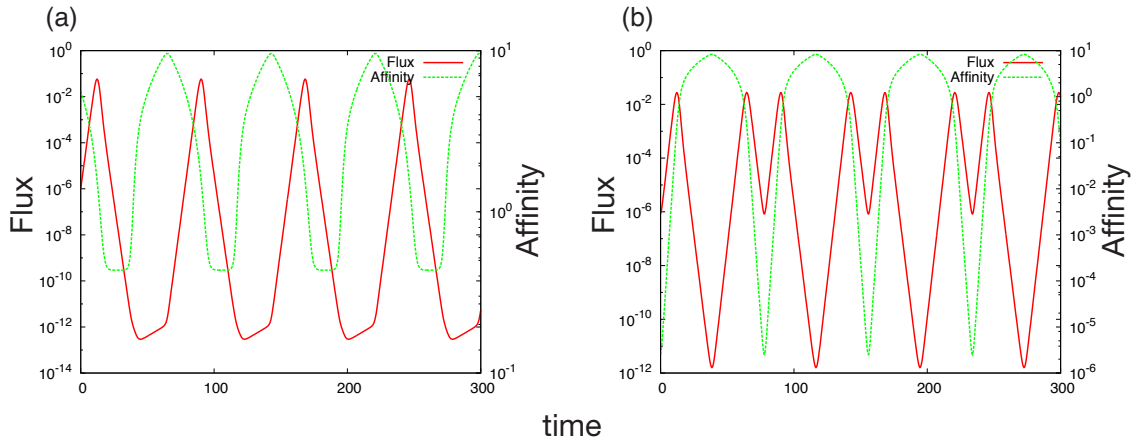

Figure 3.10: Time series of the flux (red) and affinity (green) in the reaction $x + substrate \rightleftharpoons y_1 + product$ (a), and $y_1 + substrate \rightleftharpoons z_1 + product$ (b). The flux and affinity of both reactions, $x + substrate \rightleftharpoons y_1 + product$ and $y_1 + substrate \rightleftharpoons z_1 + product$, oscillate out of phase as in the NWSP model. The time series for index $i = 1$ is shown here, and those for indices $i = 2$ and $i = 3$ are the same (except for the difference in the oscillation phase). The parameter values were chosen as described in Figure 3.8.

efficiency, as the thermodynamic loss owing to entropy production is given by the product between the flux and affinity.

In the present study, we focused only on a system with simplified, coarse-grained metabolism and elementary chemical reactions. However, improvement in the thermodynamic efficiency by such anti-phase oscillation between flux and affinity is expected to be a universal phenomenon for all biochemical processes involving catalytic reactions. In the case of an ordinary chemical reaction without catalytic enzymes, chemical reaction flux can only be controlled by the affinity, and the two are positively correlated (or proportional in the case of linear thermodynamics) [79, 83, 84]. However, for an enzymatic reaction, the flux is controlled not only by the affinity but also by the abundances of the corresponding enzymes. The enzymes do not directly alter the equilibrium condition but do facilitate the tendency toward equilibration. Hence, an increase in enzyme supply reduces dissipation for a single chemical reaction event as studied in the previous chapter. Therefore, as long as the enzyme abundance is increased with the flux, the affinity and flux will be negatively correlated if the enzyme controls the chemical reaction.

In general, biochemical reactions in microbial experiments are often facilitated and halted by simply controlling the amount of enzymes.[7, 83, 84, 85, 86, 87, 88]. Therefore, the results of the present model suggest that thermodynamic efficiency in metabolism could be improved by dynamically changing the enzyme concentrations in a microbial system. For example, oscillations in gene expression have been reported in yeast grown under nutrient limitation, which is generally referred to as the yeast metabolic cycle (YMC)[74, 75, 76, 77]. Roughly speaking, expression levels of anabolic and catabolic proteins are temporally separated in the YMC, in a similar manner to the condition of our NWSP model under an oscillatory switch of the two enzymes. Here, as the nutrients are limited, the rate of the catalytic reaction is lowered, which implies a smaller κ value (the rate constant of chemical reactions) in our NWSP model. Hence, improvement of the thermodynamic efficiency by oscillation for the small κ region observed here may provide an explanation for the experimental observations of the benefit of the YMC.

Additionally, the anti-phase oscillation between the flux and affinity also emerges in a model of the glycolytic oscillation [72]. Since glycolysis is a part of the catabolic process, we cannot adopt the same definition of the thermodynamic efficiency as adopted in this chapter. However, thermodynamic efficiency for the energy conversion, defined similarly, is shown to be improved by the glycolytic oscillation [73]. The examples of YMC and glycolytic oscillation may imply the ubiquity of the anti-phase oscillation between the reaction flux and affinity as a mechanism of improvement of the thermodynamic efficiency by enzymatic oscillation.

In general, intracellular processes include several coupled reactions that may disequilibrate each other. One potentially effective strategy to achieve higher efficiency may be to temporally separate these reactions by switching the abundances of the corresponding enzymes for each reaction in time. This issue will be addressed directly in future extensions of the present model. Furthermore, analyses of several phases in the cell cycle along these same lines may reveal new patterns and mechanisms.

3.5 Supplement

3.5.1 Increase of the thermodynamic dissipation for the oscillatory input

Here, we provide the calculation for the proof of the thermodynamic dissipation increase in the oscillatory input.

Let us consider the simplest model, which consists of a chemical reaction $x \rightleftharpoons y$, with x as the substrate and y as the product, and material flow between the internal and external environment for both chemical species x and y. We assume that the oscillatory input is given by the sinusoidal oscillation of the external concentration of x molecules, denoted by X. Then, our model is given by

$$\begin{aligned}\frac{d[x]}{dt} &= -\kappa([x]-[y]) + ([X](1+\lambda\sin(t)) - [x]) \\ \frac{d[y]}{dt} &= \kappa([x]-[y]) + ([Y]-[y]),\end{aligned} \tag{S1}$$

where κ is the rate constant of the chemical reaction $x \rightleftharpoons y$ (the rate constant of material flow is set at unity), λ is the amplitude of the oscillation, $[X]$ represents the average external concentration of x, and $[Y]$ is the external concentration of y.

The solution of this reaction system (S1) is given by

$$\begin{aligned}[x](t) &= [x]_{\rm st} + \lambda(a\sin(t) + b\cos(t))/Z \\ [y](t) &= [y]_{\rm st} + \lambda(c\sin(t) + d\cos(t))/Z,\end{aligned}$$

where $[x]_{\rm st} = \frac{(1+\kappa)[X]+[Y]}{1+2\kappa}$ and $[y]_{\rm st} = \frac{(1+\kappa)[Y]+[X]}{1+2\kappa}$ are the concentrations of each chemical species in the steady state, and the coefficients are $a = (1+\kappa)(1+2\kappa), b = -(1+\kappa), c = 1+\kappa+2\kappa^2, d = 1+\kappa$, and $Z = [X]/(2+4\kappa(1+\kappa))$.
From the solution, the average flux $< J >= 1/2\pi \int_0^{2\pi} \kappa([x]-[y])dt = \kappa([X]_0 - [Y])/(1+2\kappa)$ does not change from incorporating the oscillation. In contrast, the average entropy production rate, given by $< \sigma >= 1/2\pi \int_0^{2\pi} \kappa([x]-[y])\ln([x]/[y])/\beta dt$, with β as the inverse temperature, is changed by the oscillation. By assuming that the amplitude λ is small, $\sigma(t) = \kappa([x](t)-[y](t))\ln([x](t)/[y](t))/\beta$ is expanded into a Taylor series in λ as $\sigma(t) = \sum_n \sigma_n(t)\lambda^n$. In the series, equation $\int_0^{2\pi}\sigma_n(t)dt = 0$ holds for an odd number for n because the model (S1) is symmetric against the sign inversion of λ. This is because the sign inversion of λ is equivalent to the shift of the origin of time, because $-\sin(t) = \sin(t+\pi)$ holds. Since the choice of the origin of time does not alter the average entropy production rate, the function form of $< \sigma >$ is symmetric against λ at $\lambda = 0$; thus, the equation $\int \sigma_n(t)dt = 0$, (n:odd) holds. Therefore, $< \sigma >$ is expanded as $< \sigma >= \sigma_{\rm st} + \lambda^2 < \sigma_2 > +\mathcal{O}(\lambda^4)$, where $< \sigma_2 >$ is given by

$$< \sigma_2 >= \frac{1}{Z^2}\frac{([x]_{\rm st}+[y]_{\rm st})\Big((c[x]_{\rm st}-a[y]_{\rm st})^2 + (d[x]_{\rm st}-b[y]_{\rm st})^2\Big)}{4[x]_{\rm st}^2[y]_{\rm st}^2},$$

which is always positive regardless of the specific parameters.

We also computed $< \sigma >$ numerically over a wide range of κ and λ values. Figure 3.11 shows the dependence of $< \sigma >$ on κ and λ. It is confirmed that $< \sigma >$ is increased by the oscillation, independent of the amplitude of λ and κ, so that the energy transduction efficiency of the chemical reaction $x \rightleftharpoons y$ is decreased.

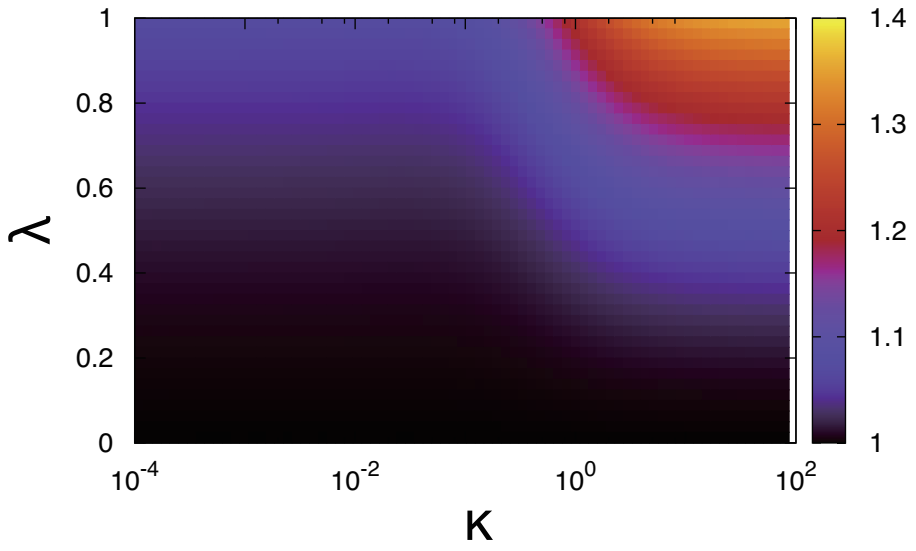

Figure 3.11: Heat map of the average entropy production rate relative to the steady value plotted against κ (horizontal axis) and λ (vertical axis). The colour bar represents $< \sigma > (\lambda, \kappa) / < \sigma > (\lambda = 0, \kappa)$. The average entropy production rate always increased with the increase in the relative amplitude λ. The parameters were set to be $[X]_0 = 10.0$ and $[Y] = 1.0$.

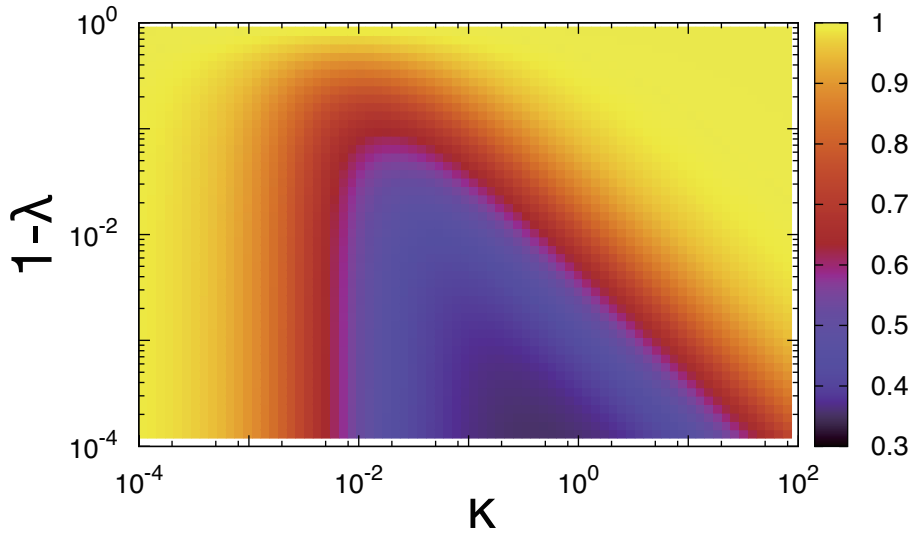

Figure 3.12: Heat map of the average flux relative to the steady value, plotted against κ (horizontal axis) and $1 - \lambda$ (vertical axis). The colour bar represents $< J > (\lambda, \kappa) / < J > (\lambda = 0, \kappa)$. The average flux always decreased with the increase in the relative amplitude λ. The parameters were set to be the same as those in Figure 3. We also calculated the first- and second-order derivatives of the average flux value $< J >$ with respect to the relative amplitude of the oscillation in the concentration of enzymes λ at $\lambda = 0$ in the NWSP model (1). Because of the symmetry of the sign inversion of λ in the model, the first derivative of the average flux is equal to zero regardless of the parameters used. The second-order derivative is extremely complicated, and is always negative if the value of the flux is positive at the steady state. This indicates that the chemical flux is never facilitated by an oscillation with a small amplitude.

Chapter 4

Theory for Transitions Between Exponential and Stationary Phases: Universal Laws for Lag Time

4.1 Introduction

Quantitative characterization of a cellular state, in terms of the cellular growth rate, concentration of external resources, as well as abundances of specific components, has long been one of the major topics in cell biology, ever since the pioneering study by Monod [3]. Such studies have been developed mainly by focusing on the microbial exponentially growing phase, in which the number of cells grows exponentially (this phase is often termed the *log phase* in cell biology, but considering the focus on exponential growth, we here adopt the term "exponential phase" throughout). This work has uncovered somewhat universal growth laws, including Pirt's equation for yield and growth [6] and the relationship between the fraction of ribosomal abundance and growth rate (experimentally demonstrated by Schaechter *et al.*[89], and theoretically rationalized by Scott *et al.* [7]), among others [37, 90, 91, 92], in which the constraint to maintain steady growth leads to general relationships[9, 41].

In spite of the importance of the discovery of these universal laws, cells under poor conditions exhibit different growth phases in which such relationships are violated. Indeed, in addition to the death phase, cells undergo a stationary phase under conditions of resource limitation, in which growth is drastically suppressed. Once cells enter the stationary phase, a certain time span is generally required to recover growth after resources are supplied, which is known as the lag time. There have been extensive studies conducted to characterize the stationary phase, including the length of lag time for resurrection and the tolerance time for starvation or antibiotics [2, 93, 94], and specific possible mechanisms for phase transitions have been proposed [95, 96, 97]. Furthermore, recent experiments have uncovered the quantitative relationships of lag time and its cell-to-cell variances[98, 99]. For

example, the lag time was shown to depend on the length of time the cells are starved. This implies that the stationary phase is not actually completely stationary but that some slow changes still progress during the starvation time, in which cells "memorize" the starvation time. Hence, a theory to explain such slow dynamics is needed that can also characterize the phase changes and help to establish corresponding quantitative laws.

The existence of these phases and lag time are ubiquitous in bacteria (as well as most microorganisms). Hence, we aimed to develop a general model that is as simple as possible, without resorting to detailed specific mechanisms, but can nonetheless capture the changes among the lag, exponential, stationary, and death phases. We first describe a simple model for a growing cell, which consists of an autocatalytic process driven by active chemical components such as ribosomes. However, this type of model with autocatalytic growth from substrates and their derivatives that is adopted for the exponential phase is not sufficient to represent all phases, as the autocatalytic process either grows exponentially or decays toward death, and thus does not account for a halting state with suppressed growth corresponding to the stationary phase. Therefore, to go one step further beyond the simplest model, we then consider the addition of an extra class of components that do not contribute to catalytic growth. Still, even the inclusion of this extra class of components cannot fully account for the transition to the stationary phase. Therefore, we further considered the interaction between the two classes of components. Here, we propose a model that includes the formation of a complex between these two types of components, which inhibits the autocatalytic process by the active components. We show that the model exhibits the transition to the stationary phase with growth suppression. By analyzing the dynamics of the model, we then uncover the quantitative characteristics of each of these phases in line with experimental observations, including the bacterial growth curve, quantitative relationships of lag time with starvation time and the maximal growth rate, and the exponentially tailed distribution of lag time. The proposed model also allows us to derive several experimentally testable predictions, including the dependence of lag time on the speed of the starvation process.

4.1.1 Model

Since molecules that contribute to autocatalytic processes are necessary for the replication of cells, models for growing cells generally consist at least of substrates (S) and active components (noted as "component A" hereafter) that catalyze their own synthesis as well as that of other components. For example, in the models developed by Scott *et al.*[7] and Maitra *et al.*[48], component A corresponds to ribosomes, whereas several models involving catalytic proteins have also been proposed[51, 52, 100]. This class of models provides a good description of the exponential growth of a cell under the condition of sufficient substrates availability; however, once the degradation rate of component A exceeds its rate of synthesis under a limited substrate supply, the cell's volume will shrink, leading to cell death. Hence, a cell population either grows exponentially or dies out, and in this cellular state it is not possible to maintain the population without growth.

However, cells often exhibit suppressed growth under substrate-poor conditions, even at a single-cell level [2, 93, 98], as observed in the stationary phase. Such cells that neither grow exponentially nor go toward death cannot be modeled with cell models that only consider autocatalytic processes[7, 48, 51, 52, 100].

Therefore, to model a state with such suppressed growth, it is important to consider additional chemical species, i.e., macromolecules that do not contribute to autocatalytic growth, in addition to the substrates (S) and component A (A) that are commonly adopted in models of cell growth. Component A represents molecules that catalyze their own growth such as ribosomes, and can include metabolic enzymes, transporters, and growth-facilitating factors. Component B represents waste products or can be other molecules that are produced with the aid of component A but do not facilitate growth. Thus, the next simplest model is given by

$$\begin{aligned} \frac{dS}{dt} &= -F_A(S)A - F_B(S)A + A(S_{\text{ext}} - S) - \mu S \\ \frac{dA}{dt} &= F_A(S)A - d_A A - \mu A \\ \frac{dB}{dt} &= F_B(S)A - d_B B - \mu B. \end{aligned} \tag{4.1}$$

Here, S_{ext} and S indicate the concentrations of the extracellular and intracellular substrate, respectively. The concentration of the intracellular substrate determines the synthesis rate of the active and non-autocatalytic proteins F_A and F_B, respectively. All chemical components are diluted due to the volume growth of a cell. In addition to dilution, macromolecules (A and B) are spontaneously degraded with slow rates (d_A and d_B). In this model, the cell takes up substrates from the external environment from which component A and the non-growth-facilitating component B are synthesized. These syntheses, $S_{\text{ext}} \rightleftharpoons S, S \to A$, and $S \to B$, as well as the uptake of substrates take place with the aid of catalysis by component A. Then, by assuming that the synthesized components are used for growth in a sufficiently rapid period, the growth rate is set to be proportional to the synthesis rate of component A. Hence, the dilution rate μ of each component due to cell volume growth is set as $\mu = F_A A$.

Now, if the ratio F_A/F_B does not depend on the substrate concentration S, the fraction A/B also does not depend on S, and the model is reduced to the original autocatalytic model; thus, the phase change to suppressed growth is not expected. Then, by introducing the S-dependence of F_A/F_B to reduce the rate of component A with the decrease in the substrate condition, we first tested whether the transition to a suppressed growth state, as in the stationary phase, occurs under a substrate-poor condition, by setting F_A/F_B to decrease in proportion to the change in S (i.e., $\frac{d}{dS}F_A/F_B > 0$). However, in this case, it is straightforwardly confirmed that there is no transition to a suppressed growth state. That is, the cells always grow exponentially without any slowing-down process, as the decrease in S simply influences the growth rate μ, while the presence of B does not influence the dynamics of A. (see also Appendix A).

Thus, we need to introduce an interaction between component A and the

non-growth-facilitating component B. Although complicated interactions that may involve other components could be considered, the simplest and most basic interaction that can also provide a basis for considering more complex processes would be formation of a complex between A and B given by the reaction $A + B \rightleftharpoons C$. This results in inhibition of the autocatalytic reaction for cell growth, as complex C does not contribute to the activity for the autocatalytic process. A schematic representation of the present model is shown in Fig. 4.1(a). Thus, our model is given by

$$\begin{aligned}
\frac{dS}{dt} &= -F_A(S)A - F_B(S)A + A(S_{\rm ext} - S) - \mu S \\
\frac{dA}{dt} &= F_A(S)A - G(A,B,C) - d_A A - \mu A \\
\frac{dB}{dt} &= F_B(S)A - G(A,B,C) - d_B B - \mu B \\
\frac{dC}{dt} &= G(A,B,C) - d_C C - \mu C
\end{aligned} \tag{4.2}$$

where $G(A,B,C)$ denotes the reaction of complex formation, given by $k_p AB - k_m C$. The catalytic activity of component A is inactivated due to the formation of complex C. Here, the complex has higher stability than that of other proteins (d_C is smaller than d_A and d_B)[1]
From Eq. (4.2), by summing up $\dot{A}$ and $\dot{C}$, we obtain $\dot{A}+\dot{C} = F_A(S)A(1-(A+C))$ if d_A and d_C are zero (or negligible). This means that once the cell reaches any steady state, the relationship $A + C = 1$ is satisfied as long as A and $F_A(S)$ are not zero. We use this relationship and eliminate C by substituting $C = 1 - A$ for the following analysis.

One plausible and straightforward interpretation of B is misfolded or mistranslated proteins that are produced erroneously during the replication of component A. Such waste molecules often aggregate with other molecules[101, 102, 103]. Alternatively, B components can be specific molecules such as HPF and YfiA[104, 105, 106], which inhibit catalytic activity by reacting with component A.

With regards to the formation of error or "waste" proteins, there are generally intracellular processes for reducing their fraction. These include kinetic proofreading, molecular chaperones, and protease systems. These error-correction or maintenance systems are energy-demanding, and require the non-equilibrium flow of substrates[107, 108]. Therefore, the performance of these mechanisms is inevitably reduced in a substrate (energy source)-poor environment. Thus, it naturally follows that the ratio of the synthesis of active proteins to wastes is an increasing function of the substrate concentration, i.e., $\frac{d}{dS}\frac{F_A(S)}{F_B(S)} > 0$. In the present model, we assume that this ratio increases with the concentration and becomes saturated at higher concentrations, as in Michaelis-Menenten's form, and choose $F_A(S) = \frac{vS}{K+S}\frac{S}{K_t+S}$ and $F_B(S) = \frac{vS}{K+S}\frac{K_t}{K_t+S}$, for example.

Note that almost all the results to be presented in this manuscript are obtained as long as $F_A \gg F_B$ holds for the nutrient-rich condition and $F_A \ll F_B$ for the

[1]The model equation (4.2) is non-dimensionalized by appropriate normalization.

nutrient- poor condition (see the section "Remarks on the choice of parameters to fit the experimental data" and *Supplemental Information*). Under this condition, specific choice of the form of F_A and F_B is not important.

This S-dependence of F_A/F_B would be biologically plausible both for the interpretations of component B as specific inhibitory proteins or "waste" (mistranslation) proteins. For the first interpretation, it is reported that such proteins related with the stationary phase (HPF, YfiA and others) are induced under stress condition such as starvation[104, 105, 109, 110], and thus it is suggested that $F_A \gg F_B$ ($F_A \ll F_B$) for a large (small) amount of S, repectively. On the other hand, by adopting the latter, waste, interpretation, $F_A(S)$ and $F_B(S)$ close to the above Michaelis-Menten's form is derived, by considering a proofreading mechanism to reduce the mistranslation (see also Appendix B).

Here we also note although the S-dependence of F_A/F_B is relevant to derive quantitative laws on the lag-time in agreement with experimental observation, it is not required just to show a transition to a suppressed growth state, as briefly discussed later (see Discussion).

4.2 Results

4.2.1 Growth phases

The steady state of the present model exhibits three distinct phases as a function of the external substrate concentration $S_{\rm ext}$ (Fig. 4.1(b)), as computed by its steady-state solution. The three phases are distinguished by both the steady growth rate and the concentration of component A, which are termed as the active, inactive, and death phases, as shown in Fig.4.1, whereas the growth rate shows a steep jump at the boundaries of the phases. The phases are characterized as follows. **(i)** In the active phase, the highest growth rate is achieved, where there is an abundance of component A molecules, which work freely as catalysts. **(ii)** In the inactive phase, the growth rate is not exactly zero but is drastically reduced by several orders of magnitude compared with that in the active phase. Here, almost all of the component A molecules are arrested through complex formation with component B, and their catalytic activity is inhibited. **(iii)** At the death phase, a cell cannot grow, and all of components A, B, and complexes go to zero. In this case, the cell goes beyond the so-called "point of no return" and can never grow again, regardless of the amount of increase in $S_{\rm ext}$, since the catalysts are absent in any form. (As will be shown below, the active and inactive phases correspond to the classic exponential and stationary phases; however, to emphasize the single-cell growth mode, we adopt these former terms for now).

The transition from the active to inactive phase is caused by the interaction between components A and B. In the substrate-poor condition, the amount of component B exceeds the total amount of catalytic proteins ($A + C$), and any free component A remaining vanishes. Below the transition point from the inactive to death phase, the spontaneous degradation rate surpasses the synthesis rate, at which point all of the components decrease. This transition point is simply

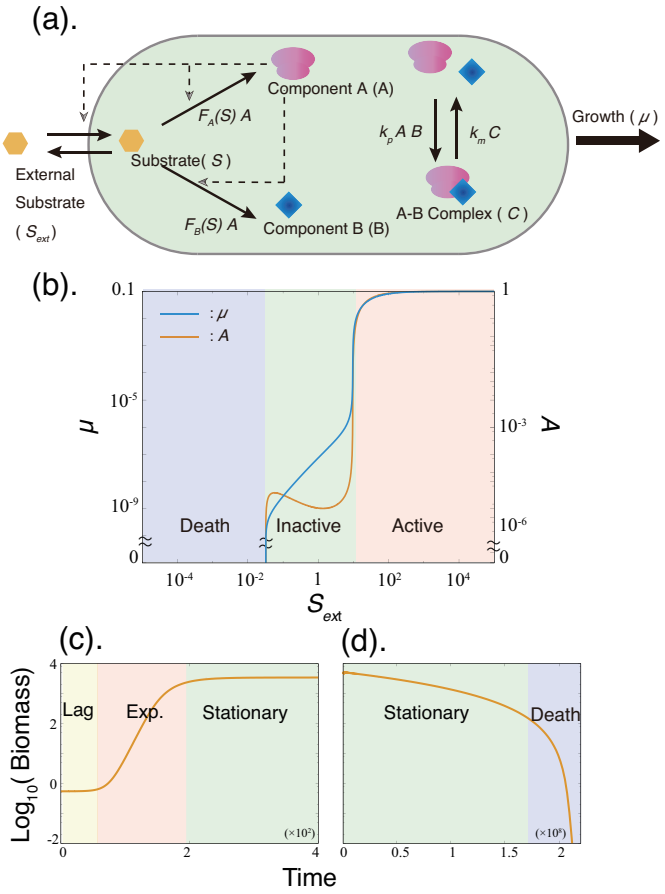

Figure 4.1: (a) Schematic representation of the components and reactions in the present model. The concentration of each chemical changes according to the listed reactions. In addition, chemicals are spontaneously degraded at a low rate, and become diluted due to volume expansion of the cell. (b) Steady growth rate and the concentration of component A are plotted as functions of the external concentration of the substrate. (c and d) Growth curve of the model. Parameters were set as follows: $v = 0.1, k_p = 1.0, k_m = 10^{-6}, K = 1.0, K_t = 10.0, d_R = d_B = 10^{-5}, d_C = 10^{-12}$. The detailed numerical method for (c) and (d) is given in Appendix C.

determined by the balance condition $F_A = d_A$. Hence, if d_A is set to zero, the inactive-death transition does not occur.

We now consider the time series of biomass (the total amount of macromolecules) that is almost proportional to the total cell number, under a condition with a given finite resource, which allows for direct comparison with experimental data obtained in a batch culture condition (Fig. 4.1(c and d)). To compute the time series of biomass, we used a model including the dynamics of S_{ext} in addition to S, A, B, and C. Details of this model are shown in Appendix C. In the numerical simulation, the condition with a given, finite amount of substrates corresponding to the increase of cell number is implemented by introducing the dynamics of the external substrate

concentration into the original model. Here, S_{ext} is decreased as the substrates are replaced by the biomass, resulting in cell growth. At the beginning of the simulation, the amount of biomass (i.e., cell number) stays almost constant, and then gradually starts to increase exponentially. After the phase of exponential growth, the substrates are consumed, and the biomass increase stops. Then, over a long time span, the biomass stays at a nearly constant value until it begins to slowly decrease. Finally, the degradation dominates and the biomass (cell number) falls off dramatically.

These successive transitions in the growth of biomass (Fig. 4.1 (c and d)) from the initially inactive phase to the active, inactive, and death phases correspond to those observed among the lag, exponential, stationary, and death phases. As the initial condition was chosen as the inactive phase under a condition of rich substrate availability, most of the component A molecules are arrested in a complex at this point. Therefore, at the initial stage, dissociation of the complex into component A and component B progresses, and biomass is barely synthesized, even though a sufficient and plentiful amount of substrate is available. After the cell escapes this waiting mode, catalytic reactions driven by component A progress, leading to an exponential increase in biomass. Subsequently, the external substrate is depleted, and cells experience another transition from the active to inactive phase. At this point, the biomass only decreases slowly owing to the remaining substrate and the stability of the complex. However, after the substrate is depleted and components A and B are dissociated from the complex, the biomass decreases at a much faster rate, ultimately entering the death phase.

In the active phase with exponential growth, the present model exhibits classical growth laws, namely **(i)** Monod's growth law, and **(ii)** growth rate vs. ribosome fraction (see Fig. 4.6).

4.2.2 Lag time dependency on starvation time T_{stv} and maximum growth rate μ_{max}

In this section, we uncover the quantitative relationships among the basic quantities characterizing the transition between the active and inactive phases; i.e., lag time, starvation time, and growth rates. We demonstrate that the theoretical predictions agree well with experimentally observed relationships.

First, we compute the dependency of lag time (λ) on starvation time (T_{stv}). Up to time $t = 0$, the model cell is set in a substrate-rich condition, $S_{\text{ext}} = S_{\text{ext}}^{\text{rich}}$, and stays at a steady state with exponential growth. Then, the external substrate is depleted to $S_{\text{ext}} = S_{\text{ext}}^{\text{poor}}$ instantaneously. The cell is exposed to this starvation condition up to starvation time $t = T_{\text{stv}}$. Subsequently, the substrate concentration S_{ext} instantaneously returns to $S_{\text{ext}}^{\text{rich}}$. After the substrate level is recovered, it takes a certain amount of time for a cell to return to its original growth rate (Fig.4.10), which is the lag time λ following the standard definition of lag time as the time period before the specific growth rate reaches its maximum value introduced by Penfold and Pirt[4, 111]. Given this, the dependency of λ on the starvation time

T_{stv} can be computed.

Next, we compute the dependency of the lag time λ on $\mu_{\max}$. We choose the steady-state solution of the cell model under $S_{\mathrm{ext}} = S_{\mathrm{ext}}^{\mathrm{poor}}$ as the initial condition and compute the lag time λ under the $S_{\mathrm{ext}} = S_{\mathrm{ext}}^{\mathrm{rich}}$ condition against different values of $\mu_{\max}(= v)$ (following the standard method to measure the relationship between λ and $\mu_{\max}$[112]).

4.2.3 Relationship between lag and starvation time: $\lambda \propto \sqrt{T_{\mathrm{stv}}}$

We found that λ increases in proportion to $\sqrt{T_{\mathrm{stv}}}$, as shown in Fig. 4.2(a). For comparison, the experimentally observed relationship between λ and T_{stv} is also plotted in Fig. 4.2(b), using reported data [93, 98, 113] that also exhibited $\lambda \propto \sqrt{T_{\mathrm{stv}}}$ dependency. Although this empirical dependency has been previously discussed[93], its theoretical origin has thus far not been uncovered.

Indeed, the origin of $\lambda \propto \sqrt{T_{\mathrm{stv}}}$ can be explained by noting the anomalous relaxation of the component B concentration, which is caused by the interaction between components A and B. A general description of this explanation is given below, and the analytic derivation is given in the *Supplementary Information*.

First, consider the time series of chemical concentrations during starvation. In this condition, cell growth is inhibited by two factors: substrate depletion and inhibition of the catalytic activity of component A. Following the decrease in uptake due to depletion of S_{ext}, the concentration of S decreases, resulting in a change in the balance between A and B (hereafter we adopt the notation such that A, B, and C also denote the concentrations of the corresponding chemicals). Under the $S_{\mathrm{ext}}^{\mathrm{poor}}$ condition, the ratio of the synthesis of B to A increases. With an increase in B, A decreases due to the formation of a complex with B. Over time, more A becomes arrested, and the level of inactivation increases with the duration of starvation.

In this scenario, the increase of the concentration of B is slow. Considering that the complex formation reaction $A + B \rightleftharpoons C$ rapidly approaches its equilibrium, i.e., $k_p AB \sim k_m C$, then A is roughly proportional to the inverse of B (recall $A + C = 1$) if B is sufficiently large. Accordingly, the synthesis rate of B, given by $F_B(S)A$, is inversely proportional to its amount, i.e.,

$$\dot{B}(t) \propto F_B(S)/B$$

, and thus

$$dB^2/dt \sim const.$$

Hence, the accumulation of component B progresses with $B(t) \propto \sqrt{t}$. (Note that due to S depletion, the dilution effect is negligible.)

Next, we consider the time series for the resurrection after recovery of the external substrate. During resurrection, A is increased while B is reduced. Since component A is strongly inhibited after starvation, the dilution effect from cell growth is the only factor contributing to the reduction of B. Noting $\mu = F_A A$ and $A \propto 1/B$, the dilution effect is given by $\mu B = F_A AB \propto B/B = const.$ at the early

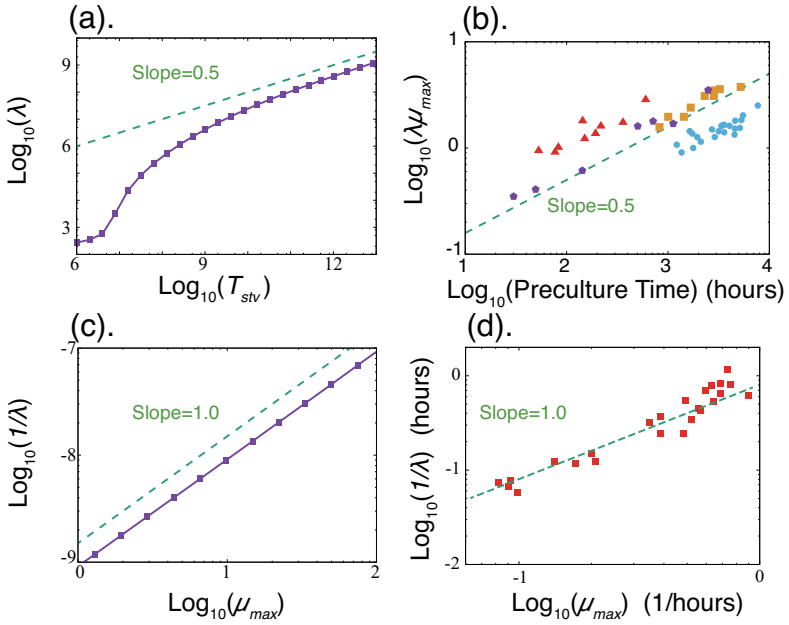

Figure 4.2: (a and b) Lag time is plotted as a function of (a) starvation time or (b) pre-incubation time. Lag time is scaled by the maximum growth rate (Inversely proportional to the shortest doubling time in the substrate-rich condition). Purple pentagons, cyan dots, and orange squares are adopted from Figures 3, 6a, and 6b of Augustin et al.[93], respectively, and the red triangles are extracted from the data in Table 1 of Pin et al.[113]. (c and d) Relationship between the lag time and maximum specific growth rate $\mu_{\max}$. Data are adopted from Table 1 of Oscar[112]. Parameters were set as follows: $S_{\text{ext}}^{\text{rich}} = 10^4, S_{\text{ext}}^{\text{poor}} = 10^{-2}, v = 0.1, k_p = 1.0, k_m = 10^{-6}, K = 1.0, K_t = 10.0$, and $d_A = d_B = d_C = 0$ (the same parameter values as in Fig. 4.1 except d_is). Lag time is computed as the time needed to reach the steady state under the $S_{\text{ext}} = S_{\text{ext}}^{\text{rich}}$ condition from an initial condition in the inactive phase. In (c), it is obtained by varying $v(= \mu_{\max})$.

stage of resurrection. Thus, the resurrection time series of B is determined by the dynamics

$$\dot{B}(t) \propto -const.,$$

leading to the linear decrease of B, i.e., $B(t) \sim B(0) - const. \times t$.

Let us briefly recapitulate the argument presented so far. The accumulated amount of component B is proportional to $\sqrt{T_{\rm stv}}$, whereas during resurrection, the dilution of B progresses linearly with time, which is required for the dissociation of the complex of A and B, leading to growth recovery. By combining these two estimates, the lag time satisfies $\lambda \propto \sqrt{T_{\rm stv}}$.

4.2.4 Relationship between the lag time and maximal growth rate: $\lambda \propto 1/\mu_{\rm max}$

Second, the relationship $\lambda \propto 1/\mu_{\rm max}$ is obtained by numerical simulation of our model, in line with experimental results [112] (Fig. 4.2(c and d)).

This relationship $\lambda \propto 1/\mu_{\rm max}$ can also be explained by the characteristics of the resurrection time series. The dilution rate of B over time is given by μB, as mentioned above; thus, at the early stage, $\dot{B} \sim -\mu B$. In the substrate-rich condition, the substrate abundances are assumed to be saturated, so that

$$\lim_{S_{\rm ext}^{\rm rich}\to\infty} \dot{B} \sim \lim_{S_{\rm ext}^{\rm rich}\to\infty} F_A \cdot B/B = \mu_{\rm max}$$

holds because $\lim_{S\to\infty} F_A(S) = \mu_{\rm max}$ is satisfied. Thus, it follows that $\lambda \propto 1/\mu_{\rm max}$.

We also obtained an analytic estimation of the lag time as

$$\lambda \sim \frac{1}{\mu_{\rm max}} \sqrt{2F_B k_p / k_m T_{\rm stv}} \tag{4.3}$$

(see the *Supplementary Information* for conditions and calculation). In this form, the two relationships $\lambda \propto \sqrt{T_{\rm stv}}$ and $\lambda \propto 1/\mu_{\rm max}$ are integrated.

4.2.5 Dependence of lag time on the starvation process

So far, we have considered the dependence of lag time on the starvation time. However, in addition to the starvation period, the starvation process itself, i.e., the speed required to reduce the external substrate, has an influence on the lag time.

For this investigation, instead of the instantaneous depletion of the external substrate, its concentration is instead gradually decreased over time in a linear manner over the span $T_{\rm dec}$, in contrast to the previous simulation procedure, which corresponds to $T_{\rm dec} = 0$. Then, the cell is placed under the substrate-poor condition for the duration $T_{\rm stv}$ before the substrate is recovered, and the lag time λ is computed [2].

[2]Here, $T_{\rm stv}$ is computed from the time point at which the external substrate concentration starts to be decreased (i.e., $T_{\rm dec} \leq T_{\rm stv}$); if it were computed from the time when the depletion is computed, a slower decrease with the increase of $T_{\rm dec}$ would effectively elongate the starvation time by itself.

The dependence of the lag time λ on $T_{\rm stv}$ and $T_{\rm dec}$ is shown in Fig. 4.3(a). While λ monotonically increases against $T_{\rm stv}$ for a given $T_{\rm dec}$, it shows drastic dependence on $T_{\rm dec}$. If the external concentration of the substrate is reduced quickly (i.e., a small $T_{\rm dec}$), the lag time is rather small. However, if the decrease in the external substrate concentration is slow (i.e., a large $T_{\rm dec}$), the lag time is much longer. In addition, this transition from a short to long lag time is quite steep.

This transition against the timescale of the environmental change manifests

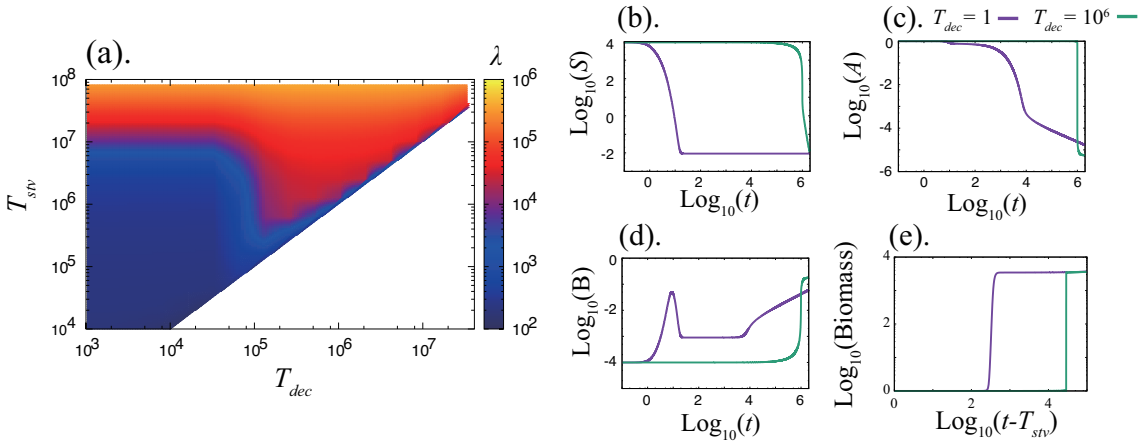

Figure 4.3: (a) Dependence of lag time λ on the time required to decrease the substrate $T_{\rm dec}$ and starvation time $T_{\rm stv}$. (b-d) Time series of starvation for different $T_{\rm dec}$ ($T_{\rm dec} = 10^6$ (green) and $T_{\rm dec} = 1.0$ (purple)) values, the internal concentrations of substrate S (b), component A (c), and component B (d). (e) Time series of biomass during resurrection. The same parameter values as indicated in Fig.4.2 were adopted. The batch culture model (which is used to compute a bacterial growth curve) was adopted to compute the time series of biomass accumulation(e).Time series of μ is shown in Fig.4.12.

itself in the time series of chemical concentrations (see Fig. 4.3(b)). With rapid environmental change, S decreases first, whereas with slow environmental change, component A decreases first. In addition, the value of component B is different between the two cases, indicating that the speed of environmental change affects the degree of inhibition, i.e., the extent to which component A is arrested by component B to form a complex.

Now, we provide an intuitive explanation for two distinct inhibition processes. When $S_{\rm ext}$ starts to decrease, a cell is in the active phase in which A is abundant. If the environment changes sufficiently quickly, there is not enough time to synthesize the chemicals A or B, because of the lack of S, and the concentrations of chemical species are frozen near the initial state with abundant A. However, if the rate of environmental change is slower than that of the chemical reaction, the concentration of B (A) increases (decreases). Hence, A remains rich in the case of fast environmental change, whereas B is rich for a slow environmental change. In the former case, when the substrate is increased again, component A molecules are ready to work, so that the lag time is short, which can be interpreted as a kind of "freeze-dry" process. Note that the difference in chemical concentration caused

by different $T_{\rm dec}$ values is maintained for a long time because in the case of slow (fast) environmental change, chemical reactions are almost completely halted due to the decrease of A (S). Thus, the difference of lag time remains even for large $T_{\rm stv}$, as shown in Fig. 4.3(a).

This lag time difference can also be explained from the perspective of dynamical systems[114]. For a given S, the temporal evolution of A and B is given by the flow in the state space of (A, B). Examples of the flow are given in Fig. 4.4. The flow depicts $(dA/dt, dB/dt)$, which determines the temporal evolution. The flow is characterized by $A-$ and $B-$ nullclines, which are given by the curves satisfying $dA/dt = 0$ and $dB/dt = 0$, as plotted in Fig. 4.4.

Note that at a nullcline, the temporal change of one state variable (either A or B) vanishes. Thus, if two nullclines approach each other, then the time evolution of both concentrations A and B are slowed down, and the point where two nullclines intersect corresponds to the steady state. As shown in Fig. 4.4, nullclines come close together under the substrate-depleting condition, which provides a dynamical systems account of the slow process in the inactive phase discussed so far.

For a fast change (i.e., small $T_{\rm dec}$, Fig. 4.4(a)), S is quickly reduced at the point where the two nullclines come close together. First, B reaches the B-nullcline quickly. Then, the state changes along the almost coalesced nullclines where the dynamics are slowed down. Thus, it takes a long time to decrease the A concentration, so that at resumption of the substrate, sufficient A can be utilized.

In contrast, for a slow change (i.e., large $T_{\rm dec}$), the flow in (A, B) gradually changes as shown in Fig. 4.4(b–d). Initially, the state (A, B) stays at the substrate-rich steady state. Due to the change in substrate concentration, two nullclines moderately move and interchange their vertical locations. Since the movement of nullclines is slow, the decrease in A progresses before the two nullclines come close together (i.e., before the process is slowed down). The temporal evolution of A and B is slowed down only after this decrease in A (Fig. 4.4(c and d)). Hence, the difference between cases with small and large $T_{\rm dec}$ is determined according to whether the nullclines almost coalesce before or after the A decrease, respectively.

These analyses allow us to estimate the critical time for a substrate decrease $T^*_{\rm dec}$ beyond the point at which λ increases dramatically. The value of a fixed point $(A_{\rm st}, B_{\rm st})$ depends on the substrate concentration, which drastically changes at the active-inactive transition point. If the relaxation to the fixed point is faster than the substrate decrease $T_{\rm dec}$, the system changes 'adiabatically' to follow the fixed point at each substrate time during the course of a "slow decrease". The relaxation time is estimated by the smallest eigenvalue around the fixed point at the transition point. In $k_m \to 0$ limit, this eigenvalue is equal to the growth rate at the active-inactive transition point. Since it is inversely proportional to v, the critical time $T^*_{\rm dec}$ for the substrate decrease is estimated as $T^*_{\rm dec} \propto 1/v$. This dependence was also confirmed numerically (Fig.4.13 in *Supplementally Information*).

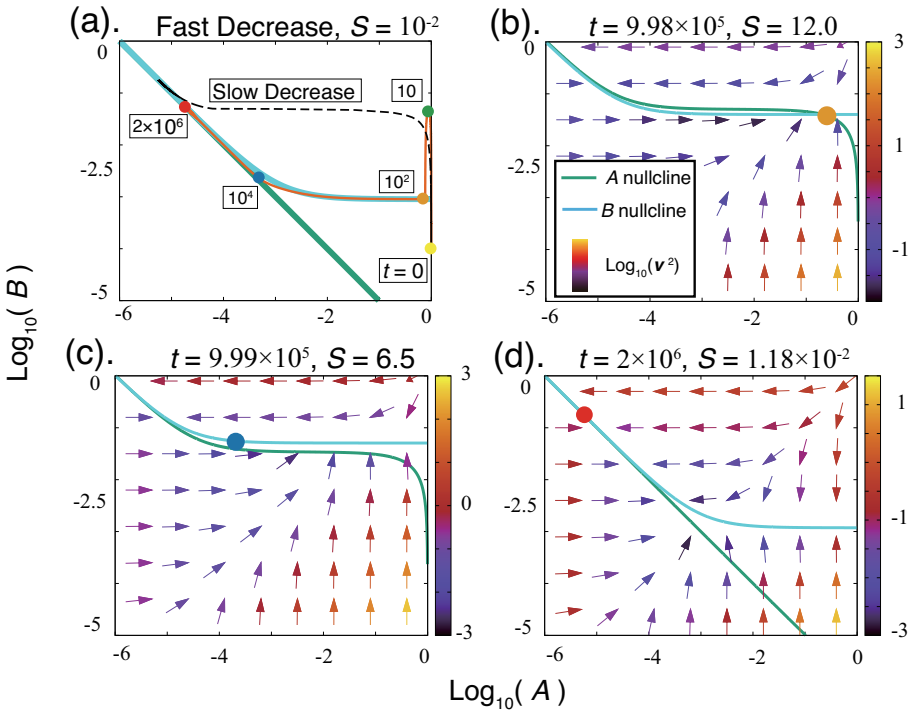

Figure 4.4: Movement of nullclines and time evolution of state variables (circles within the state space (A, B)). (a) The case of a fast substrate decrease (the orange line indicates the orbit and numbers in white boxes indicate the time points). The orbit of a slow substrate decrease is also plotted (black dashed line). (b–d) The case of a slow substrate decrease. Each point is the value of the state variable at the indicated time and substrate concentration. The vector field $\boldsymbol{v} = (dA/dt, dB/dt)$ is also depicted. Parameters are identical to those described in Fig. 4.2.

4.2.6 Distribution of lag time

So far, we have considered the average change of chemical concentrations using the rate equation of chemical reactions. However, a biochemical reaction is inherently stochastic, and thus the lag time is accordingly distributed. This distribution was computed by carrying out a stochastic simulation of chemical kinetics using the Gillespie algorithm[115].
By increasing the starvation time, two types of lag time distributions are obtained: (1) a skewed type, and (2) a skewed type with an exponential long time tail type. Each distribution type changes as follows:

(1) When the starvation time is sufficiently long, the system enters the phase with the slow accumulation of B. Here, the relaxation is anomalous, leading to a skewed type distribution. This skewed distribution is understood as follows. The number of component A molecules among cells takes on a Gaussian-like distribution just before the recovery of the external substrate concentration[3], whereas the lag time λ is proportional to B and thus to $1/A$, as discussed in last section. Then, the lag time distribution λ is obtained as the transformation of $1/A \to \lambda$ from the Gaussian distribution of component A. This results in a skewed distribution with a long time tail as shown in Fig. 4.5(a).

(2) When the starvation time is too long, the decrease in A comes to the stage where its molecular number reaches 0 or 1. This results in a long time tail in the distribution. This effect occurs when the number of component A molecules becomes zero due to the inhibition by component B. When the number of component A molecules becomes zero, the only reaction that can take place is a dissociation reaction ($C \to A + B$). Since we assume that the time evolution of molecule numbers follows a Poisson process, the queueing time of dissociation obeys an exponential distribution Prob(queueing time $= t$) $\sim N_C k_m \exp(-N_C k_m t)$, where N_C is the number of complexes formed. This exponential distribution is added to the skewed distribution, resulting in a long tail.

The distributions of the two cases are plotted in Fig. 4.5, together with experimental data adopted from[98]. The skewed distribution fits the experimental observations for the 0-day starvation data, whereas the distribution including the exponential tail is a good fit to the 1-day, 2-day, and 3-day distributions.

Here, each kinetic parameter alters the critical starvation time around which the shape of the distribution starts to change; for example, a small k_m makes it easier to obtain the type three distribution. However, kinetic parameters do not change the shape of the distribution directly as confirmed computationally.

The distribution of lag time was traditionally thought to follow the normal distribution[92, 118] until single-cell measurements for a long time span were carried out[98]. The preset model also generates the normal distribution of lag time if the starvation time is too short, whereas the normal distribution of lag time in earlier experiments would originate from the limitation of experimental procedures. For example, a cell that regains growth in a colony ends up dominating the colony, and thus the fluctuation of the shortest lag time governs the behavior.

[3]Note that the log-normal or Gamma distribution of chemicals in a cell has been well observed and mathematically explained for an exponentially growing cell[116, 117].

However, identification of the small fraction of bacteria with a long lag time is difficult owing to the limited capacity of cell tracking (as indicated in [98]).

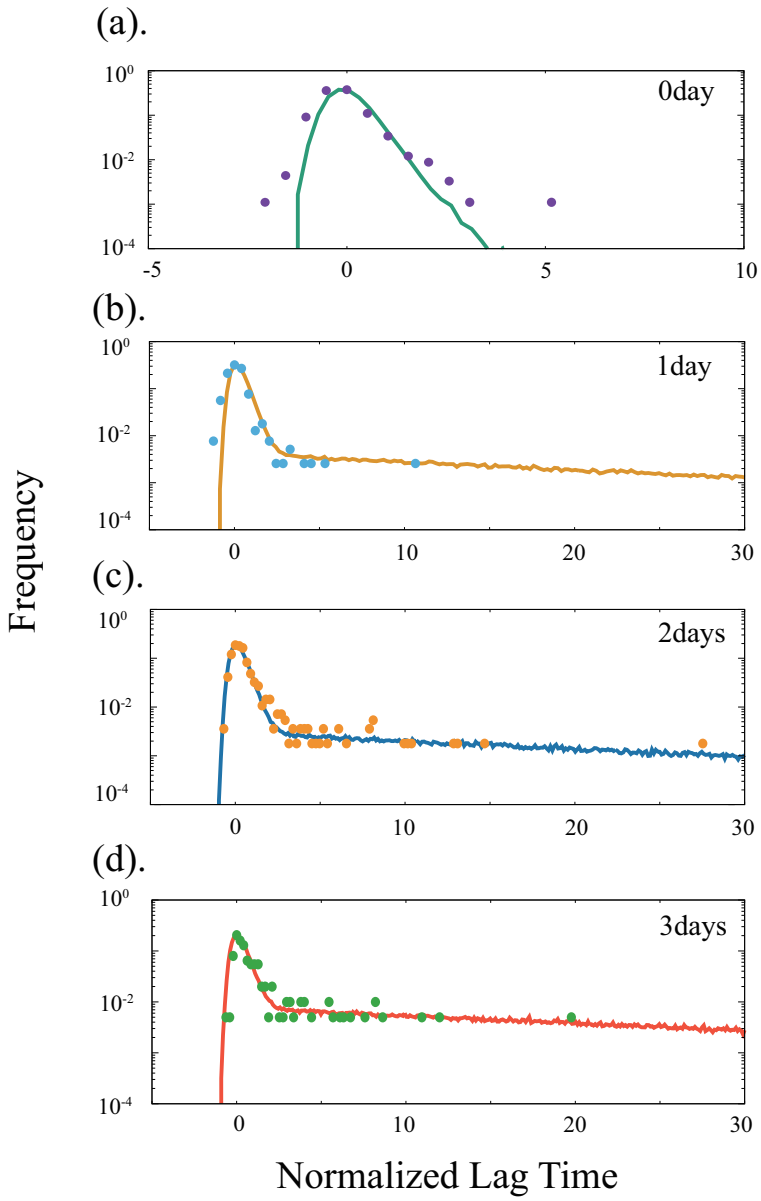

Figure 4.5: Distribution of lag time obtained by model simulation (solid line) with experimental data (lag time distribution of cultures starved for the indicated days) overlaid. The horizontal axis of each distribution was normalized by using its peak point (Peak) and the full width half maximum (FWHM) as $\lambda \rightarrow (\lambda - \text{Peak})/\text{FWHM}$. Experimental data were extracted from those presented in Fig. 1e of Reismann et al.[98]. Methods of stochastic simulations, the procedure used to compute Peak and FWHM, and parameter values are given in Appendix C.

4.2.7 Remarks on the choice of parameters to fit the experimental data

Although there are several parameters in the model and the results depend on these values, the basic results on the active-inactive transition, suppression of growth, and quantitative relationships with lag time are obtained for a large parameter region. Conditions of the parameter values to obtain these main results are given in the *Supplemental Information* and are summarized in Table 4.1. Here, an important parameter is k_m, which we assumed to be the smallest among all other parameters values. This choice was made to facilitate analytic calculations, and this condition for k_m can be relaxed. For example, we plotted the growth rate at the steady state in Fig.4.14, indicating that the active-inactive transition occurs as long as $k_m < k_p$ holds.

Next, we estimated realistic parameter values such as the value of v from the

Result	Assumption	Condition (Prediction)
Active-Inactive Transition Point	$k_m \sim 0$	$1 + 2F_A(S_{\rm st}(S_{\rm ext}^{\rm act-inact}))/k_p = \sqrt{1 + 4F_B(S_{\rm st}(S_{\rm ext}^{\rm act-inact}))/k_p}$.
Inactive-Death Transition Point	–	$F_A(S_{\rm st}(S_{\rm ext}^{\rm inact-death})) = d_A$
Analytic Estimation of Lag Time	$k_m \sim 0$, Dynamics of S is faster than (A, B)	$\lambda \sim \frac{1}{F_A(S_{\rm st}(S_{\rm ext}^{\rm rich}))}\sqrt{2F_B(S_{\rm st}(S_{\rm ext}^{\rm poor}))k_p/k_m T_{\rm stv}}$
Contiguity of Nullclines (Slow Relaxation)	-	$A_{\rm A-nullcline}(B) \sim \frac{G(0,B)}{F_A(S)-G'(0,B)}$ $A_{\rm B-nullcline}(B) \sim \frac{G(0,B)}{F_B(S)-F_A(S)B-G'(0,B)}$

Table 4.1: Predictions and Assumptions

literature. However, several parameter values could not be estimated directly from experimentally reported data because this would require quantitative studies at the stationary phase, which are not currently available. Thus, we estimated other parameter values by fitting Monod's growth law [3] as well as from the reported relationship between the ribosome fraction and growth rate[7, 119, 120] (Fig.4.6)[4]. Since the number of parameters is greater than the minimum number required to fit the two laws in Fig. 4.6, the choice of parameter values is not unique. A possible set of of parameter values is listed in Table 4.2 in Appendix D.

In fitting the two growth laws in Fig.4.6, we have also found that v is proportional

[4]Recall that Eq.(4.2) is already non-dimensionalized with appropriate scaling. To make a quantitative comparison with experimental data, we replaced each term in Eq.(4.2) as follows: $S_{\rm ext} \to m \cdot S_{\rm ext}/f_1, S \to m \cdot S/f_1, A \to m \cdot A, B \to m \cdot B, C \to m \cdot C, v \to v \cdot \psi \cdot r/(f_0 \cdot D/m), k_p \to k_p/(f_0 \cdot D), k_m \to k_m/(f_0 \cdot D/m), K \to m \cdot K/f_1, K_t \to m \cdot K_t/f_1$, and $t \to t \cdot (f_0 \cdot D/m)$, with additional parameters f_0, f_1, r, m, ψ, and D, which indicates the stoichiometry between external substrates and substrates, stoichiometry between substrates and macromolecular components (components A and B), fraction of ribosomal proteins to component A, fraction of actively translating ribosomes, volume growth per synthesis of component A, and speed of the $S_{\rm ext} \rightleftharpoons S$ reaction, respectively. To fit the experimental data, we adopt an interpretation that the external substrate, substrate, and both components A and B correspond to glucose, amino acids, and proteins, respectively. Thus, we adopt the stoichiometry between glucose and amino acids, that between amino acids and typical (average size of) proteins, and that between amino acids and ribosomal proteins as f_0, f_1, and f_2, respectively. To compare with the data of [7, 119, 120], the ribosomal fraction ϕ is defined as $\phi = \psi \frac{f_2}{f_1} \frac{A+C}{A+B+2C}$.

to the maximum growth rate and negatively correlates to the slope of the linear relationship between ribosome fraction and growth rate, while r (the fraction of actively translating ribosome) decreases and k_p increases the y-offset of the linear relation, respectively [5].

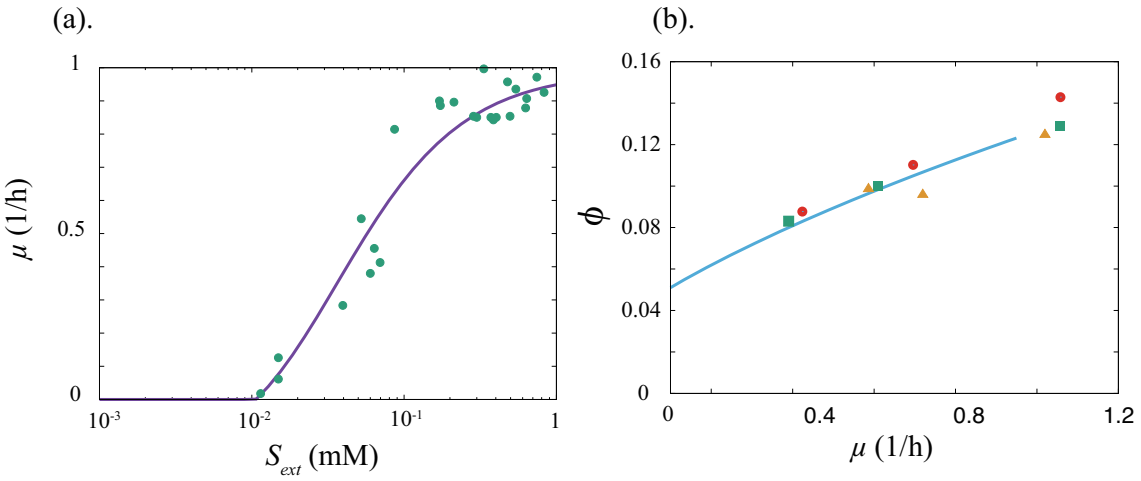

Figure 4.6: Comparison of the model results using estimated values (Table 4.2) with experimental values. (a) The specific growth rate is plotted as a function of the external substrate (glucose) concentration. Experimental data are adopted from Monod[3]. (b)Fraction of ribosomal proteins (component A) to total proteins as a function of the specific growth rate: orange squares are from Scott et al.[7], red circles are from Bremer and Dennis[119], and green triangles are from Forchhammer et al.[120]. In (b), the theoretical curve from the model is plotted up to ~ 1.0, because we obtained the parameter values by fitting the $\mu - \phi$ relation and the Monod equation with the maximum growth rate of $\mu_{\max} \sim 1.0$.

4.3 Discussion

Here, we developed a coarse-grained model consisting of a substrate, autocatalytic active protein (component A), non-growth-facilitating component (component B), and A-B complex, C. In the steady state, the model shows distinct phases, i.e., the active, inactive, and death phases. In addition, the temporal evolution of total biomass is consistent with the bacterial growth curve. The present model not only satisfies the already-known growth laws in the active phase but also demonstrates two relationships, $\lambda \propto \sqrt{T_{\rm stv}}$ and $\lambda \propto 1/\mu_{\max}$, concerning the duration of the lag time λ. Although these two relationships have also been observed experimentally, their origins and underlying mechanisms had not yet been elucidated. The present model can explain these relationships based on the formation of a complex between

[5] Addition of antibiotics may correspond to the increase in k_p in our model, while Scott et al.[7] showed experimentally that addition of antibiotics increases the y-offset of the linear relation.

components A and B, whose increase in the starvation condition hinders the catalytic reaction.
The above two laws are also generally derived for the inactive phase, which corresponds to the stationary phase, as long as the ratio of the synthesis of component B to that of component A is increased along with a decrease in the external substrate concentration. This condition can also be interpreted as a natural consequence of the waste-reducing (or error-correcting) process that is ubiquitous in a cell, which demands energy when assuming that component B consists of waste molecules. These laws are also derived if the waste is interpreted as a product of erroneous protein synthesis, where a proofreading mechanism to correct the error, which also requires energy, works inefficiently in a substrate-poor condition. The inhibition of growth by waste proteins is experimentally discussed by Nucifora et al. and others[101, 102, 103]. Aggregation of such waste proteins can inhibit the catalytic activity of proteins, although its role in the transition to the inactive phase remains to be elucidated. Alternatively, instead of waste proteins, we can also interpret such non-autocatalytic proteins as specific inhibitory molecules binding ribosomes such as YfiA and HPF [104, 105, 106].

For a simpler model, one could eliminate the substrate dependence of $F_B(S)/F_A(S)$. Indeed, even in this simpler form, the active/inactive transition itself is observed if we tune the parameter values finely, as the decrease in substrate flow decreases the dilution, which in turn increases the fraction of complexes formed. Nevertheless, the accumulation of non-autocatalytic proteins is not facilitated with a substrate decrease, and the increase in the lag time as $\lambda \propto \sqrt{T_{\rm stv}}$ does not follow. Hence, this simpler model will not be appropriate to explain the behavior of the present cells, although it might provide relevant insight as a general mechanism for the "inactive" or "dormancy" phase in the context of protocells.

Although the cell state with exponential growth has been extensively analyzed in previous theoretical models, the transition to the phase with suppressed growth has thus far not been theoretically explained. Our model, albeit simple, provides an essential and general mechanism for this transition with consideration of the complex formation between components A and B, which can be experimentally tested.

The model here may also be relevant to study growth arrest such as stringent response[121, 122]. There, ppGpp, the effector molecule of the stringent response, is known to destabilize the open complex of all promoters causing the global reduction of macromolecular synthesis, playing the similar role as the component B in this chapter[123, 124, 125, 126]. Additionally, rpoS, sigma factor of stationary-phase genes, lies downstream of ppGpp[127], and it is reported that the mutant lacking ppGpp (which might correspond to inhibition of the component B in our model) shows a physiological state reminiscent of exponentially growing bacteria even under starvation [128].

Moreover, the model predicts that the lag time differs depending on the rate of external depletion of the substrate, which can also be examined experimentally. Recently, the bimodal distribution of growth resumption time from the stationary phase was reported in a batch culture experiment[99]. The heterogeneous depletion of a substrate due to the spatial structure of a bacterial colony is thought to

be a potent cause of this bimodality, and progress toward gaining a deeper understanding of this concept is underway. Since the present model shows different lag times for different rates of environmental change, it can provide a possible scenario for helping to explain this bimodality.

4.4 Appendix A: Model without interaction between the two components

To clarify the necessity of the interaction between the two components to obtain the main results, we remove the complex formation between A and B (by setting k_p and k_m to be zero). Then, the A-B complex is eliminated, and our model is given as

$$\dot{A} = F_A(S)A - F_A(S)A^2 - d_A A, \tag{4.4}$$
$$\dot{B} = F_B(S)A - F_A(S)AB - d_B B. \tag{4.5}$$

(We assume that the internal concentration of the substrate is equal to that of the external concentration of the substrate, and ignore the substrate dynamics.) The steady solution is

$$A_{st} = 1 - \frac{d_A}{F_A(S)}, \quad B_{st} = F_B(S)\frac{1 - d_A/F_A(S)}{F_A(S) - d_A + d_B},$$

and the steady growth rate is given as $\mu_{st} = F_A(S)A_{st} = F_A(S) - d_A$. Therefore, the present model without an interaction between components A and B exhibits only the active-death transition at S^*, satisfying $F_A(S^*) = d_A$.
In addition, the dynamics of the system are calculated as

$$A(t) = \frac{1}{1 - \exp(-F_A t)(1 - A(0)^{-1})}$$
$$B(t) = \frac{F_B}{F_A}\frac{1 - \exp(-F_A t)(1 - \frac{B(0)F_A}{A(0)F_B})}{1 - \exp(-F_A t)(1 - A(0)^{-1})},$$

where we neglect d_i. Therefore, if the model cell Eq. (4.5) restarts growth in a high S (S_{rich}) value environment after exposure to the starvation condition (low S value), $A(t)$ and $B(t)$ exponentially converge to the substrate-rich steady state. Hence the time for growth recovery $T_{\rm rec}$ is quite short, which is calculated

$$T_{\rm rec} = \frac{1}{F_A(S_{rich})}\ln\left(\left(\frac{B_p}{B_r} - 1\right)(1 - e^{-F_A(S_{poor})T_{\rm stv}})\right) + const.,$$

as a function of starvation time $T_{\rm stv}$. Here, B_p and B_r are the steady concentrations of component B under the substrate-poor and substrate-rich environment, respectively. Obviously this relationship is far from the relationship between lag and startvation time.

4.5 Appendix B: Reduction of the kinetic proofreading model

In the main text, the concrete forms of F_A and F_B were predetermined by assuming the characteristic $\frac{d}{dS}(F_A/F_B) > 0$, which is essential for the active-inactive transition. In this section, we show that this characteristic is derived from a simple polymer elongation model with a kinetic proofreading scheme[108] by assigning a correct polymer as A and an erroneous one as B. Indeed, $\frac{d}{dS}(F_A/F_B) > 0$ originates from an error in the synthesis of component A that consequently inhibits the synthetic reactions.

Polymer elongation is essential to synthesize macromolecules. It is well known that ribosomes elongate a polypeptide chain following receipt of the information from messenger RNA. However, since the transfer RNA (tRNA) discrimination by a ribosome is not perfect, there is always a certain probability for mistranslation (i.e., the wrong choice of tRNA). Kinetic proofreading is one of the possible error-correction mechanisms in such a polymerization system, which demands energy. We derive that the synthesis ratio of mistranslated proteins to a "correct" protein increases under the substrate-depleting condition.

For the polymerization reaction, we introduce two monomers, "correct" and "wrong" monomers, as simplified from real amino acids. In reality, there are 20 amino acids and one tRNA that specifies one amino acid, i.e., one correct and 19 wrong monomers with a certain affinity lower than that of the correct monomer.

In the model, a polymer is elongated up to the length L with the aid of the catalytic activity of the "correct" protein, i.e., the ribosome. The matured polymer with length L is spontaneously folded into a protein; the proteins consisting of only correct monomers are correct proteins with catalytic activity, whereas those with other monomer sequences turn into mistranslated proteins. The elongation process progresses under a kinetic proofreading mechanism (Fig. 4.7).

As in the original model, mistranslated proteins inhibit the correct protein's catalytic activity by forming a complex with it, while the growth is facilitated by the activity of correct proteins.

The dynamics of the polymer elongation part are given by

$$
\begin{aligned}
\frac{d[A_i(x)]}{dt} &= -\hat{k}_0 \sum_{Y=C,D} ([A_i(x)][M_Y] - \rho_Y \hat{l}_0 [A_i(x)M_Y]) \\
&- \hat{k}_2 \sum_{Y=C,D} ([A_i(x)][M_Y] - \rho_Y \hat{l}_2 [A_i(x)M_Y^*]) \\
&+ \hat{v}[A_{i-1}(x^-)M^*_{\mathrm{ter}(x)}], \quad (1 \le i \le L-1) \\
\frac{d[A_i(x)M_Y]}{dt} &= \hat{k}_0([A_i(x)][M_Y] - \rho_Y \hat{l}_0 [A_i(x)M_Y]) \\
&- \hat{k}_1([A_i(x)M_Y]\alpha - \hat{l}_1 [A_i(x)M_Y^*]\beta), \quad (0 \le i \le L-1) \\
\frac{d[A_i(x)M_Y^*]}{dt} &= \hat{k}_1([A_i(x)M_Y]\alpha - \hat{l}_1 [A_i(x)M_Y^*]\beta) + \hat{k}_2([A_i(x)][M_Y] - \rho_Y \hat{l}_2 [A_i(x)M_Y^*]) \\
&- \hat{v}[A_i(x)M_Y^*] \quad (0 \le i \le L-1),
\end{aligned}
$$

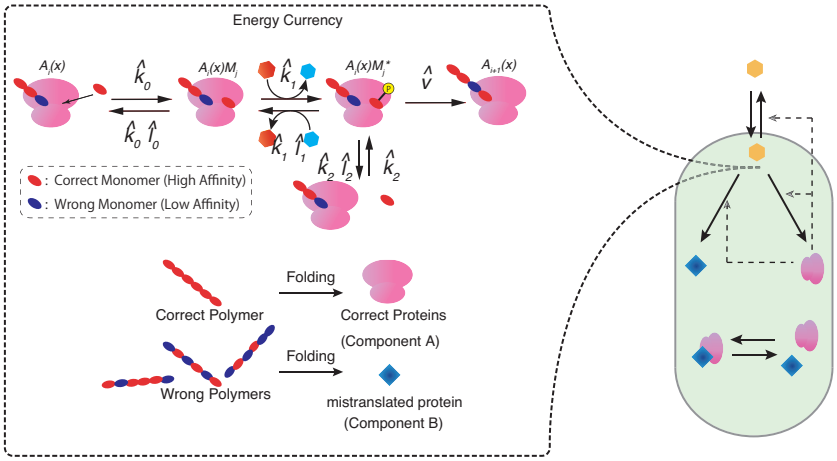

Figure 4.7: Schematic representation of a polymer elongation system with kinetic proofreading. The reactions other than the synthesis part ($F_A(S)A$ and $F_B(S)A$) are identical to those of the original model (4.2).

where $[M_C]$ and $[M_D]$ denote the concentrations of correct and wrong monomers, respectively. $[A_i(x)], [A_i(x)M_Y]$, and $[A_i(x)M_Y^*]$ represent the concentration of a complex of correct proteins and a polymer with length i, a correct protein-polymer-monomer complex, and an activated correct protein-polymer-monomer complex, respectively, where x denotes a monomer sequence such as $CCDC\cdots$, with C and D indicating the correct and wrong monomer, respectively. $\mathrm{ter}(x)$ and x^- indicate the last monomer (C or D) of a monomer sequence x and the partial monomer sequence of x from which the last monomer (i.e., $\mathrm{ter}(x)$) has been removed, respectively. Here, $[A_0]$ denotes the concentration of the correct protein. $\hat{v}$ and $\hat{k}_i$s are the rate constants of the chemical reactions, and the $\hat{l}_i$s are the Boltzman factors of each chemical reaction. We assume that dissociation of the matured polymer from correct proteins and polymer folding into proteins take place instantaneously. α and β are the concentration energy currencies, for example, GTP and GDP, respectively. ρ_i reflects the difference in affinity between the wrong monomer (D) and the correct monomer (C) (we set ρ_C as unity).

At the steady state, the synthesis rates of correct and mistranslated proteins, J_{A}^L and J_{B}^L, are given by

$$\begin{aligned} J_{\mathrm{A}}^L &= \hat{v}[A_0][M_C]H_C\Xi_C^{L-1} \\ J_{\mathrm{B}}^L &= \hat{v}[A_0](H_C[M_C]+H_D[M_D])(\Xi_C+\Xi_D)^{L-1} - J_{\mathrm{A}}^L, \end{aligned}$$

where functions Ξ_i and H_i are given by

$$\begin{aligned}
\Xi_i &= \frac{\hat{v}H_i[M_i]}{\hat{k}_0\sum_j(1-\rho_j\hat{l}_0Z_j[M_j])+\hat{k}_2\sum_j(1-\rho_j\hat{l}_2H_j[M_j])} \\
H_i &= \frac{\hat{k}_2(\hat{k}_1\alpha+\hat{k}_0\rho_i\hat{l}_0)+\hat{k}_0\hat{k}_1\alpha}{(\hat{k}_1\alpha+\hat{k}_0\rho_i\hat{l}_0)(\hat{k}_1\hat{l}_1\beta+\hat{k}_2\rho_i\hat{l}_2+\hat{v})-\hat{k}_1^2\hat{l}_1\alpha\beta} \\
Z_i &= \frac{\hat{k}_0+\hat{k}_1\hat{l}_1\beta H_i}{\hat{k}_0\rho_i\hat{l}_0+\hat{k}_1\alpha}
\end{aligned}$$

Ξ_0 and Ξ_1 denote the rate of polymer elongation with the wrong and correct monomers, respectively.

Now, we set the functional form of α and monomer concentrations $[M_C]$ and $[M_D]$ to obtain the concrete values of $J_{\rm c}^L$ and $J_{\rm w}^L$. It is natural to assume that α and $[M_i]$ are increasing functions of the internal substrate concentration $[S]$. Here, we adopt a Michaelis-Menten's type form $\alpha = [S]/(K_a+[S])$, $\beta = K_a/(K_a+[S])$, and $[M_C] = [M_D] = [M]_{\max}[S]/(K_S+[S])$.

Although $J_{\rm A}^L([S])$ and $J_{\rm w}^L([S])$ do not completely agree with the form we adopted for $F_A(S)A$ and $F_B(S)A$ in the original model, the conditions discussed in Section 2 of the Supplementary Information are nevertheless satisfied, as shown in Fig. 4.8. In particular, $\frac{d}{d[S]}J_{\rm A}^L/J_{\rm B}^L > 0$ holds. Indeed, using this model, we obtained the same active, inactive, and death phases, as well as the same growth curve and other quantitative laws. As an example, Fig. 4.9 shows the steady growth rate as a function of the external substrate concentration $[S]_{\rm ext}$. Furthermore, for any L, the same behaviors are obtained, as $J_{\rm A}^L$ and $J_{\rm B}^L$ satisfy the condition outlined in Section 2 of the Supplementary Information. It is also confirmed that the ratio of $J_{\rm A}^L([S])$ to $J_{\rm B}^L([S])$ increases as $[S]$ increases for any L.

4.6 Appendix C: Details of Models and Simulation Procedures

To obtain the growth curve shown in Fig. 1(c) and (d), we added the dynamics of the substrates in the external environment, as well as cell volume growth. By representing the dynamics according to the amounts of chemicals rather than their

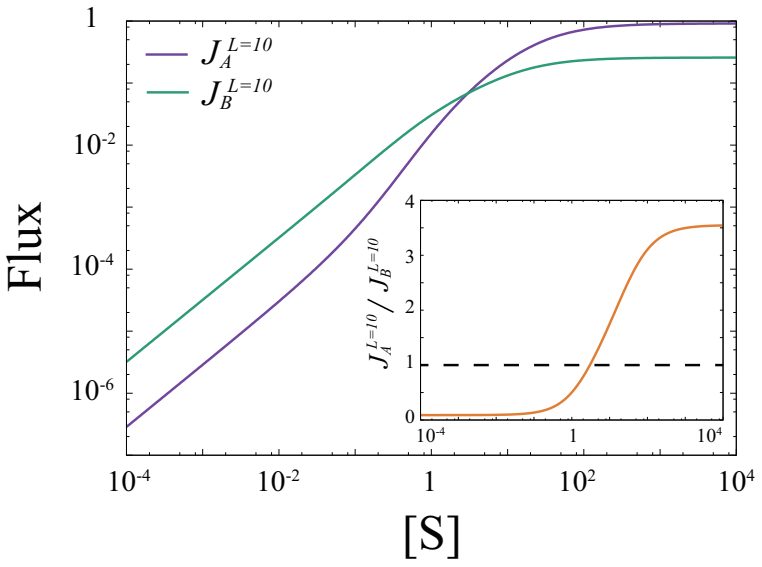

Figure 4.8: $J_{\mathrm{A}}^{L=10}$ and $J_{\mathrm{B}}^{L=10}$ are plotted against the substrate concentration $[S]$. The ratio of $J_{\mathrm{A}}^{L=10}$ to $J_{\mathrm{B}}^{L=10}$ is also plotted in the inset of the figure. Parameters for the polymer elongation part are set to be $\hat{v} = 0.1, \rho_C = 1.0, \rho_D = 10.0, \hat{k}_0 = 10^5, \hat{k}_1 = 10^2, \hat{k}_2 = 10.0, \hat{l}_0 = \hat{l}_1 = \exp(-1), \hat{l}_2 = \exp(1), K_a = 10.0, K_S = 1.0, [M]_{\max} = 1.0$, and $[A_0] = 1.0$.

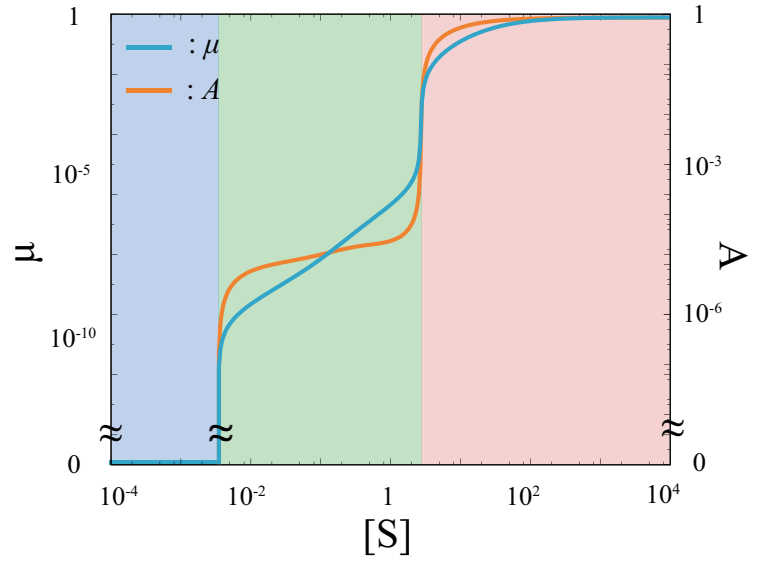

Figure 4.9: Steady growth rate of the model with polymerization and kinetic proofreading. $J_{\mathrm{A}}^{L=10}$ and $J_{\mathrm{B}}^{L=10}$ are adopted for the synthetic reaction rate of components A and B. Parameters for $J_{\mathrm{A}}^{L=10}$ and $J_{\mathrm{B}}^{L=10}$ are identical to those in Fig. 4.8, and others are set to be the same.

concentrations, the model is given by

$$\frac{dN_{S_{\rm ext}}}{dt} = -N_A(N_{S_{\rm ext}}/V_{\rm bath} - N_S/V) \tag{4.6}$$
$$\frac{dN_S}{dt} = -F_A(N_S/V)N_A - F_B(N_S/V)N_P + N_A(N_{S_{\rm ext}}/V_{\rm bath} - N_S/V) \tag{4.7}$$
$$\frac{dN_A}{dt} = F_A(N_S/V)N_A - k_pN_AN_B/V + k_mN_C - d_AN_A \tag{4.8}$$
$$\frac{dN_B}{dt} = F_B(N_S/V)N_A - k_pN_AN_B/V + k_mN_C - d_BN_B \tag{4.9}$$
$$\frac{dN_C}{dt} = k_pN_AN_B/V - k_mN_C - d_CN_C \tag{4.10}$$
$$\frac{dV}{dt} = F_A(N_S/V)N_A, \tag{4.11}$$

where $N_{S_{\rm ext}}$ is the amount of substrate in the external environment at volume $V_{\rm bath}$, and N_S, N_A, N_B, and N_C are the amounts of each chemical within the cell at volume $V(t)$, respectively. $V(t)$ is the volume of a cell. The dilution effect is introduced by dividing the amount of each chemical by $V(t)$. $S_{\rm ext}$ is the total amount of the external substrate contained in the culture system with volume $V_{\rm bath}$ (set to be unity). For all other parameters, the same values as shown in Fig. 4.1 were adopted.

To obtain the lag time distribution, we performed a stochastic simulation. We computed the model equation according to the volume change

$$\frac{dN_S}{dt} = -F_A(N_S/V)N_A - F_B(N_S/V)N_A + N_A(N_{S_{\rm ext}}/V_{\rm bath} - N_S/V) \tag{4.12}$$
$$\frac{dN_A}{dt} = F_A(N_S/V)N_A - k_pN_AN_B/V + k_mN_C \tag{4.13}$$
$$\frac{dN_B}{dt} = F_B(N_S/V)N_A - k_pN_AN_B/V + k_mN_C \tag{4.14}$$
$$\frac{dN_C}{dt} = k_pN_AN_B/V - k_mN_C \tag{4.15}$$
$$\frac{dV}{dt} = F_A(N_S/V)N_A. \tag{4.16}$$

Here, we introduced cell division and simulated the dynamics of only one daughter cell (to reduce the simulation time). When the cell volume V reaches the division volume $V_{\rm div}$, V halves and chemicals are distributed to two doughter cells in equal probability. After computing these equations for a sufficiently long time under the $N_{S_{\rm ext}^{\rm rich}}$ condition, $N_{S_{\rm ext}}$ suddenly changed to $N_{S_{\rm ext}^{\rm poor}}$, and was then set at this value over the starvation period $T_{\rm stv}$. Then, $N_{S_{\rm ext}}$ returned to the original value $N_{S_{\rm ext}^{\rm rich}}$. The lag time λ is computed as the time needed to double the volume from V_0; i.e., the volume at which $S_{\rm ext}$ recovers. The numerical results indicated that the absolute value of the correlation coefficient between V_0 and λ is small. Here, the difference in V_0 in cells does not affect the distribution of the lag time. Stochastic simulation was carried out using the Gillespie algorithm. Parameter values were set to be $V_{\rm div} = 2 \times 10^3, V_{\rm bath} = 1.0, N_{S_{\rm ext}^{\rm rich}} = 10^4, N_{S_{\rm ext}^{\rm poor}} = 10^{-3}$, and the others

were the same as those described in Fig. 4.2. The length of starvation time T_{stv} was set to be $5 \times 10^4, 10^6, 2 \times 10^6$, and 10^7 for Fig. 4.5 (a), (b), (c), and (d), respectively.
From the lag time distribution obtained by numerical simulation, we could compute the peak and FWHM values directly. Since the experimental data did not include a sufficient amount of samples, we applied a smoothing filter to determine the FWHM, while the peak point was determined directly.

4.7 Appendix D: Estimated parameter values

Symbol	Meaning	Estimated Value (Unit)	Reference
f_0	Stoichiometry of glucose and amino acids (measured by carbon, average)	1.1(-)	[129]
f_1	Stoichiometry of amino acids and average proteins	209(-)	[8]
f_2	Stoichiometry of amino acids and ribosomal protein	7336(-)	[7]
v	synthesis rate of protein per ribosome 20(a.a/sec)$/209$(a.a) $\times 3600$(sec)	345 (1/hour)	[7, 8]
m	volume growth per synthesis of growth factor $1.0\mu m^3$ (*E. Coli* volume) divided by 5×10^5 (# of proteins)	1.2×10^{-2} (1/mM)	[8]
r	Fraction of actively translating ribosomes	0.8 $(-)$	[119]
ψ	Fraction of ribosomal proteins to component A	$3.6 \times 10^{-3}(-)$	Fitting
D	Speed of phenomenological catabolism	10^5(1/mM/hour)	Fitting
K	Saturation constant of $F_A + F_B$	1.8×10^{-2}(mM)	Fitting
K_t	Phenomenological constant changing A/B balance	2.3×10^{-2}(mM)	Fitting
k_p	Rate of association between A and B	10^{-3}(1/mM/hour)	Fitting
k_m	Rate of dissociation between A and B	10^{-6}(1/hour)	Fitting

Table 4.2: Estimated parameter values

4.8 Supplemental Information

4.8.1 Analytic estimation of lag time λ

Here, we are not concerned with the death process, which occurs over a much longer time scale. Hence, we assume that the spontaneous degradation rates d_A, d_B, and d_C are negligibly small and are thus set to be zero. Therefore, the

model equation is given by

$$\begin{aligned}
\frac{dS}{dt} &= -F_A A - F_B A + A(S_{\text{ext}} - S) - F_A AS \\
\frac{dA}{dt} &= F_A A - k_p AB + k_m C - F_A A^2 \\
\frac{dB}{dt} &= F_B A - k_p AB + k_m C - F_A AB \\
\frac{dC}{dt} &= k_p AB - k_m C - F_A AC
\end{aligned}$$

From the above equations, we obtain

$$\frac{d}{dt}(A + C) = F_A(S)A(1 - (A + C)). \tag{4.17}$$

Eq. (4.17) implies that once the model (4.17) reaches a steady state, the sum of A and C cannot be altered by any parameter. Thus, the concentrations of A and C change over time while maintaining $A + C = 1$, even if the external substrate concentration S_{ext} is changed. Thus, C is substituted by $1 - A$ and can be eliminated in the calculation below.

Relationship between the initial value and lag time

First, we calculate the relaxation time from an initial starved condition (S_0, A_0, B_0) to the substrate-rich steady state (S_1, A_1, B_1). Considering the present setup of the model, the following three conditions are assumed:

- A and B relax after the relaxation of S, and the substrate uptake part $A(S_{\text{ext}} - S)$ is dominant in the dynamics of S.
- The cell is initially in the inactive phase. As a result, the concentration of component B exceeds a certain value B^*_{rich}, where $B^*_{\text{rich}} = F_A(S_1)/k_p$.
- Dissociation of the A-B complex hardly ever occurs, i.e., k_m is the smallest parameter among all parameters.

It has been experimentally confirmed that the uptake of a substrate occurs at the very beginning of growth resurrection[92], and the relaxation of S and (A, B) are separated in the numerical simulation (Fig.4.10). Note that the initial state (S_0, A_0, B_0) does not need to be the steady state under the substrate-poor condition.

Under these conditions, we first estimate the relaxation time of S. According to the assumptions, A is fixed to A_0 during the relaxation of S, while the dominant part of the change in S is given by its uptake, so that $\dot{S}$ is approximated by

$$\dot{S} \sim A_0(S^{\text{rich}}_{\text{ext}} - S).$$

Then, the relaxation time λ_S is obtained by solving this equation with $S(0) = S_0, S(\lambda_S) = S_1$ as

$$\lambda_S \sim \frac{1}{A_0} \ln\left(\frac{S_{\text{ext}}^{\text{rich}} - S_0}{S_{\text{ext}}^{\text{rich}} - S_1}\right)$$

. Next, we estimate the relaxation time of A and B, where S is fixed at the steady value S_1 throughout the estimation. We adiabatically eliminate the dynamics of A, in order to represent A as a function of B, $A = A(B)$, obtained by $\dot{A} = 0$. (In other words, the relaxation progresses along the A null cline, as validated later). Then, from the assumption of a small k_m, we get

$$\frac{dB}{dt} = -k_m \frac{(F_A - F_B + F_A B)}{k_p B - F_A} + \mathcal{O}(k_m^2), \tag{4.18}$$

where the last term is neglected below. This expression is valid in the region $B_{\text{rich}}^* < B$, i.e., $k_p B > F_A(S_1)$. As will be shown later, the concentration of component B changes linearly with time, and this relaxation is much slower than that observed in the exponential relaxation region with $B_{\text{rich}}^* > B$. By integrating $B(t)$ from $t = 0$ to $t = \lambda_B$ with the condition $B(0) = B_0$ and $B(\lambda_B) = B_{\text{rich}}^*$, the relaxation time λ_B is obtained as

$$\lambda_B \sim \frac{K_A}{F_A}\left\{(B_0 - B_{\text{rich}}^*) - \left(1 + \frac{1}{k_p F_A} - \frac{F_B}{F_A}\right) \ln\left(\frac{F_A(1 + B_0) - F_B}{F_A(1 + B_{\text{rich}}^*) - F_B}\right)\right\}, \tag{4.19}$$

where $K_A = k_p/k_m$. Recalling that k_m is the smallest parameter, and accordingly $K_A \gg 1$ and $\lambda_S \ll \lambda_B$, the relaxation time λ is approximated as $\lambda \approx \lambda_B$. Here, we assume $F_B/F_A \sim 0$, then

$$\lambda_B \sim \frac{K_A}{F_A}\left\{(B_0 - B_{\text{rich}}^*) - \left(1 + \frac{1}{k_p F_A}\right) \ln\left(\frac{1 + B_0}{1 + B_{\text{rich}}^*}\right)\right\} \tag{4.20}$$

holds. Since we consider the asymptotic behavior of lag time λ under a sufficiently long starvation time T_{stv}, $B_0 \gg B_{\text{rich}}^*$ holds. Therefore, the second term in Eq. (4.20) with logarithmic dependence is neglected as compared to the linear part, and $(B_0 - B_{\text{rich}}^*)$ is approximated as B_0. Thus, we obtain a simple relationship between the initial amount of component B and the lag time given by

$$\lambda \sim \frac{K_A}{F_A(S_1)} B_0. \tag{4.21}$$

Relationship between accumulation of component B and starvation time

In this section, we estimate the relationship between the accumulation of component B and starvation time, i.e., the relationship between B_0 and T_{stv}. The initial point is set at the steady state under the substrate-rich condition (S_1, B_1, A_1). As discussed in the previous subsection, the relaxation of S is fast, so that the time required for this relaxation is negligible. Using Eq. (4.18) and

noting $F_A(S_0) \ll F_B(S_0)$, i.e., the ratio of the synthesis of component B to that of component A is larger under the substrate-poor condition, we get

$$\frac{dB}{dt} \sim \frac{F_B}{K_A B}. \tag{4.22}$$

The solution with the initial condition $B(0) = B^*_{\rm poor} = F_A(S_0)/k_p$ is given by

$$B(t) \sim \sqrt{2\frac{F_B(S_0)}{K_A}t + \frac{F_A(S_0)}{k_p}}.$$

As $F_A(S_0)/F_B(S_0) \approx 0$, its solution is obtained as

$$B(t) \sim \sqrt{2\frac{F_B(S_0)}{K_A}t} \tag{4.23}$$

Substituting Eq. (4.23) into Eq.(4.21) with $t = T_{\rm stv}$, we get

$$\lambda \sim \frac{1}{F_A(S_1)}\sqrt{2F_B(S_0)K_A T_{\rm stv}}. \tag{4.24}$$

Thus, the lag time increases with the square root of starvation time.

In addition, since $\lim_{S\to\infty} F_A(S) = \mu_{\rm max}$ holds, the relationship between lag time and the maximum specific growth rate $\mu_{\rm max}$ is obtained as

$$\begin{aligned}\lim_{S^{\rm rich}_{\rm ext}\to\infty} \lambda &\sim \lim_{S^{\rm rich}_{\rm ext}\to\infty} \frac{1}{F_A(S_1)}\sqrt{2F_B(S_0)K_A T_{\rm stv}} \\ &= \frac{1}{\mu_{\rm max}}\sqrt{2F_B(S_0)K_A T_{\rm stv}}\end{aligned} \tag{4.25}$$

Recall that to derive the relationship $\lambda \propto \sqrt{T_{\rm stv}}$, only the assumption $F_A(S_0) \ll F_B(S_0)$ and $F_A(S_1) \gg F_B(S_1)$ is required here, while to derive $\lambda \propto 1/\mu_{\rm max}$, only $\lim_{S\to\infty} F_A(S) = \mu_{\rm max}$ is needed. Thus, these relationships hold irrespective of the detailed function form of F_is. For example, we can chose a form close to step function for F_is.

Finally, we confirm that the relaxation between (A_0, B_0) and (A_1, B_1) occurs along the A null cline. For this purpose, we calculate the difference between $\dot{A}/A$ and $\dot{B}/B$.

Fig.4.11 is a phase diagram dividing (A, B) space into the regimes with

$$\left(\frac{\dot{A}}{A}\right)^2 > \left(\frac{\dot{B}}{B}\right)^2$$

and

$$\left(\frac{\dot{A}}{A}\right)^2 < \left(\frac{\dot{B}}{B}\right)^2.$$

The figure demonstrates that the former region occupies the greatest area in (A, B) space, which is the region of interest here. In addition, we obtain the boundaries $B_{b,1}(A), B_{b,2}(A)$, and $B_{b,3}(A)$ of these regions by solving $\left(\frac{\dot{A}}{A}\right)^2 - \left(\frac{\dot{B}}{B}\right)^2 = 0$ with respect to B. By comparing them, it is confirmed that $(\dot{A}/A)^2 > (\dot{B}/B)^2$, and thus $\dot{A} = 0$, is reached at a much faster rate as long as k_m is sufficiently small.

4.8.2 Condition for the main results

Growth phases

We chose the specific rate functions $F_A(S)$, $F_B(S)$, and $G(A, B, C)$. However, the main results were not altered by changing the choice of rate functions as long as certain conditions are fulfilled. In this section, we discuss the conditions required for the three growth phases (Fig.1(b)) to exist.

In general, $F_A(S), F_B(S) > 0$ for $S > 0$, and $F_A(0) = F_B(0) = 0$, while $F_A(S) + F_B(S)$, so that the total synthesis rate monotonically increases with S. We assume that k_m is sufficiently small. Although F_A and F_B are functions of S, we use an abbreviated representation of $F_A(S_{\rm ext})$ and $F_B(S_{\rm ext})$ as $F_A(S_{\rm st}(S_{\rm ext}))$ and $F_B(S_{\rm st}(S_{\rm ext}))$, respectively.

First, the transition point between the inactive and death phases $S_{\rm ext}^{\rm inact-death}$ is simply and generally obtained as the point satisfying $F_A(S_{\rm ext}^{\rm inact-death}) = d_A$. For estimating the transition point between the active and inactive phase $S_{\rm ext}^{\rm act-inact}$, the spontaneous degradation rate of all chemical species can be set to zero. Following the earlier argument, C is eliminated by using $C = 1 - A$, and the model equation is given by

$$\begin{aligned} \frac{dA}{dt} &= F_A A - k_p AB - F_A A^2 \\ \frac{dB}{dt} &= F_B A - k_p AB - F_A AB, \end{aligned} \tag{4.26}$$

where the reaction term $k_m(1 - A)$ is neglected as $k_m \to 0$. The bifurcation of the system occurs at $S_{\rm ext}^{\rm act-inact}$, where $F_A(S_{\rm ext}^{\rm act-inact}) = k_p B_{\rm st}(S_{\rm ext}^{\rm act-inact}) - F_A(S_{\rm ext}^{\rm act-inact}) A_{\rm st}(S_{\rm ext}^{\rm act-inact})$.

By substituting the steady solution of Eq. (4.26), we obtain the relationship between F_A and F_B at $S_{\rm ext}^{\rm act-inact}$ as

$$1 + 2F_A(S_{\rm ext}^{\rm act-inact})/k_p = \sqrt{1 + 4F_B(S_{\rm ext}^{\rm act-inact})/k_p}.$$

If there exists $S_{\rm ext}^{\rm act-inact} > 0$ satisfying this equation, there also exists an active-inactive transition, while the region $1+2F_A(S_{\rm ext}^{\rm act-inact})/k_p \geq \sqrt{1 + 4F_B(S_{\rm ext}^{\rm act-inact})/k_p}$ corresponds to the active phase.

In summary, the transition points for the active/inactive phases and inactive/death phases are given by

- $1 + 2F_A(S_{\rm ext}^{\rm act-inact})/k_p = \sqrt{1 + 4F_B(S_{\rm ext}^{\rm act-inact})/k_p}$.
- $F_A(S_{\rm ext}^{\rm inact-death}) = d_A$.

As long as the functions F_A and F_B allow for such equalities given certain $S_{\rm ext}$ values, there exist three phases against the change in $S_{\rm ext}$, and essentially the same results are obtained as in the original model, including the time series of biomass (Fig.1(c and d)).

Condition for the contiguity of null clines

We here discuss the condition for the contiguity of null clines, which causes slow relaxation. We assume that the inhibitory reaction takes place among A, B, and C, and mass is conserved in the reaction, although we do not specify the process of inhibition. To clarify the constraint imposed by the mass conservation, we set the mass per unit volume of each chemical species as dynamical variables. Then, the model equations are given by

$$M_A \frac{dA}{dt} = M_A F_A(S) A - \xi_A M_A G(A,B,C) - M_A F_A(S) A^2, \tag{4.27}$$

$$M_B \frac{dB}{dt} = M_B F_B(S) A - \xi_B M_B G(A,B,C) - M_B F_A(S) AB, \tag{4.28}$$

$$M_C \frac{dC}{dt} = \xi_C M_C G(A,B,C) - M_C F_A(S) AC, \tag{4.29}$$

where M_i and ξ_i $(i = A, B, C)$ are the mass and the stoichiometry coefficient of the inhibition reaction in the rate of $G(A, B, C)$, respectively, while S is regarded as a parameter. Following the same argument to derive $A + C = 1$ as introduced in Section 2 above, $C = \xi_C/\xi_A(1 - A)$ is satisfied after the system reaches the steady state, and thus C is eliminated. By calculating the A and B null clines for a small A region, we obtain

$$A_{A-nullcline}(B) \sim \frac{G(0,B)}{F_A(S)/\xi_A - G'(0,B)} \tag{4.30}$$

$$A_{B-nullcline}(B) \sim \frac{G(0,B)}{(F_B(S) - F_A(S)B)/\xi_B - G'(0,B)}, \tag{4.31}$$

where $G'(0, B)$ represents $\frac{\partial G}{\partial A}(0, B)$. The only difference between the two null clines lies in the first term in the denominators. Since $F_A(S)$ and $F_B(S)$ approach zero as S goes to zero, the first term is vanishingly small in the substrate-poor condition, and the two null clines come close together for small A values.

The central point of null cline contiguity lies in the mass conservation in the reaction $G(A, B)$, which is commonly introduced in the equations for both A and B. The rate of all reactions other than the inhibition reaction decreases as S decreases. However, the inhibition reaction is not slowed down, because the reaction is independent of the substrate concentration. This reaction is dominant for both A and B under the starving condition. Therefore, A and B are almost completely determined by the same dynamics.

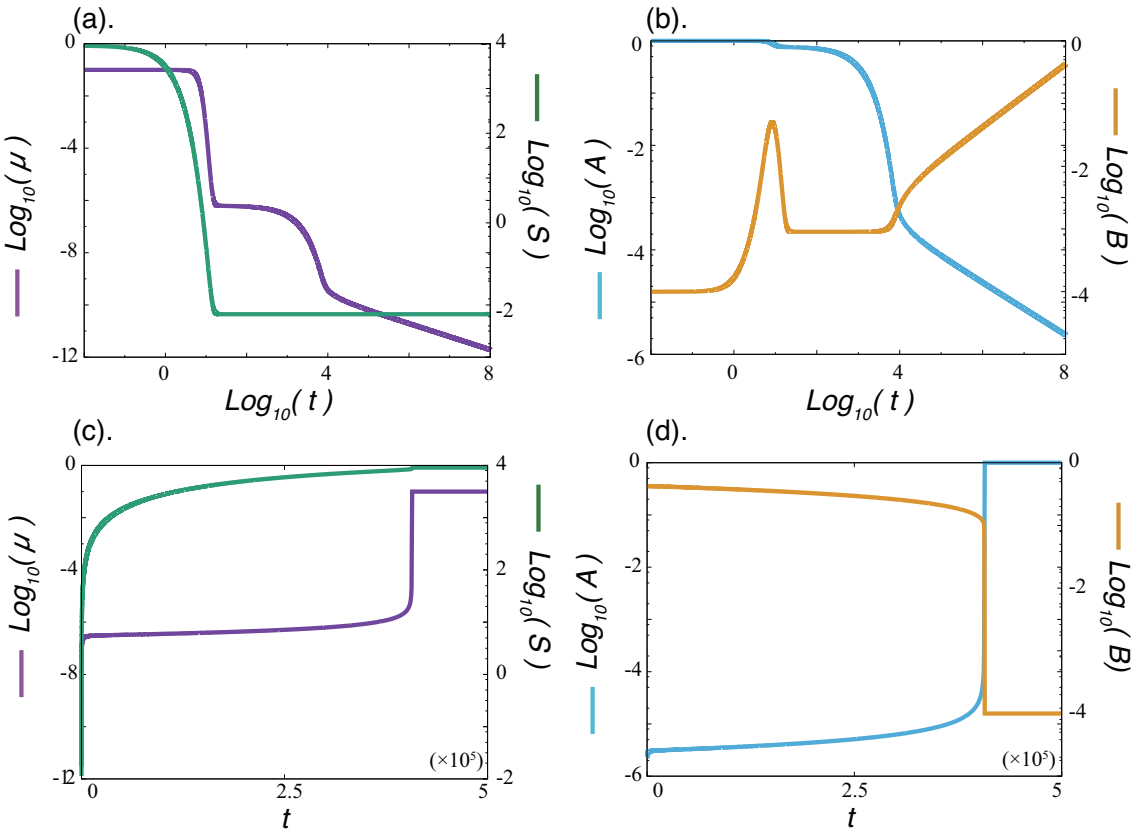

Figure 4.10: Time series of the starvation-mimicking simulation. (a and b) Time series of the (a) growth rate μ and internal substrate S, and (b) components A and B during the starvation period. (c and d) Time series of the (c) growth rate μ and internal substrate S, and (d) components A and B after recovery of the external substrate concentration. At $t = 0$, the cell stays at the steady state under the substrate-rich $S_{\rm ext} = S_{\rm ext}^{\rm rich}$ condition, and $S_{\rm ext}$ changes to $S_{\rm ext}^{\rm poor}$. After the $T_{\rm stv} = 10^8$ starvation period, $S_{\rm ext}$ is returned to $S_{\rm ext}^{\rm rich}$ (For (c and d), the origin of time is set to the time point at which the external substrate concentration is recovered). Recovery to the original concentration other than S requires a long lag time. The same parameter values are adopted as described for Fig. 2 .

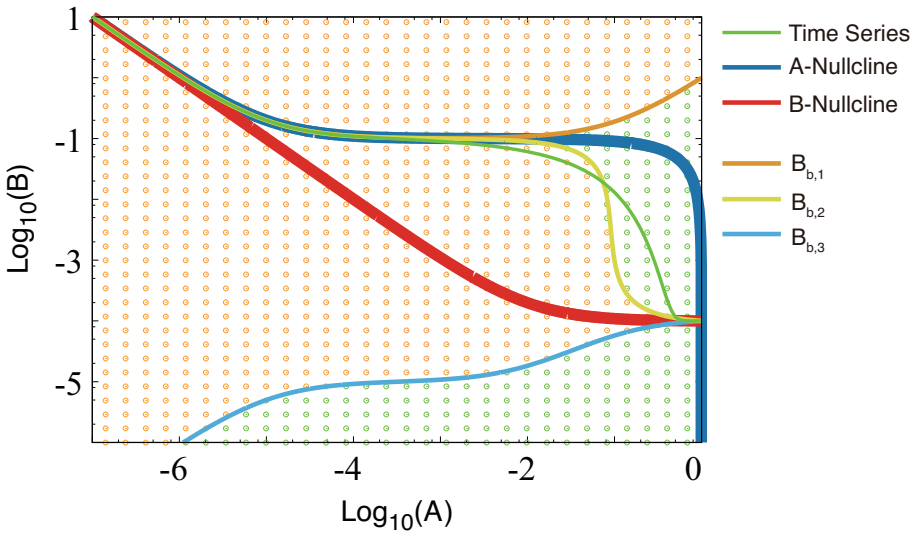

Figure 4.11: Phase diagram dividing (A, B) space into the A-fast region and B-fast region. The orange region and green region correspond to the $(\dot{A}/A)^2 > (\dot{B}/B)^2$ and $(\dot{A}/A)^2 < (\dot{B}/B)^2$ regions, respectively. A time series (orbit) is obtained by numerical simulation of the model. The parameters are the same as those described in Fig. 4.10. The initial point for the time series is given as $S(0) = S_1, B(0) = 10.0$, and $A(0) = A_{A-nullcline}(S_1, B(0))$.

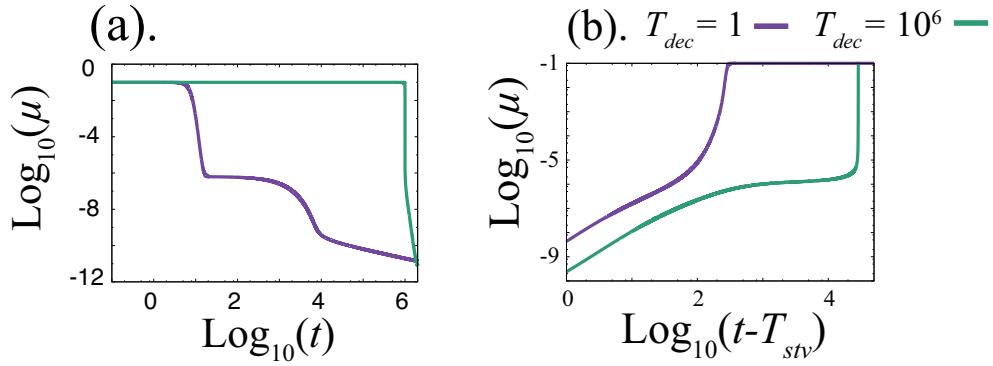

Figure 4.12: (a) Time series of growth rate μ during starvation for different $T_{\rm dec}$ values ($T_{\rm dec} = 10^6$ (green) and $T_{\rm dec} = 1.0$ (purple)). (b)The resurrection of growth rate is plotted against time after recovery of the external substrate concentration. The same parameter values as indicated in Fig.2 were adopted.

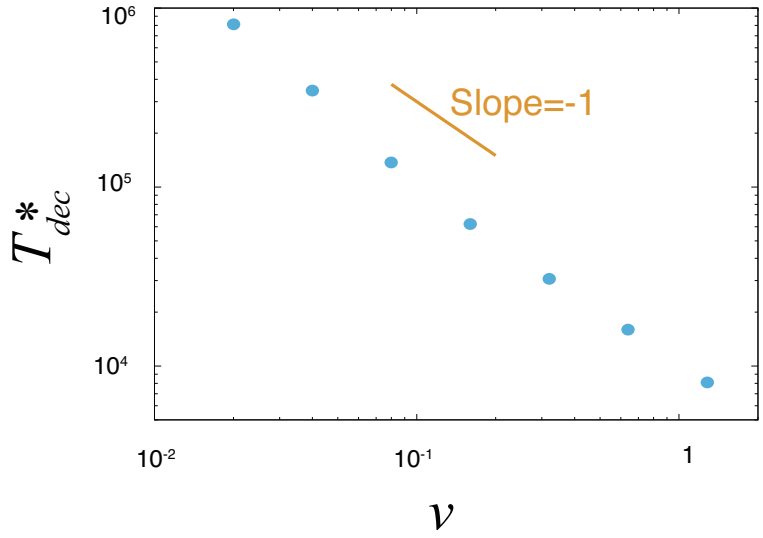

Figure 4.13: Relationship between the critical $T_{\rm dec}(T^*_{\rm dec})$ and synthesis rate v. The same parameter values as indicated in Fig.2 were adopted.

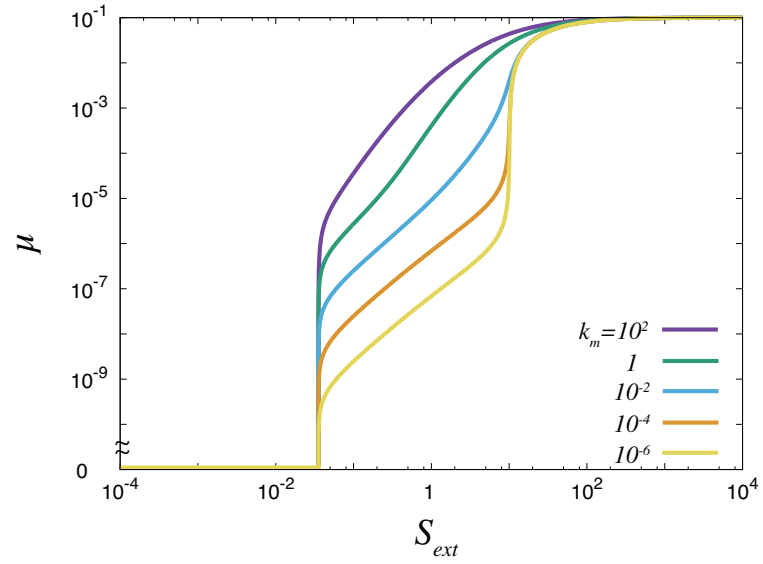

Figure 4.14: The steady growth rate for different k_m values. A sharp decline of the steady growth rate is observed as long as k_m is smaller than $k_p(=1.0)$. Other parameter values are chosen to be same as those indicated in Fig.1.

Chapter 5

Substrates can kill cells : A phenomenological model for Sugar Induced Cell Death

5.1 Introduction

In the previous chapter, we constructed coarse-grained model consisting of three components of macromolecules, namely, an autocatalytic component which facilitates cellular growth (A), a component which does not facilitate cellular growth (B), and the complex (C) consisting of component A and B. The model (ABC model) exhibits three distinct phases (active, inactive, and death phases), and the obtained dynamics of the amounts of macromolecules are similar to those observed in the bacterial growth curve. It also reproduces the well-known growth laws in exponential growth phase (Monod's equation and the relationship between rRNA and growth rate).
In the inactive phase, novel phenomenological relationships are obtained. The lag time for growth resurrection increases in square-root of starvation time and is inversely proportional to the maximum growth rate. The distribution of lag time exhibits a long-time tail. These two results were confirmed to be consistent with the experimental results. While there is no direct experimental evidence, it is also found that the length of lag time depends on how the cell is starved. If the substrate depletes gradually, the lag time becomes much longer than that of a cell under immediate depletion of the substrate.
Here, additional question arises. The ABC model predicts that "how starved" matters on the cell's behavior, but "how waken up" does not matter. As will be discussed, it is known that the recovery processes of environmental conditions affect a resurrection of cells from starved conditions. Especially, in a phenomenon known as Sugar Induced Cell Death (SICD), incubation of starved cells (*E.coli* or some yeasts) into a medium with glucose as a sole nutrient source leads to cell death[130, 131, 132]. SICD was first reported by Granot et. al[131] in starved cells of *S.Cerevisiae*. The authors incubated the starved cells into three types

of nutrients, namely, water, sorbitol[1], and glucose medium. Any other nutrient sources, such as nitrogen sources, vitamins, and inorganic salts, were not added to these media. Then, the cells incubated in the glucose medium were reported to die faster than the cells in the water and sorbitol medium[2]. Also, they found that the cells in glucose medium had more reactive oxygen species (ROS) than those in water and sorbitol medium. Because of the observation of toxicity, ROS was thought to lead the SICD. SICD was also reported, however, in the petite mutant of yeast cells which lack the respiratory chain[132]. Thus, SICD has also triggered mechanisms other than the accumulation of ROS. To elucidate general mechanisms and phenomenological laws of SICD, we extend the model which is proposed in Chapter.4 by introducing energy currency molecules in this chapter. We show that the model exhibits distinct growth phases, and dies depending on the temporal order of the recovery of substrates.

5.2 model

Here, we extend our previous model by introducing the energy currency molecules such as ATP and ADP into the ABC model and modifying the synthesis rate of component A and B so that the synthesis ratio between them is determined by the ratio of ATP to ADP. We add another type of substrate which is used for the conversion reaction from ADP to ATP. This extra substrate is denoted as S_1, while the substrate (S) in ABC model is renamed as S_0. Also, we assume that the total concentration of ATP and ADP is kept constant just for the sake of simplicity. Then, our model is given by

$$\begin{aligned}
\frac{dA}{dt} &= fF_A(S_0,\alpha)A - G(A,B,C) - d_A A - \mu A, \\
\frac{dB}{dt} &= fF_B(S_0,\alpha)A - G(A,B,C) - d_B B - \mu B, \\
\frac{dC}{dt} &= G(A,B,C) - d_C C - \mu C, \\
\frac{d\alpha}{dt} &= (1-f)J(S_1,\alpha)A - F_A(S_0,\alpha)A - F_B(S_0,\alpha)A - d_\alpha \alpha.
\end{aligned}$$

Here, α represents the concentration of ATP. Since the total concentration of ATP and ADP is kept constant value $\alpha_{\rm tot}$, the concentration of ADP is given as $\alpha_{\rm tot} - \alpha$. ATP is converted from ADP using the substrate S_1 with the aid of catalytic ability of component A. ATP is used for the macromolecular synthesis, and spontaneously deactivated into ADP. Decrease in ATP and ADP by the dilution effect is compensated, for example, by the supply of such phosphate molecules. f denotes the fraction of component A used for the synthesis of macromolecules ($0 \leq f \leq 1$), and $1-f$ is the fraction of component A which is used for the production of ATP.

[1] *S.Cerevisiae* cannot utilize sorbitol as a carbon source, sorbitol was used for the pH control.

[2] Of course, since there is no nutrient sources in the water and sorbitol medium, the cells in these media will die. The speed of cell death, however, is quite slow.

A schematic representation of the present model is shown in Fig.5.1.(a).
Definitions of G and μ are identical to the previous ABC model, given as $G(A, B, C) = k_p AB - k_m C$ and $\mu = F_A A$, respectively. The expressions of F_A and F_B are slightly modified. We set these as $F_A(S_0, \alpha) = \frac{vS_0}{K+S_0}\frac{\alpha}{\alpha_{\rm tot}}\alpha$ and $F_B(S_0, \alpha) = \frac{vS_0}{K+S_0}\frac{\alpha_{\rm tot}-\alpha}{\alpha_{\rm tot}}\alpha$. The first part of F_* is derived from normal Michaelis-Menten type reaction kinetics. The second part determines the ratio of the synthesis of component A to that of B. In this model, if a cell has ATP sufficiently, it produces component A, while in the opposite case, it produces the component B. The last term, α, is added because macromolecular synthesis reactions are typically endothermic processes, and thus, they need the consumption of energy currency molecules. One can obtain this type of functions also as a consequence of error-correcting mechanisms of the macromolecular synthesis as discussed in Chapter.4. $J(S_1, \alpha)$ represents the rate of conversion reaction from ADP to ATP which consumes substrate S_1 given as $J(S_1, \alpha) = \frac{uS_1(\alpha_{\rm tot}-\alpha)}{K_\alpha+S_1+(\alpha_{\rm tot}-\alpha)+S_1(\alpha_{\rm tot}-\alpha)}$.

5.3 Growth Phases and lag time

By computing the steady state of the present model, we obtain again the three growth phases. Fig.5.1.(b) shows the three-dimensional plot of the steady growth rate. In contrast to the ABC model, the present model has death attractor within all (S_0, S_1) region. Also, by decreasing S_0 with keeping S_1 at high values, there is no distinct transition between active and inactive phases as observed in the previous chapter, whereas, there are such transitions by decreasing S_1 with keeping S_0 at high values. This difference is consistent with result of the previous chapter. In the ABC model, the active-inactive transition occurs when the substrate concentration satisfies an equation $1 + F_A(S)/k_p = \sqrt{1 + 4F_B(S)/k_p}$ as discussed in Appendix of the previous chapter. By assuming $4F_B(S)/k_p \ll 1$, this equation is approximated as $F_A(S)/F_B(S) \sim 1$ indicating that the transition point does not depend on each synthesis rate of A and B, but depends critically on the synthesis ratio of A and B. In ABC model, change in the concentration of substrate alters both the whole synthesis rate and synthesis ratio of A and B, and it cannot distinguish the influence of the two to the transition. Here, by introducing the energy currency molecules, these two effects are separated. The transition between active and inactive phases is triggered by the change in the synthesis ratio. On the other hand, the active/death and inactive/death transition occurs when the spontaneous degradation rate of component A exceeds its synthesis rate. Both the changes are relevant to this transition in whole synthesis rate and synthesis.
The death phase in the substrate-rich condition emerges by an overproduction of component B. If we chose an initial condition with a low α and A, the macromolecular synthesis is directed mostly to component B due to the low concentration of α. Also, since the concentration of component A is low, the production rate of α is slow. Besides the slow production of ATP, it is also degraded (deactivated) spontaneously, which further decreases the synthesis ratio of component A to component B. Thus, the cell cannot change the synthesis ratio unless the concentration of component A exceeds a certain value so that the production rate of α exceeds

its spontaneous degradation rate. There are the initial points from which the concentration of component A cannot exceed such critical value, and the state from such initial points are attracted into death attractor with zero-growth.
Also, we computed the growth rate in the mixed medium made by blending S_0 and S_1 in a certain proportion. Fig.5.1(c) shows the steady growth rate for several blending proportion medium. As a result of the differences between the roles of S_0 and S_1 on the transition, three growth phases emerge under limited blending proportion.
The present model exhibits similar behavior of lag time with the ABC model, as shown in Fig.5.2. We computed the dependency of lag time on starvation time and the maximum specific growth rate. Up to time $t = 0$, a cell is put in the substrate rich condition ($S_0 = S_1 = S_{\rm rich}$). Then, the concentrations of both substrates is decreased immediately ($S_0 = S_1 = S_{\rm poor}$). After the starvation period $T_{\rm stv}$, the concentrations of both substrates are recovered to the rich condition immediately. The lag time was computed as the relaxation time necessary to return to the original, non-zero growth state. If the starvation time is sufficiently long, the lag time increases with square-root of the starvation time. In contrast to the previous ABC model, however, if the starvation time is too long, the cell cannot return to the original non-zero growth state mainly due to the spontaneous degradation of ATP. As the starvation time approaches this "point of no return", the lag time starts to diverge. In this case, the square-root dependency, is not observed due to the cell death if the spontaneous degradation rate is large. The cell dies before it satisfies the condition discussed in Supplemental Information of Chapter.4.
Also, the inverse proportionality between lag time and the maximum specific growth rate is obtained. The cell is starved for the fixed starvation time $T_{\rm stv} = 10^{10}$, and the substrate concentrations return to the original rich value. Here, we changed v and u when the substrate concentrations are recovered to compute the lag time for various $\mu_{\rm max}$[3].

5.4 Growth resurrection depending on the recovery process of environmental condition

In this section, we study the relationship between the resurrection of cells from starving conditions and the recovery process of the external substrate concentrations. A cell is starved up to $t = T_{\rm stv}$ as explained above. After the starvation period, the substrate concentration starts to recover. We compute two different temporal orders of the substrate restoration. That is, first S_0 is returned to $S_{\rm rich}$ and then S_1 is returned to $S_{\rm rich}$ after the period of time $T_{\rm interval}$. In the other process, S_1 is recovered first, and subsequently, S_0 is recovered after $T_{\rm interval}$.
Fig.5.3 shows the phase diagram on the recovery processes plotted against the change in the starvation and interval time. We examined if the cell resurrects, i.e., returns to the original growth after the above two orders of resource recov-

[3]We used the same parameter set for the starvation, i.e. we computed the relaxation time from a single initial condition, for various v and u values.

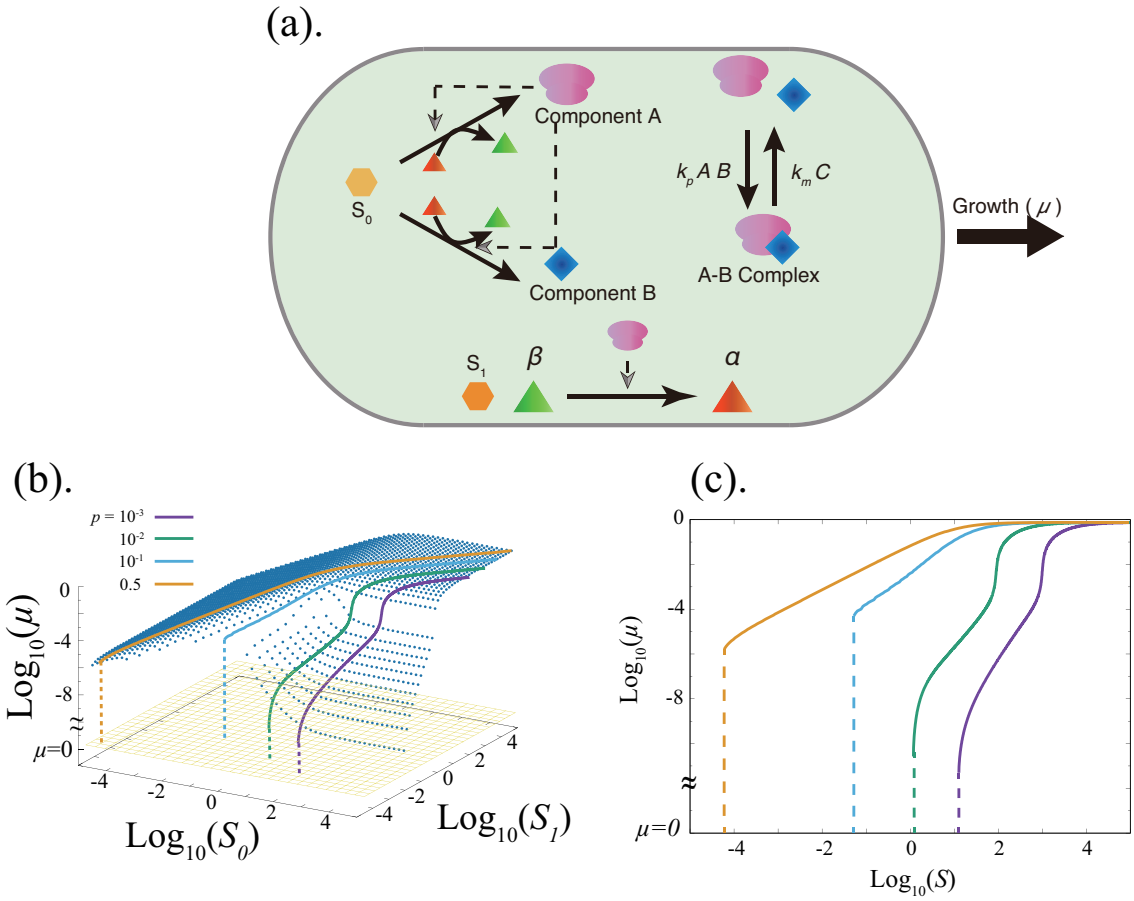

Figure 5.1: (a). Schematic representation of the components and reactions in the present model. The concentration of each chemical changes according to the listed reactions. In addition, chemicals are spontaneously degraded at a low rate, and chemicals other than ATP and ADP are diluted following the volume expansion of the cell. (b). The steady growth rate is plotted as a function of the concentrations of S_0 and S_1. Blue dots indicate non-zero growth state and the yellow surface is the death state with zero growth rate. The growth rate of the steady state is plotted as a function of the concentrations of S_0 and S_1, for different values of p. (c). The steady growth rate is plotted as a function of total concentration of substrate $S(= S_0 + S_1)$ for several p values. Line colors correspond to those in (b). Parameter values are set as $v = 2.0, u = 20.0, f = 0.5, k_p = 1.0, k_m = 10^{-3}, K = 10.0, K_a = 10.0, d_A = 10^{-7}, d_B = d_C = 0.0, d_\alpha = 10^{-5}$, and $\alpha_{\mathrm{tot}} = 1.0$.

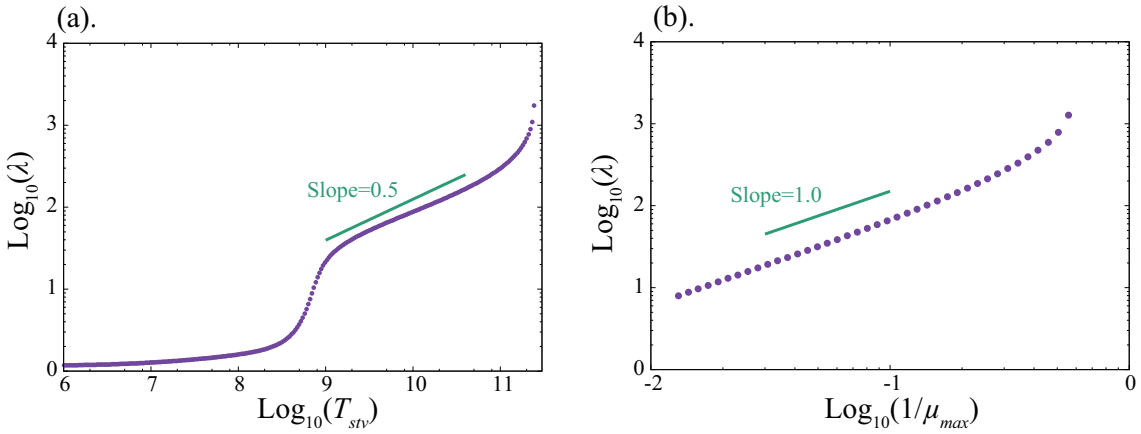

Figure 5.2: (a). Lag time as a function of starvation time. Lag time diverges at $T_{\rm stv} \sim 10^{12}$ because of the cell death.(b). Relationship between the lag time and maximum specific growth rate $\mu_{\rm max}$. Starvation time is set as $T_{\rm stv} = 10^{10}$. We changed the values of v and u with keeping a relationship $v = 0.1 \times u$. Parameters are set as $v = 20.0, u = 200.0, k_p = 1.0, k_m = 10^{-6}, K = 10.0, K_\alpha = 10.0, S_{\rm rich} = 10^3, S_{\rm poor} = 10^{-7}, d_A = 10^{-8}, d_B = d_C = 0.0, d_\alpha = 10^{-2}, f = 0.5$, and $\alpha_{\rm tot} = 1.0$.

ery processes. For too small $S_{\rm poor}$ (Fig.5.3(a)), the cell cannot recover the growth against both recovery processes unless $T_{\rm stv}$ and $T_{\rm interval}$ are small. In the other value of $S_{\rm poor}$ (Fig.5.3(b)), however, the order of substrate concentration recovery determines whether the cell returns to the high growth rate or not. The first increase of S_0 concentration leads to the cell death in a wide range of $T_{\rm stv}$ and $T_{\rm interval}$. We have confirmed for other parameter choices that the cell can return to the high growth state, except a special case described below, if the concentration of S_0 recovers after the recovery of S_1 the cell resurrects the growth[4].
The recovery process of substrate concentration affects the resurrection of the cell because it leads the overproduction of component B. The synthesis ratio of component B is typically higher in small S_1 conditions than that of high concentration situation due to the low concentration of α. Thus, if the concentration of S_0 increases keeping the concentration of S_1 low, the synthesis rate of component A and B increases, but the synthesis ratio of A to B is not improved, so that more component A is not synthesized. Moreover, since the increased production rate of both A and B consumes more ATP. Therefore, an addition of S_0 in low S_1 results in the induction of the synthesis of component B. If the duration of induction ($T_{\rm interval}$) is short, and S_1 is soon added, the cell restores the high growth rate. If the induction lasts for a long time, however, the state enters the basin of death

[4]Note that the growth recovery is always worse in the alternate recovery of substrate concentrations than the simultaneous increase of the concentrations of both substrates. When the concentrations of both substrates return to the high value after the starvation period $T_{\rm stv}$ simultaneously, the cell can restore the high growth rate as long as the cell can resurrect by either way of substrate recovery ($S_0 \to S_1$ or $S_1 \to S_0$). Therefore we can see that the addition of S_0 as a sole nutrient source is nothing but a just toxic operation for the cell.

attractor, and the cell will die.
When S_{poor} is very small (Fig.5.3(a)), there is a region in which cells are resurrected only for the case in which S_0 is first recovered ($\mathrm{S}_0 \rightarrow \mathrm{S}_1$) This occurs when the cell stays near the basin boundary of death attractor when the starvation is finished. It is explained accordingly: The active/death and inactive/death transitions occur when the spontaneous degradation rate of component A (d_A) exceeds the production rate of it (F_A). Whereas the concentration of S_1 does not directly increase the production rate F_A because the ATP production reaction is necessary, an increase of S_0 directly increase the production rate. Near the boundary, the concentration of component A is exceedingly small, and thus, the ATP production hardly progresses. Thus, the first increase of S_1 effectively prolongs the starvation time under such situations, and the recovery process ($\mathrm{S}_1 \rightarrow \mathrm{S}_0$) fails to resurrect the starved cells[5].

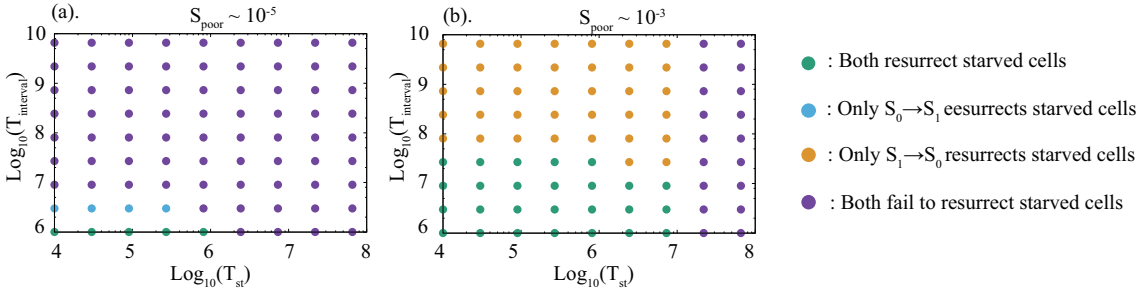

Figure 5.3: Processes which lead the resurrection of the starved model cell are plotted as a function of T_{stv} and T_{interval} for different S_{min} values. (a). Since the substrate concentration in starvation condition is too low ($S_{\mathrm{min}} \sim 10^{-5}$), the cell cannot recover the growth. (b). If both T_{stv} and T_{interval} are small, the cell can resurrect the growth by both processes of substrate recovery. However, if the cell is exposed at S_0-rich and S_1-poor environment for a long time, it fails to recover the growth. Parameter values are set as $v = 2.0, u = 20.0, f = 0.5, k_p = 1.0, k_m = 10^{-3}, K = 10.0, K_a = 10.0, d_A = d_B = 10^{-5}, d_C = 10^{-7}, d_\alpha = 10^{-2}$, and $\alpha_{\mathrm{tot}} = 1.0$.

5.5 Summary and Discussion

Here, we developed a phenomenological model consisting of two types of substrates, autocatalytic component (A), non-growth-facilitating component(B), A-B complex,(C) and energy currency molecules such as ATP and ADP. In contrast to the model introduced in Chapter.4, present model has death attractor for a whole range of the concentrations of substrates. Also, the model exhibits the square-root

[5]If we simultaneously increase the concentrations of both substrates at $t = T_{\mathrm{stv}} + T_{\mathrm{interval}}$, the cell dies for the values of T_{stv} and T_{interval} at which the first increase of S_0 only succeeds the resurrection. Thus, the first increase of S_1 itself is not toxic, but an effective prolongation of starvation period leads to the cell death. Also, this situation emerges very limited choices of T_{stv} and T_{interval}.

dependency of lag time to the length of starvation time.
It is shown that the resurrection of the cellular growth in the present model from the starved conditions is determined by how the substrate concentration returns to high values. If macromolecular synthesis rate is increased first without filling the energy currency molecules, the macromolecular synthesis triggers cell death. This cell death is induced by the positive feedback of component B production. The active synthesis of component B under lower ATP level hinders ATP production further, because component B forms a complex with component A and inhibits its catalytic ability. Thus, if the production rate (or ratio) of component B exceeds a certain value, this positive feedback mechanism triggers cell death. In Chapter.4, we discussed a possible scenario interpreting the main results as consequences of error-correcting mechanisms of macromolecular synthesis in cellular systems. The cell death induced by the substrate is possibly seen as a consequence of the mechanisms which work inefficiently under substrate-poor conditions. The aggregate body formation of denatured proteins is experimentally reported by Ncifora and others [101, 102, 103], and they can inhibit the catalytic ability of active proteins. Also, we can interpret component B as a reactive oxygen species to some extent. One of the toxicities of ROS is denaturation of proteins[131]. When we set the dissociation rate k_m to zero, the complex formation reaction can be interpreted as an irreversible denaturation of component A caused by component B, and we can infer that the resistant systems against ROS molecules supported by antioxidant enzymes work ineffectively under substrate-poor conditions.
While our model is too simple to discuss the detailed mechanisms which lead to the cell death, it can provide abstract concepts of the cell death led by the chemical species which positively contribute to the cellulaer growth under the typical conditions.

Chapter 6

Summary and Discussions

6.1 Summary

6.1.1 Energetically efficient growth of cellular system

In Chapter.2 and Chapter.3, we have studied the energetic (thermodynamic) efficiency of cellular growth and metabolism. As discussed in Introduction, biological systems need to produce the catalytic enzymes to proceed biochemical reactions. In other words, the protein production is sustained by protein production, itself. We found that biological systems do not achieve the highest efficiency at the quasi-static limit as a consequence of this autonomous nature.

Based on a simple cell model consisting of substrate, catalytic enzyme, and membrane precursor, we have found that the total entropy production during one generation of cell division is minimized at a non-zero, finite, growth rate. This optimality at a finite speed stemmed from two effects; the equilibration effect led by the increase of the abundance of catalytic enzyme and the increase of entropy production rate due to the overproduction of macromolecules. The qualitatively same result is obtained also in the catalytic reaction network model with multiple chemical species.

In Chapter.3, we found that the temporal separation of different chemical reactions enhances the thermodynamically efficient growth by using a simple model of metabolism. Our model consists of simplified "catabolic" and "anabolic" reactions connected by the energy currency molecules. When the concentrations of the two distinct enzymes needed for catabolic and anabolic reactions oscillate in anti-phase with each other, the catabolic reaction and anabolic reaction are temporally separated, which allows each reaction to progress in close to the chemical equilibrium. We examined the advantage of the temporal separation of metabolism by imposing non-autonomous oscillation of the concentration of enzymes as a first step. Next, the temporal separation is shown to be beneficial also in the catalytic reaction model which exhibits an autonomous oscillation in the concentrations of enzymes. It implies that the temporal separation of chemical reactions might be advantageous even if the energetic cost for autonomous oscillation is considered, as is a typical phenomenon in non-equilibrium dissipative systems.

The common message of these two studies is that cells realize the states being

close to chemical equilibrium not in the non-growing or static conditions but in growing or dynamic states because external chemical environments are inherently far-from-equilibrium and cells obtain energy by facilitating equilibration of chemical reactions with the aid of catalytic enzymes. This concept will be common to living things.
We will try to construct a quantitative theory which bridges the thermodynamic efficiency and yield of cellular growth with such error-correcting mechanisms. Also, we have to discuss the biological relevance of this optimality at a finite speed.

6.1.2 Phenomenological theory for slowly growing cell

In Chapter.4, we constructed a simple, coarse-grained cell model that includes an extra class of macromolecular component in addition to the autocatalytic active components that facilitate cellular growth, while this additional component forms a complex with the autocatalytic component. Depending on nutrient conditions, the cell exhibited typical transitions among the lag, exponential, stationary, and death phases. Furthermore, the lag time needed for growth recovery after the starvation followed the square root of the starvation time and was inverse to the maximal growth rate, in agreement with experimental observations. Moreover, the lag time distributed among cells was skewed with a long time tail, also in agreement with experiments.
In Chapter.5, we extended our model introduced in Chapter.4 to study the phenomenon called sugar induced cell death. An extended model has another substrate and energy currency molecules such as ATP and ADP in addition to the original model. The model also showed three distinct phases depending also on the compositional ratio of two substrates. If the concentration of substrate for protein synthesis is high and the concentration of the substrate for energy currency production is low, the model cell does not exhibit "inactive" phase. The model showed the same dependency of the lag time to the starvation time and the maximum specific growth rate. In contrast to the original model, however, the extended model has death attractor over a whole range of substrate concentrations, and after the starvation, the cell could be attracted to the death attractor depending on which substrate concentration was recovered first. This model might give us the insight to establish a theory for cell death caused by the process of substrate recovery.

6.2 Future Directions

Here, we discuss the limitation of our studies and the future directions for a few topics.

6.2.1 Energetics of cellular growth

Energetics, or in other words, the economics of cell growth has gathered much attention. Thermodynamic efficiency of cellular growth have been actively stud-

ied in the 1980s[6, 13, 14, 15, 16, 17, 18]. In these studies, relationships between the thermodynamic efficiency and the yield seemed to be blindly trusted to exist. In fact, no clear relationships between them are found. Lack of this relationship imposes limitations on our studies.
Normally, the thermodynamic efficiency of chemical reactions increases if the chemical reactions progress in the state being close to the chemical equilibrium. However, cells have to change the stoichiometry of chemical reactions to increase the yield of certain reactions. To change the stoichiometry according to the thermodynamic efficiency, the cell has to sense the efficiency, and regulate the reactions. It is not clear whether the thermodynamically efficient reaction always leads to high yield or not, even if we omit the costs of the sensing and regulation.
One candidate which possibly connect the thermodynamics and yield is error-correcting mechanism such as kinetic proofreading. In the original model of kinetic proofreading proposed by J. J. Hopfield[107, 108], the production ratio of desired protein to that of other mistranslated proteins changes according to the GTP/GDP ratio. If we can naïvely expect that the thermodynamically efficient metabolism realizes high GTP/GDP ratio, it can lead to accurate translation, and high yield states.

6.2.2 Universality theory of lag time

Experimental studies for the lag time study described in Chapter.4 are needed in future. We list up some topics to be done, and briefly explain each.

Confirm square-root dependency

Since the experimental data we have used to validate our theory in Chapter.4 were obtained from the low- temperature experiments, there may be a possibility that they may not reflect the bacterial physiology under the normal temperature (from room temperature to 37°C). Thus, an experiment performed at normal temperature is needed.

Memory for the starvation process

We found that the lag time in our model cell drastically changed depending on how the cell was starved. The difference in the starvation process somehow preserved in a cell state over a long time. Hence the starvation process is memorised in a cell state. While this result on starvation-process dependence has not yet confirmed experimentally, there is a suggestive experiment done by Radzikowski et.al. They performed an experiment in which bacteria grown in glucose medium are separated into two groups by re-incubating to the different media: fumarate and no-carbon source medium. They found that the gene expression level of ribosome modification factor (RMF) for the fist (fumarate) group is significantly higher than that of the second (without carbon source) group. Since fumarate is a carbon source inferior to glucose, we possibly regard the incubation of bacteria to fumarate medium as

the slow decrease in the concentration of the substrate. If this expectation is valid, the up-regulation of RMF might support the increase of component B in our model induced by slow decrease in the substrate concentration, because RMF is similar in function to component B.
While we expect that this study can be indirect support for our prediction about the memory of starvation processes, the direct confirmation of the memory is necessary.

Mechanism of the emergence of heavy tail in the distribution of lag time

We found the long-time-tailed distribution of lag time in our model. According to our study, this tail appears if all the component A (or ribosome) of a bacterium binds to component B. By monitoring the binding of ribosome and the ribosome-binding factors such as hibernation promoting factor(HPF) and YfiA, and examining if all ribosomes are bound to such factors, this hypothesis has to be tested.

Model for Sugar Induced Cell Death

The model cell introduced in Chapter.5 resurrects its growth from starved conditions depending on the substrate recovery process. The cell fails the resurrection if the concentration of substrate used for the macromolecular synthesis is recovered fist. It is discussed as a potential mechanism of SICD that the increase in the abundance of glucose triggers the active production of macromolecules regardless of other substrates[131]. Of course, it is not obvious whether such discussions on the real cells is straightforwardly applicable for our simple model, or not. Both in such experimental studies and in our model, however, launching the macromolecular synthesis without preparing other reactions such as ATP production would harm the integrity of cells, leading to cell death. It will be important to study the cell death induced by the substrate addition by constructing a detailed model of SICD, and extract the central mechanism of SICD.

6.3 Concluding Remarks

In this thesis, we have studied the energetics of cellular growth (Chapter.2 and Chapter.3) and the growth laws and the growth resurrection from starved conditions (Chapter.4 and Chapter.5). Whereas we found that the thermodynamic efficiency of cellular growth is optimized at a finite speed as a consequence of the autonomous nature of cells, we have not yet understood how the thermodynamics efficiency of biochemical reactions affect the growth yield, and whether the cell growth matters the thermodynamic efficiency, or not.
In Chapter.4, novel phenomenological growth laws of cells in stationary and lag phases were found. Whereas these laws agree with the experimental result well, still, the generality of the laws has to be validated both experimentally and theoretically.

It is still far to answer the questions presented in Introduction. However, we hopefully succeeded in grabbing some aspects of living things. The author is honored if we can make even a little contribution to approach the problems.

Acknowledgements

I am deeply grateful to Prof. Kunihiko Kaneko who offered continuing support and constant encouragement.
I would like to appreciate Prof. Chikara Furusawa for his kind help and suggestions. I also owe a very important debt to the members of Kunihiko Kaneko lab., especially, Dr. Nobuto Takeuchi, Dr. Atsushi Kamimura, Dr. Nen Saito, Dr. Tetsuhiro Hatakeyama, and Dr. Takahiro Kohsokabe whose comments and supports were an enormous help to me.
Finally, I would also like to express my gratitude to my parents for their warm encouragements and financial supports.

References

[1] Gregoire Nicolis, Ilya Prigogine, et al. Self-organization in nonequilibrium systems, volume 191977. Wiley, New York, 1977.

[2] Orit Gefen, Ofer Fridman, Irine Ronin, and Nathalie Q Balaban. Direct observation of single stationary-phase bacteria reveals a surprisingly long period of constant protein production activity. Proceedings of the National Academy of Sciences, 111(1):556–561, 2014.

[3] Jacques Monod. The growth of bacterial cultures. Annual Reviews in Microbiology, 3(1):371–394, 1949.

[4] S John Pirt et al. Principles of microbe and cell cultivation. Blackwell Scientific Publications., 1975.

[5] Bernhard Palsson and Bernhard Ø Palsson. Systems biology. Cambridge university press, 2015.

[6] S. J. Pirt. The maintenance energy of bacteria in growing cultures. Proceedings of the Royal Society of London. Series B. Biological Sciences, 163(991):224–231, 1965.

[7] Matthew Scott, Carl W Gunderson, Eduard M Mateescu, Zhongge Zhang, and Terence Hwa. Interdependence of cell growth and gene expression: origins and consequences. Science, 330(6007):1099–1102, 2010.

[8] Ron Milo, Rob Phillips, and Orme Nigel. CELL BIOLOGY by the numbers. Garland Science, 2016.

[9] Kunihiko Kaneko, Chikara Furusawa, and Tetsuya Yomo. Universal relationship in gene-expression changes for cells in steady-growth state. Physical Review X, 5(1):011014, 2015.

[10] E. Schrödinger. What is life?: With mind and matter and autobiographical sketches. Cambridge University Press, 1992.

[11] K. A. Katchalsky and P. F. Curran. Nonequilibrium thermodynamics in biophysics. Harvard books in biophysics. Harvard University Press, 1967.

[12] M. C. M van Loosdrecht J. J. Hoijnen and L. Tijhuis. A black box mathematical model to calculate auto- and heterotrophic biomass yields based on

gibbs energy dissipation. Biotechnology and Bioengineering, 40(10):1139–1154, 1992.

[13] R. Otto H. V. Westerhoff, J. S. Lolkema and K. J. Hellingwerf. Thermodynamics of growth non-equilibrium thermodynamics of bacterial growth the phenomenological and the mosaic approach. Biochimica et Biophysica Acta (BBA)-Reviews on Bioenergetics, 683(3):181–220, 1982.

[14] V. P. Skulachev. The laws of cell energetics. European Journal of Biochemistry, 208(2):203–209, 1992.

[15] R.T.J.M. van der Heijden H.H. Beeftink and J.J. Heijnen. Maintenance requirements: energy supply from simultaneous endogenous respiration and substrate consumption. FEMS Microbiology Letters, 73(3):203 – 209, 1990.

[16] JY. Zhu XD. Hao, QL. Wang and M. CM. Van Loosdrecht. Microbiological endogenous processes in biological wastewater treatment systems. Critical Reviews in Environmental Science and Technology, 40(3):239–265, 2010.

[17] J. B. Russell and G. M. Cook. Energetics of bacterial growth: balance of anabolic and catabolic reactions. Microbiological reviews, 59(1):48–62, 1995.

[18] J. B. Russell and RL. Baldwin. Comparison of substrate affinities among several rumen bacteria: a possible determinant of rumen bacterial competition. Applied and environmental microbiology, 37(3):531–536, 1979.

[19] K. J. Hellingwerf H. V. Westerhoff and K. Van Dam. Thermodynamic efficiency of microbial growth is low but optimal for maximal growth rate. Proceedings of the National Academy of Sciences, 80(1):305–309, 1983.

[20] H. M. L. van der Gulden M. Rutgers and K. van Dam. Thermodynamic efficiency of bacterial growth calculated from growth yield of pseudomonas oxalaticus ox1 in the chemostat. Biochimica et Biophysica Acta (BBA)-Bioenergetics, 973(2):302–307, 1989.

[21] J. Liu I. W. Marison V. U. Stockar, T. Maskow and R. Patino. Thermodynamics of microbial growth and metabolism: an analysis of the current situation. Journal of Biotechnology, 121(4):517–533, 2006.

[22] K. Jungermann R. K. Thauer and K. Decker. Energy conservation in chemotrophic anaerobic bacteria. Bacteriological reviews, 41(1):100, 1977.

[23] KY. Teh and A. E. Lutz. Thermodynamic analysis of fermentation and anaerobic growth of baker ' s yeast for ethanol production. Journal of biotechnology, 147(2):80–87, 2010.

[24] and K. van Dam M. Rutgers and H. V. Westerhoff. Control and thermodynamics of microbial growth: rational tools for bioengineering. Critical reviews in biotechnology, 11(4):367–395, 1991.

[25] E. Smith. Thermodynamics of natural selection ii: Chemical carnot cycles. Journal of theoretical biology, 252(2):198–212, 2008.

[26] Richard Wolfenden and Mark J Snider. The depth of chemical time and the power of enzymes as catalysts. Accounts of chemical research, 34(12):938–945, 2001.

[27] D. Ben-Eli D. Segré and D. Lancet. Compositional genomes: prebiotic information transfer in mutually catalytic noncovalent assemblies. Proceedings of the National Academy of Sciences, 97(8):4112–4117, 2000.

[28] K. Kaneko. Recursiveness, switching, and fluctuations in a replicating catalytic network. Physical Review E, 68(3):031909, 2003.

[29] S. A. Kauffman. The Origins of Order: Self-organization and Selection in Evolution. Oxford University Press, 1993.

[30] S. Jain and S. Krishna. Large extinctions in an evolutionary model: the role of innovation and keystone species. Proceedings of the National Academy of Sciences, 99(4):2055–2060, 2002.

[31] FL Curzon and B Ahlborn. Efficiency of a carnot engine at maximum power output. American Journal of Physics, 43(1):22–24, 1975.

[32] Christian Van den Broeck. Thermodynamic efficiency at maximum power. Physical review letters, 95(19):190602, 2005.

[33] Yuki Izumida and Koji Okuda. Efficiency at maximum power of minimally nonlinear irreversible heat engines. EPL (Europhysics Letters), 97(1):10004, 2012.

[34] Ken Sekimoto and Shin-ichi Sasa. Complementarity relation for irreversible process derived from stochastic energetics. Journal of the Physical Society of Japan, 66(11):3326–3328, 1997.

[35] AWC Lau, David Lacoste, and Kirone Mallick. Nonequilibrium fluctuations and mechanochemical couplings of a molecular motor. Physical review letters, 99(15):158102, 2007.

[36] Juan MR Parrondo and Pep Español. Criticism of feynman's analysis of the ratchet as an engine. American Journal of Physics, 64(9):1125–1129, 1996.

[37] Stefan Klumpp, Zhongge Zhang, and Terence Hwa. Growth rate-dependent global effects on gene expression in bacteria. Cell, 139(7):1366–1375, 2009.

[38] M. Scott and T. Hwa. Bacterial growth laws and their applications. Current opinion in biotechnology, 22(4):559–565, 2011.

[39] Y. Kondo and K. Kaneko. Growth states of catalytic reaction networks exhibiting energy metabolism. Phys. Rev. E, 84:011927, Jul 2011.

[40] A. Awazu and K. Kaneko. Relaxation to equilibrium can be hindered by transient dissipative structures. Physical review letters, 92(25):258302, 2004.

[41] Chikara Furusawa and Kunihiko Kaneko. Zipf's law in gene expression. Physical review letters, 90(8):088102, 2003.

[42] Akiko Kashiwagi, Itaru Urabe, Kunihiko Kaneko, and Tetsuya Yomo. Adaptive response of a gene network to environmental changes by fitness-induced attractor selection. PloS one, 1(1):e49, 2006.

[43] Chikara Furusawa and Kunihiko Kaneko. A generic mechanism for adaptive growth rate regulation. PLoS Computational Biology, 4(1):e3, 2008.

[44] Yasuji Sawada. A thermodynamic variational principle in nonlinear non-equilibrium phenomena. Progress of Theoretical Physics, 66(1):68–76, 1981.

[45] Axel Kleidon, Ralph Lorenz, and Ralph D Lorenz. Non-equilibrium thermodynamics and the production of entropy: life, earth, and beyond. Springer, 2005.

[46] J. J. Heijnen and J. P. Van Dijken. In search of a thermodynamic description of biomass yields for the chemotrophic growth of microorganisms. Biotechnology and Bioengineering, 39(8):833–858, 1992.

[47] J. A. Roels. Energetics and kinetics in biotechnology. Elsevier Biomedical Press, 1983.

[48] Arijit Maitra and Ken A Dill. Bacterial growth laws reflect the evolutionary importance of energy efficiency. Proceedings of the National Academy of Sciences, 112(2):406–411, 2015.

[49] Yohei Kondo and Kunihiko Kaneko. Growth states of catalytic reaction networks exhibiting energy metabolism. Physical Review E, 84(1):011927, 2011.

[50] Peter R Bergethon. The physical basis of biochemistry: the foundations of molecular biophysics. Springer Science & Business Media, 2013.

[51] Daniel Segré, Dafna Ben-Eli, and Doron Lancet. Compositional genomes: prebiotic information transfer in mutually catalytic noncovalent assemblies. Proceedings of the National Academy of Sciences, 97(8):4112–4117, 2000.

[52] Kunihiko Kaneko. Recursiveness, switching, and fluctuations in a replicating catalytic network. Physical Review E, 68(3):031909, 2003.

[53] Stuart A. Kauffman. The origins of order: Self organization and selection in evolution. Oxford university press, 1993.

[54] Sanjay Jain and Sandeep Krishna. Large extinctions in an evolutionary model: the role of innovation and keystone species. Proceedings of the National Academy of Sciences, 99(4):2055–2060, 2002.

[55] Cyril N Hinshelwood. 136. on the chemical kinetics of autosynthetic systems. Journal of the Chemical Society (Resumed), pages 745–755, 1952.

[56] Yuki Izumida and Koji Okuda. Onsager coefficients of a finite-time carnot cycle. Physical Review E, 80(2):021121, 2009.

[57] Ian S FARMER and Colin W JONES. The energetics of escherichia coli during aerobic growth in continuous culture. European Journal of Biochemistry, 67(1):115–122, 1976.

[58] Anke Kayser, Jan Weber, Volker Hecht, and Ursula Rinas. Metabolic flux analysis of escherichia coli in glucose-limited continuous culture. i. growth-rate-dependent metabolic efficiency at steady state. Microbiology, 151(3):693–706, 2005.

[59] OM Neijssel, MJ Teixeira De Mattos, and DW Tempest. Growth yield and energy distribution. 1996.

[60] GN Vemuri, E Altman, DP Sangurdekar, AB Khodursky, and MA Eiteman. Overflow metabolism in escherichia coli during steady-state growth: transcriptional regulation and effect of the redox ratio. Applied and environmental microbiology, 72(5):3653–3661, 2006.

[61] David Owen Morgan. The cell cycle: principles of control. New Science Press, 2007.

[62] Andrew Wood Murray and Tim Hunt. The cell cycle: an introduction, volume 251. Oxford University Press New York, 1993.

[63] Jean-Louis Martiel and Albert Goldbeter. A model based on receptor desensitization for cyclic amp signaling in dictyostelium cells. Biophysical journal, 52(5):807, 1987.

[64] Albert Goldbeter. Biochemical oscillations and cellular rhythms: the molecular bases of periodic and chaotic behaviour. Cambridge university press, 1997.

[65] John B Hogenesch and Hiroki R Ueda. Understanding systems-level properties: timely stories from the study of clocks. Nature Reviews Genetics, 12(6):407–416, 2011.

[66] LNM Duysens and G Sweep. Fluorescence spectrophotometry of pyridine nucleotide in photosynthesizing cells. Biochimica et biophysica acta, 25:13–16, 1957.

[67] Britton Chance, Benno Hess, and Augustin Betz. Dpnh oscillations in a cell-free extract of s. carlsbergensis. Biochemical and biophysical research communications, 16(2):182–187, 1964.

[68] A Ghosh and B Chance. Oscillations of glycolytic intermediates in yeast cells. Biochemical and biophysical research communications, 16(2):174–181, 1964.

[69] Joseph Higgins. The theory of oscillating reactions-kinetics symposium. Industrial & Engineering Chemistry, 59(5):18–62, 1967.

[70] EE Sel'Kov. Self-oscillations in glycolysis. Eur. J. Biochem, 4(1):79–86, 1968.

[71] Britton Chance, Kendall Pye, and Joseph Higgins. Waveform generation by enzymatic oscillators. Spectrum, IEEE, 4(8):79–86, 1967.

[72] Albert Goldbeter and René Lefever. Dissipative structures for an allosteric model: application to glycolytic oscillations. Biophysical Journal, 12(10):1302, 1972.

[73] Yves Termonia and John Ross. Oscillations and control features in glycolysis: numerical analysis of a comprehensive model. proceedings of the national academy of sciences, 78(5):2952–2956, 1981.

[74] Benjamin P Tu, Andrzej Kudlicki, Maga Rowicka, and Steven L McKnight. Logic of the yeast metabolic cycle: temporal compartmentalization of cellular processes. Science, 310(5751):1152–1158, 2005.

[75] Sunil Laxman, Benjamin M Sutter, and Benjamin P Tu. Behavior of a metabolic cycling population at the single cell level as visualized by fluorescent gene expression reporters. PloS one, 5(9):e12595, 2010.

[76] Benjamin P Tu, Rachel E Mohler, Jessica C Liu, Kenneth M Dombek, Elton T Young, Robert E Synovec, and Steven L McKnight. Cyclic changes in metabolic state during the life of a yeast cell. Proceedings of the National Academy of Sciences, 104(43):16886–16891, 2007.

[77] Douglas B Murray, Manfred Beckmann, and Hiroaki Kitano. Regulation of yeast oscillatory dynamics. Proceedings of the National Academy of Sciences, 104(7):2241–2246, 2007.

[78] Robert R Klevecz, James Bolen, Gerald Forrest, and Douglas B Murray. A genomewide oscillation in transcription gates dna replication and cell cycle. Proceedings of the National Academy of Sciences of the United States of America, 101(5):1200–1205, 2004.

[79] A. Katzir-Katchalsky and P.F. Curran. Nonequilibrium thermodynamics in biophysics. Harvard books in biophysics. Harvard University Press, 1967.

[80] O Kedem and S Roy Caplan. Degree of coupling and its relation to efficiency of energy conversion. Transactions of the Faraday Society, 61:1897–1911, 1965.

[81] Yuansheng Cao, Hongli Wang, Qi Ouyang, and Yuhai Tu. The free-energy cost of accurate biochemical oscillations. Nature Physics, 2015.

[82] Michael B Elowitz and Stanislas Leibler. A synthetic oscillatory network of transcriptional regulators. Nature, 403(6767):335–338, 2000.

[83] Henrik Kacser and Luis ACERENZA. A universal method for achieving increases in metabolite production. European journal of biochemistry, 216(2):361–367, 1993.

[84] H Kacser and JA Burns. The control of flux. In Symp. Soc. Exp. Biol., volume 27, pages 65–104, 1973.

[85] Douwe Molenaar, Rogier van Berlo, Dick de Ridder, and Bas Teusink. Shifts in growth strategies reflect tradeoffs in cellular economics. Molecular systems biology, 5(1):323, 2009.

[86] AH Stouthamer and Corry Bettenhaussen. Utilization of energy for growth and maintenance in continuous and batch cultures of microorganisms: A reevaluation of the method for the determination of atp production by measuring molar growth yields. Biochimica et Biophysica Acta (BBA)-Reviews on Bioenergetics, 301(1):53–70, 1973.

[87] Pablo A Iglesias and Brian P Ingalls. Control theory and systems biology. MIT Press, 2010.

[88] Reinhart Heinrich and Tom A Rapoport. A linear steady-state treatment of enzymatic chains. European Journal of Biochemistry, 42(1):89–95, 1974.

[89] Moselio Schaechter, Ole Maaløe, and Niels O Kjeldgaard. Dependency on medium and temperature of cell size and chemical composition during balanced growth of salmonella typhimurium. Microbiology, 19(3):592–606, 1958.

[90] PM Bennett and O Maaløe. The effects of fusidic acid on growth, ribosome synthesis and rna metabolism in escherichia coli. Journal of molecular biology, 90(3):541–561, 1974.

[91] Nobuyoshi Ishii, Kenji Nakahigashi, Tomoya Baba, Martin Robert, Tomoyoshi Soga, Akio Kanai, Takashi Hirasawa, Miki Naba, Kenta Hirai, Aminul Hoque, et al. Multiple high-throughput analyses monitor the response of e. coli to perturbations. Science, 316(5824):593–597, 2007.

[92] Daniel Madar, Erez Dekel, Anat Bren, Anat Zimmer, Ziv Porat, and Uri Alon. Promoter activity dynamics in the lag phase of escherichia coli. BMC systems biology, 7(1):136, 2013.

[93] Jean-Christophe Augustin, Laurent Rosso, and Vincent Carlier. A model describing the effect of temperature history on lag time for listeria monocytogenes. International Journal of Food Microbiology, 57(3):169–181, 2000.

[94] Farida K Vasi and Richard E Lenski. Ecological strategies and fitness tradeoffs in escherichia coli mutants adapted to prolonged starvation. Journal of Genetics, 78(1):43–49, 1999.

[95] IAM Swinnen, Kdens Bernaerts, Els JJ Dens, Annemie H Geeraerd, and JF Van Impe. Predictive modelling of the microbial lag phase: a review. International journal of food microbiology, 94(2):137–159, 2004.

[96] Clara Prats, Daniel López, Antoni Giró, Jordi Ferrer, and Joaquim Valls. Individual-based modelling of bacterial cultures to study the microscopic causes of the lag phase. Journal of Theoretical Biology, 241(4):939–953, 2006.

[97] J Baranyi, PJ McClure, JP Sutherland, and TA Roberts. Modeling bacterial growth responses. Journal of Industrial Microbiology, 12(3-5):190–194, 1993.

[98] Irit Levin-Reisman, Orit Gefen, Ofer Fridman, Irine Ronin, David Shwa, Hila Sheftel, and Nathalie Q Balaban. Automated imaging with scanlag reveals previously undetectable bacterial growth phenotypes. Nature Methods, 7(9):737–739, 2010.

[99] Arvi Jõers and Tanel Tenson. Growth resumption from stationary phase reveals memory in escherichia coli cultures. Scientific reports, 6, 2016.

[100] Stuart A Kauffman. The origins of order: Self-organization and selection in evolution. Oxford University Press, USA, 1993.

[101] Frederick C Nucifora, Masayuki Sasaki, Matthew F Peters, Hui Huang, Jillian K Cooper, Mitsunori Yamada, Hitoshi Takahashi, Shoji Tsuji, Juan Troncoso, Valina L Dawson, et al. Interference by huntingtin and atrophin-1 with cbp-mediated transcription leading to cellular toxicity. Science, 291(5512):2423–2428, 2001.

[102] Yaohui Chai, Jianqiang Shao, Victor M Miller, Aislinn Williams, and Henry L Paulson. Live-cell imaging reveals divergent intracellular dynamics of polyglutamine disease proteins and supports a sequestration model of pathogenesis. Proceedings of the National Academy of Sciences, 99(14):9310–9315, 2002.

[103] Rahul S Rajan, Michelle E Illing, Neil F Bence, and Ron R Kopito. Specificity in intracellular protein aggregation and inclusion body formation. Proceedings of the National Academy of Sciences, 98(23):13060–13065, 2001.

[104] Yasushi Maki, Hideji Yoshida, and Akira Wada. Two proteins, yfia and yhbh, associated with resting ribosomes in stationary phase escherichia coli. Genes to cells, 5(12):965–974, 2000.

[105] Masami Ueta, Ryosuke L Ohniwa, Hideji Yoshida, Yasushi Maki, Chieko Wada, and Akira Wada. Role of hpf (hibernation promoting factor) in translational activity in escherichia coli. Journal of biochemistry, 143(3):425–433, 2008.

[106] Antón Vila-Sanjurjo, Barbara-S Schuwirth, Cathy W Hau, and Jamie HD Cate. Structural basis for the control of translation initiation during stress. Nature structural & molecular biology, 11(11):1054–1059, 2004.

[107] Jens Tyedmers, Axel Mogk, and Bernd Bukau. Cellular strategies for controlling protein aggregation. Nature reviews Molecular cell biology, 11(11):777–788, 2010.

[108] John J Hopfield. Kinetic proofreading: a new mechanism for reducing errors in biosynthetic processes requiring high specificity. Proceedings of the National Academy of Sciences, 71(10):4135–4139, 1974.

[109] R Hengge-Aronis. Regulation of gene expression during entry into stationary phase. Escherichia coli and Salmonella typhimurium, pages 1497–1511, N/A.

[110] Herb E Schellhorn, Jonathon P Audia, Linda IC Wei, and Lily Chang. Identification of conserved, rpos-dependent stationary-phase genes of escherichia coli. Journal of bacteriology, 180(23):6283–6291, 1998.

[111] William Jas Penfold. On the nature of bacterial lag. Journal of Hygiene, 14(02):215–241, 1914.

[112] Thomas E Oscar. Validation of lag time and growth rate models for salmonella typhimurium: acceptable prediction zone method. Journal of Food Science, 70(2):M129–M137, 2005.

[113] Carmen Pin and József Baranyi. Single-cell and population lag times as a function of cell age. Applied and environmental microbiology, 74(8):2534–2536, 2008.

[114] Steven H Strogatz. Nonlinear dynamics and chaos: with applications to physics, biology, chemistry, and engineering. Westview press, 2014.

[115] Daniel T Gillespie. Exact stochastic simulation of coupled chemical reactions. The journal of physical chemistry, 81(25):2340–2361, 1977.

[116] Chikara Furusawa, Takao Suzuki, Akiko Kashiwagi, Tetsuya Yomo, and Kunihiko Kaneko. Ubiquity of log-normal distributions in intra-cellular reaction dynamics. Biophysics, 1:25–31, 2005.

[117] Long Cai, Nir Friedman, and X Sunney Xie. Stochastic protein expression in individual cells at the single molecule level. Nature, 440(7082):358–362, 2006.

[118] A Elfwing, Y LeMarc, J Baranyi, and A Ballagi. Observing growth and division of large numbers of individual bacteria by image analysis. Applied and Environmental Microbiology, 70(2):675–678, 2004.

[119] Hans Bremer and Patrick P Dennis. Modulation of chemical composition and other parameters of the cell at different exponential growth rates. EcoSal Plus, 3(1), 2008.

[120] Jes Forchhammer and Lasse Lindahl. Growth rate of polypeptide chains as a function of the cell growth rate in a mutant of escherichia coli 15. Journal of molecular biology, 55(3):563–568, 1971.

[121] Margot K Sands and Richard B Roberts. The effects of a tryptophan-histidine deficiency in a mutant of escherichia coli. Journal of bacteriology, 63(4):505, 1952.

[122] Gunther S Stent and Sydney Brenner. A genetic locus for the regulation of ribonucleic acid synthesis. Proceedings of the National Academy of Sciences, 47(12):2005–2014, 1961.

[123] Brian J Paul, Melanie M Barker, Wilma Ross, David A Schneider, Cathy Webb, John W Foster, and Richard L Gourse. Dksa: a critical component of the transcription initiation machinery that potentiates the regulation of rrna promoters by ppgpp and the initiating ntp. Cell, 118(3):311–322, 2004.

[124] M Kajitani and A Ishihama. Promoter selectivity of escherichia coli rna polymerase. differential stringent control of the multiple promoters from ribosomal rna and protein operons. Journal of Biological Chemistry, 259(3):1951–1957, 1984.

[125] Arvind Raghavan and Dipankar Chatterji. Guanosine tetraphosphate-induced dissociation of open complexes at the escherichia coli ribosomal protein promoters rplj and rpsa p1: nanosecond depolarization spectroscopic studies. Biophysical chemistry, 75(1):21–32, 1998.

[126] Melanie M Barker, Tamas Gaal, Cathleen A Josaitis, and Richard L Gourse. Mechanism of regulation of transcription initiation by ppgpp. i. effects of ppgpp on transcription initiation in vivo and in vitro. Journal of molecular biology, 305(4):673–688, 2001.

[127] Lisa U Magnusson, Anne Farewell, and Thomas Nyström. ppgpp: a global regulator in escherichia coli. Trends in microbiology, 13(5):236–242, 2005.

[128] Lisa U Magnusson, Thomas Nyström, and Anne Farewell. Underproduction of ς70 mimics a stringent response a proteome approach. Journal of Biological Chemistry, 278(2):968–973, 2003.

[129] ChemSpider. http://www.chemspider.com/.

[130] Sara Oliveira. Glucose as a potent inducer of cell death in yeast. Master Dissertation, 2011.

[131] David Granot, Alex Levine, and Edan Dor-Hefetz. Sugar-induced apoptosis in yeast cells. FEMS Yeast Research, 4(1):7–13, 2003.

[132] Hiroyuki Yoshimoto, Rie Ohuchi, Kumiko Ikado, Satoshi Yoshida, Toshiko Minato, Tatsuji Ishiguro, Satoru Mizutani, and Osamu Kobayashi. Sugar induces death of the bottom fermenting yeast saccharomyces pastorianus. Journal of bioscience and bioengineering, 108(1):60–62, 2009.